INFORMATION TO USERS

This manuscript has been reproduced from the microfilm master. UMI films the text directly from the original or copy submitted. Thus, some thesis and dissertation copies are in typewriter face, while others may be from any type of computer printer.

The quality of this reproduction is dependent upon the quality of the copy submitted. Broken or indistinct print, colored or poor quality illustrations and photographs, print bleedthrough, substandard margins, and improper alignment can adversely affect reproduction.

In the unlikely event that the author did not send UMI a complete manuscript and there are missing pages, these will be noted. Also, if unauthorized copyright material had to be removed, a note will indicate the deletion.

Oversize materials (e.g., maps, drawings, charts) are reproduced by sectioning the original, beginning at the upper left-hand corner and continuing from left to right in equal sections with small overlaps. Each original is also photographed in one exposure and is included in reduced form at the back of the book.

Photographs included in the original manuscript have been reproduced xerographically in this copy. Higher quality 6" x 9" black and white photographic prints are available for any photographs or illustrations appearing in this copy for an additional charge. Contact UMI directly to order.

UMI

University Microfilms International
A Bell & Howell Information Company
300 North Zeeb Road, Ann Arbor, MI 48106-1346 USA
313/761-4700 800/521-0600

Reproduced with permission of the copyright owner. Further reproduction prohibited without permission.

Reproduced with permission of the copyright owner. Further reproduction prohibited without permission.

Order Number 9417448

Nuclear magnetic resonance studies of water in perfluorinated ion exchange membranes

Chen, Rensheng, Ph.D.

City University of New York, 1994

U·M·I
300 N. Zeeb Rd.
Ann Arbor, MI 48106

Reproduced with permission of the copyright owner. Further reproduction prohibited without permission.

Reproduced with permission of the copyright owner. Further reproduction prohibited without permission.

NUCLEAR MAGNETIC RESONANCE STUDIES

OF WATER IN PERFLUORINATED ION EXCHANGE MEMBRANES

by

Rensheng Chen

A dissertation submitted to the Graduate Faculty in
Physics in partial fulfillment of the requirements
for the degree of Doctor of Philosophy,
The City University of New York.

1994

Reproduced with permission of the copyright owner. Further reproduction prohibited without permission.

This manuscript has been read and accepted for the Graduate Faculty in Physics in satisfaction of the dissertation requirement for the degree of Doctor of Philosophy.

18 January 1994
Date

Professor Steve G. Greenbaum, Chair of Examining Committee

20 Jan 1994
Date

Professor Joseph Krieger, Executive Officer

Professor Ying-Chih Chen

Professor John J. Fontanella

Professor Robert A. Marino

Professor Ruth E. Stark

Supervisory Committee

The City University of New York

Reproduced with permission of the copyright owner. Further reproduction prohibited without permission.

Abstract

NUCLEAR MAGNETIC RESONANCE STUDIES

OF WATER IN PERFLUORINATED ION EXCHANGE MEMBRANES

by

Rensheng Chen

Advisor: Professor Steve G. Greenbaum

Perfluorinated ion-exchange membranes such as NAFION (DuPont) serve as both electrolyte and separators employed in fuel cells. The presence of the water in these membranes is critical to fuel cell operation. Water molecular diffusion and charge transport across the membrane are correlated. Through the availability of water isotopically enriched in deuterium or ^{17}O, nuclear magnetic resonance (NMR) can be employed to study molecular dynamics by utilizing quadrupolar nuclei as probes. In this thesis, Deuteron and oxygen-17 NMR measurements in NAFION-117 membranes with variable water (D_2O or $H_2{}^{17}O$) content (3 ~ 18% by weight) have been carried out. Measurements were taken at variable temperature (room T down to 115 K), high pressure (up to 0.25 GPa), and on stretched samples. One of the main results concerns the observation of anisotropic molecular motion in the membrane plane, with dramatic enhancement of the anisotropy in modestly stretched membranes. Glassy behavior of the water domains at low temperature is evidenced by the specific nature of the ^2H NMR line shapes at 109 K. Activation energies extracted from both ^2H and ^{17}O spin-lattice

Reproduced with permission of the copyright owner. Further reproduction prohibited without permission.

relaxation data exhibit a steady increase with increasing water content. Activation volumes extracted from both ^{1}H and ^{2}H T_1 pressure dependence show a decrease with increasing water content, at room temperature. Analysis of these observations suggests a water cluster model for water organization in NAFION membranes. The relatively free water and motionally restricted (by interaction with the polymer host) water exchange each other rapidly yielding an averaged response at room T, while the hydrogen bonds become more rigid at low temperature. Deuteron and oxygen-17 NMR studies of NAFION-117 containing either deuterated methanol (CH_3OD) or oxygen-17 enriched methanol ($CH_3{}^{17}OH$) demonstrate that the methanol molecular motion in NAFION-117 is considerably faster than for water in NAFION. This supports the conclusion that the methanol transport across the NAFION membrane is probably too high for fuel cell applications. Comparison of the water behavior in NAFION-127 with in NAFION-117 supports the conclusion that proton transport is more effective in NAFION-117.

Reproduced with permission of the copyright owner. Further reproduction prohibited without permission.

ACKNOWLEDGEMENTS

I OWE SPECIAL THANKS to my advisor, Professor Steve Greenbaum, who generously advised me on a variety of academic issues as I was working on my Ph.D. degree. His special guidance, patience and encouragement were always appreciated. He also made his invaluable suggestions in reviewing this manuscript.

Professor Robert Marino, my "second" advisor, is gratefully thanked for his knowledge, helpful discussion and kindness, especially his supervision during Professor Greenbaum's sabbatical leave.

I am very grateful to Mr. Richard Krumm for his technical assistance in fabrication of high pressure feed-through plugs used in high pressure NMR studies.

Professor Ying-Chih Chen, Professor John J. Fontanella, and Professor Ruth E. Stark of my supervisory committee are great appreciated for their friendly participation and reading of this manuscript.

Dr. J.R.P. Jayakody, who collaborated with me for nearly two years, deserves my thanks for his friendship and many useful discussions. I would like to express my gratitude to Dr. Shizhe Li for his knowledge and help in NMR techniques, as well as to Dr. P.E. Stallworth, Dr. Yiu Sun Pak for their useful discussions. People in the NMR lab are thanked for their friendship, especially Ms. Jiali Li, who assisted in plotting partial data for me.

I owe my wife and son the commitment of companionship, their support and understanding were essential for the completion of this work.

This work was supported partly by a grant from the US Office of Naval Research.

Reproduced with permission of the copyright owner. Further reproduction prohibited without permission.

DEDICATION

This Thesis is Dedicated to

The Memory

of

My Beloved Mother

for her great commitment to her children with heart and soul

though herself suffering from both poverty and sickness

Reproduced with permission of the copyright owner. Further reproduction prohibited without permission.

Table of Contents

Reproduced with permission of the copyright owner. Further reproduction prohibited without permission.

Reproduced with permission of the copyright owner. Further reproduction prohibited without permission.

Reproduced with permission of the copyright owner. Further reproduction prohibited without permission.

List of Tables

Reproduced with permission of the copyright owner. Further reproduction prohibited without permission.

List of Figures

Reproduced with permission of the copyright owner. Further reproduction prohibited without permission.

Reproduced with permission of the copyright owner. Further reproduction prohibited without permission.

Reproduced with permission of the copyright owner. Further reproduction prohibited without permission.

Reproduced with permission of the copyright owner. Further reproduction prohibited without permission.

Reproduced with permission of the copyright owner. Further reproduction prohibited without permission.

Reproduced with permission of the copyright owner. Further reproduction prohibited without permission.

Reproduced with permission of the copyright owner. Further reproduction prohibited without permission.

Chapter 1. Introduction

1-1. Materials Under Investigation

Power systems for electric vehicles are receiving increasing attention[1]. The fuel cell is considered particularly attractive for mobile power since it could provide a driving range and refueling time comparable to the conventional internal combustion automobile. The solid-polymer-electrolytes fuel cell is considered by many to be the most promising type of fuel cell for transportation applications because of its low-temperature operation and ease of construction[2,3]. Perfluorosulfonate ion-exchange membranes such as NAFION act both as the electrolyte and the separator in fuel cells[2,4]. However, the presence of the water in these membranes is critical to fuel cell operation. Thus, the behavior of water in these ion-exchange polymers is of great technological interest. The main rationale of this thesis is to shed light on the specific role that water plays in proton transport in the NAFION membranes using wide-line NMR techniques. In particular, an important goal is to obtain an improved understanding of the behavior of water in NAFION as compared to that of bulk water.

1-1.1. NAFION

The NAFION brand perfluorosulfonate polymers were manufactured by E. I. du Pont de Nemours and Co.. These materials were developed during the middle 1960's, and have been available in various forms for study since the early 1980's[5-8]. Recently, the commercial preparation NAFION available in acid and various salt forms are receiving a great deal of attention with regard to their high ion-exchange properties, great

Reproduced with permission of the copyright owner. Further reproduction prohibited without permission.

thermal stabilities, high chemical stabilities to most reagents, and the potential use in fuel cells. In addition, NAFION is one of the candidates for low temperature electrochemistry studies as pioneered by Stimming and co-workers with other solid electrolyte systems[9-10].

1-1.2. The Chemical Structure of NAFION-117 Membrane

A general formula of NAFION in either the acid form or the salt form is[4]:

$$\sim (CF_2CF_2)_n\text{-}CF_2CF \sim$$

$$|$$

$$O(CF_2CF\text{-}O)_mCF_2CF_2SO_2X$$

$$|$$

$$CF_3$$

where X = F denotes NAFION-F, the precursor; X = O^-K^+ denotes NAFION-K; X = OH, denotes NAFION-H. For commercial materials, m is usually equal to one and n varies from about 5 to 11. This generates an equivalent weight (EW), the weight of acid polymer per SO_3H group, in a range of about 1000 to 1500 grams of dry hydrogen ion form polymer per mole of exchange sites. Membranes are produced in nominal thicknesses from about 0.1 mm to 0.3 mm. The membrane that we investigated extensively in this thesis is NAFION-117, named NAFION-H, the acid form of the material. Its EW is 1100, the repeat number n is 6.5 ~ 7 and m = 1. Its thickness is about 0.19 mm. Structurally, NAFION consists of a backbone of tetrafluoroethylene with pendent side chains of perfluorinated vinyl ethers which terminate in sulfonic acid groups

Reproduced with permission of the copyright owner. Further reproduction prohibited without permission.

or a metal sulfonate. The acid and salt forms are hydrophilic. Gierk[11] on the basis of small-angle x-ray results concluded that the ionic domains are about 40 Å in diameter and are separated by walls of fluorocarbon about 10 Å thick. Starkweather reported that NAFION has significant levels of crystallinity. The size of the crystallites is greater than the average separation between side groups. The polymer is thought to be arranged in bilayers with ionizable side groups extending on either side[12]. Figure 1 shows the scheme of NAFION-117 structure.

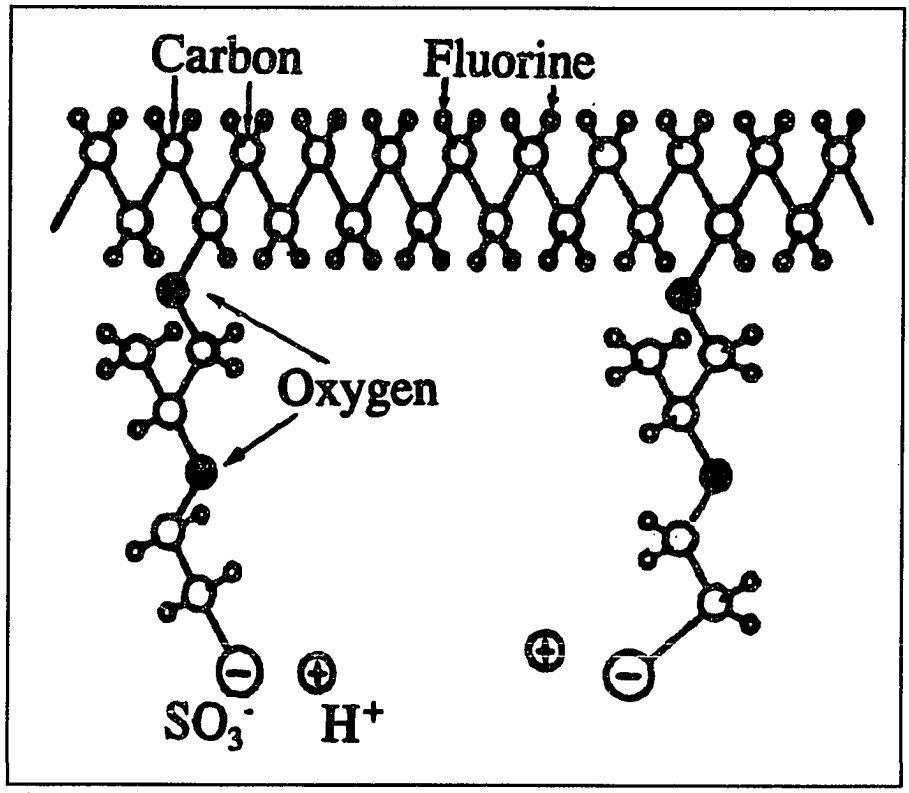

Figure 1.1: The scheme of NAFION-117 structure.

1-1.3. The Significance of Water in NAFION Membranes

It is well known that the presence of water, readily incorporated into the structure of the polymer in amounts ranging from several to 25% by weight, facilities rapid self-

Reproduced with permission of the copyright owner. Further reproduction prohibited without permission.

diffusion of protons and other cations in the membrane, which enables ionic diffusive properties to be maintained through the membrane phase. The amount of the water present in these membranes greatly influences the performance of the fuel cell. If the membrane is too dry, its conductivity falls, resulting in reduced cell performance. An excess of water in the fuel cell can lead to cathode flooding problems, also resulting in less than optimal performance[13]. Several studies have examined the water behavior in the membranes[14-23] which will be discussed later.

1-2. A Brief Literature Review of Studies of Water in NAFION

1-2.1. The Structural Models of NAFION Containing Water

An interesting and important practical aspect of NAFION perfluorosulfonate membranes is their ability to absorb relatively large amounts of water and other solvents. The NAFION membranes typically absorb 10-25% of water by weight, depending upon their EW, counterion form and temperature of equilibration. They absorb even larger amounts of other solvents as well, particularly alcohols and other protonic solvents[24]. Structural models of NAFION have been proposed. Since the sulfonate groups are far more hydrophilic than the fluorocarbon backbone, the molecules are arranged to maximize the interaction of similar fragments. The ionizable sulfonate groups form clusters, which cause the production of water-containing pockets in a hydrophobic matrix, the latter comprised of the fluorocarbon backbone of the polymer[4]. Several models have been proposed to describe the structural organization of NAFION. The first group of models suggests that all the sulfonate groups are in an aqueous phase, consisting of well-defined clusters and channels, as shown in Figure 1.2. This cluster-network

Reproduced with permission of the copyright owner. Further reproduction prohibited without permission.

model develops the concept of spherical ionic regions separated by inter-connecting channels. These channels are seen to have an important role in hydroxide ion rejection in chlor-alkali cells[25]. Another group of models proposed by Rodmacq et al. is a three phase model in which fluorocarbon microcrystallites, ion water clusters, and a second ionic region of low water content coexist[26]. Yeager et al. proposed a model of NAFION which is consistent with ionic diffusion within three regions in the polymer, as shown in Figure 1.3, Region A consists of fluorocarbon backbone material, some of which is in a microcrystalline form. Ion clusters form Region C, in which the majority of sulfonate exchange sites, counterions, and sorbed water exist. The interfacial Region B is seen as one of relatively large fractional void volume, containing pendent side chain material, a smaller amount of water, some sulfonate exchange sites which have not been incorporated into clusters, and a corresponding fraction of counterions[27].

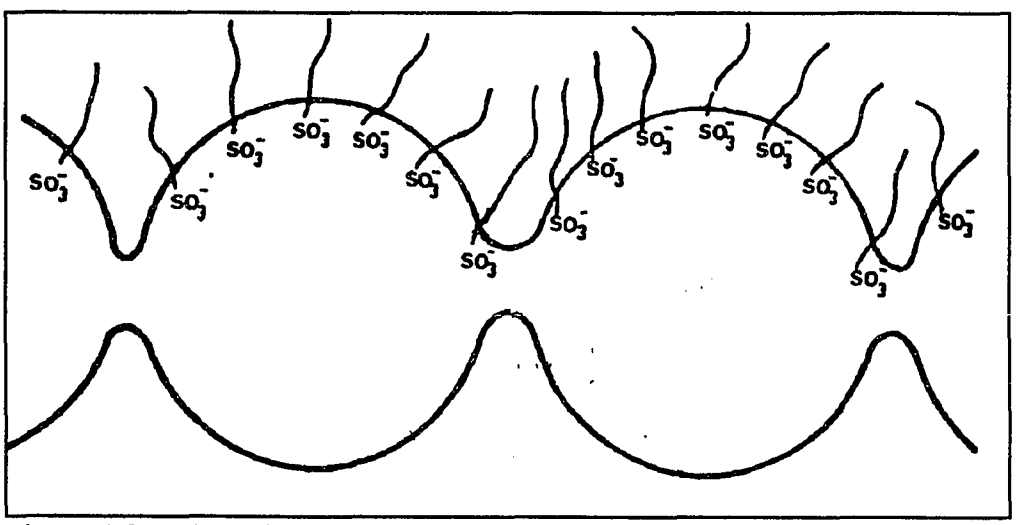

Figure 1.2: Schematic representation of the molecular organization of a cluster (reproduced from Ref.[4])

Reproduced with permission of the copyright owner. Further reproduction prohibited without permission.

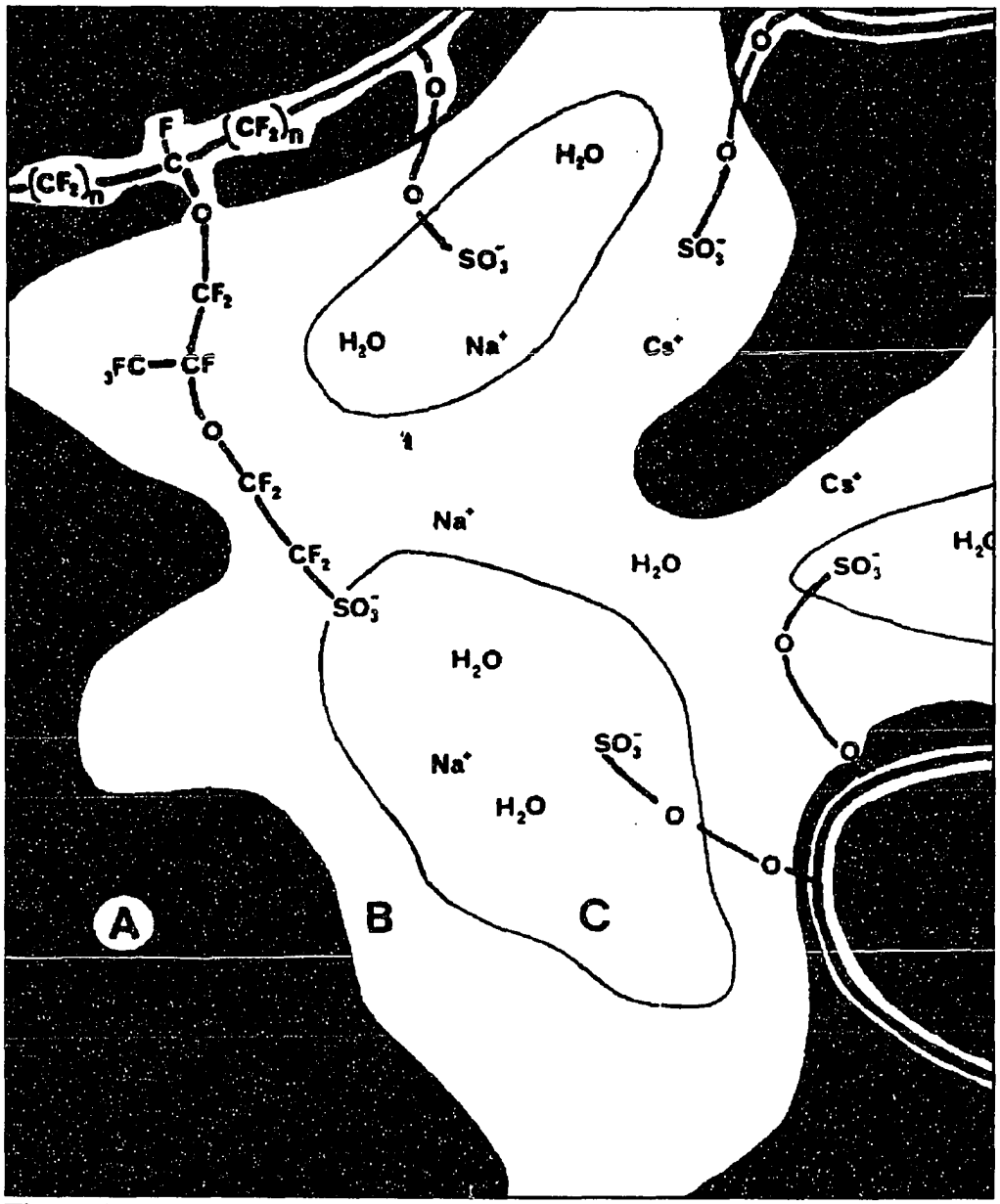

Figure 1.3: Three region structural models for NAFION: A, fluorocarbon; B, interfacial zone; C, ionic clusters. (reproduced from [27])

Reproduced with permission of the copyright owner. Further reproduction prohibited without permission.

Evidence to support these models of NAFION has been obtained for NAFION acid or salt forms (other than EW 1100) by several techniques. The transmission electron microscopy of NAFION sample whose salt ions were exchanged to lead ions shows a regular pattern of clusters 3-6 nm in diameter[28], indicating that in the polymer the clusters are spherical. Falk reported evidence for two environments of sorbed water in NAFION from infrared spectroscopic studies[29]. The first environment appears to be aqueous in nature, with the strength of intermolecular hydrogen bonding slightly reduced from that in bulk water. In the second environment, the water molecules are not hydrogen bonded and appear to be exposed mainly to fluorocarbon. In small-angle x-ray (SAXS) and small-angle neutron scattering (SANS) studies, Gierke found a reflection which was assigned to the clusters associated with a Bragg spacing of 30 to 50 Å in NAFION-H and its salts but it was not observed in the precursor, NAFION-F. He found that both the position and intensity were dependent on EW and cation. Moreover, the size of the clusters is also highly dependent on the amount of water present. The calculated diameter of the clusters for NAFION-H varied from 1.9 nm for the dry polymer up to 4.08 nm for the one containing 20% water[25].

1-2.2. Water Behavior in NAFION

The behavior of the water itself within the membrane is complex and poorly understood. Several attempts have been made to obtain a detailed appreciation of the structure of the aqueous phase in the NAFION[30-32].

Neutron quasi-elastic scattering (NQES) has been used to study the motion of water in NAFION[30,31]. In this technique the energy of the scattered neutrons is

Reproduced with permission of the copyright owner. Further reproduction prohibited without permission.

measured; the change in energy of the scattered neutrons from the energy of the incident radiation is dependent on the motion of the scattering particles. Two peaks were observed, a broad peak provides evidence of a disordered scattering center in rapid motion, while a sharp peak yields evidence of a rigid structure. Dry NAFION-H shows a much sharper peak than wet NAFION-H.

Duplessix et al.[32] studied solid NAFION-H containing 2.7 to 20 wt% water by proton NMR. At all water contents only a single proton resonance was observed. This could be explained even though there is more than one environment for the protons in NAFION-H, — all the NMR active protons undergo rapid exchange on the NMR time scale. The line width decreases and the chemical shift moves to higher field as the water content increases from 2.7% to 4.4%. But the line width and chemical shift are nearly independent of water content at water content above 4.4%. The major change in the chemical shift and the line width at the lower water content is taken as evidence of two regimes of water absorption. The change in the line width implies that there is a significant increase in the mobility of the water protons at water contents higher than 4%. The temperature dependence of the line width shows a decrease in the line width as the temperature is increased from 200 K to room temperature. This could be due to either an increase in the spin-spin relaxation time (T_2) or to decreasing anisotropy as the water becomes more mobile at higher temperature. That the proton NMR measurements are less sensitive in detecting of molecular anisotropic motion invites deuteron NMR as a probe of anistropy which will be most of our work in this thesis. The temperature dependence of the spin-lattice relaxation time (T_1) is a function of water content too; it is observed that the larger the water content the smaller the T_1. There is a single

Reproduced with permission of the copyright owner. Further reproduction prohibited without permission.

minimum T_1 at room temperature (~280 K) for a relatively dry sample (2.7%), this behavior implies that a single molecular motion mechanism can describe the water and acid protons in these samples and that long-range diffusion is not a major factor because the water molecules are restricted within certain regions in the dry sample. For wet samples the situation is more complicated. The T_1 value shows two minima, one near room temperature and a second at low temperature. The position of the low temperature minimum is 200 K for sample containing 20% water and it shifts to higher temperatures in drier samples. The line width versus temperature also exhibits a maximum point at room temperature for NAFION containing 20% water. These results indicate that water in NAFION does not exhibit a single simple motion. Other proton NMR studies of water in NAFION have been reported by Boyle and co-workers[22,23]. They have performed the temperature dependence of T_1, $T_{1\rho}$, and T_2 for 25% hydrated NAFION acid form at Larmor frequency = 40 MHz. The data indicate a glasslike transition near 193 K, which is consistent with dielectric results reported by Yeo and Eisenberg[17]. Below this temperature the three relaxation times reflect non-exponential processes. The magnitude of the ratio T_1/T_2=2.6 at the T_1 minimum exceeds the 1.6 predicated by the BPP theory[33]. This implies the relaxation cannot be assigned to unique correlation times and is probably associated with two different and segregated proton populations with different relaxation times. Boyle et al. suggested that these two types of protons could arise from exchange between two populations of water in different regions of the polymer, possibly varying in acidity. A similar suggestion was made by Duplessix et al.[32]: there are two types of motions, one is long-range diffusion and the other is shorter. Starkweather et al. have reported proton NMR results at 90 MHz for NAFION-H, Na^+, and K^+ forms of

Reproduced with permission of the copyright owner. Further reproduction prohibited without permission.

EW 970, 1100, 1200, and 1375. NAFION-H EW 1500 was also done. In each case, there was a minimum in T_1 near 218 K. The activation energies calculated from the dependence of T_1 on temperature near the minima are 5-6 kcal/mol(0.22-0.26 eV). Above 283 K, the slope is smaller and corresponds to an activation energy close to the value of 3.7 kcal/mol(0.15 eV) for bulk water. They concluded that the larger activation energies are indicative of more cooperative motion[34]. Their T_1 results for NAFION-H EW 1200 are somewhat different from that of Duplessix and co-workers[32]. The reasons for the difference are unknown.

Sivashinsky and Tanny[35] took both NMR and differential scanning calorimetry (DSC) measurements. The NMR data also show a single minimum between 200 and 300 K in T_1 temperature dependence measurements. In addition, their measurements of the intensity of the FID showed that the intensity decreased linearly with the inverse of the temperature. Since the intensity of the NMR line is proportional to the number of mobile protons, the observed results indicate that about 50% of the total number of water protons in NAFION become significantly less mobile around 273 K for NAFION containing more than 8% water. As for the DSC results, the authors analyzed the DSC peaks as corresponding to freezing or melting of water in small diameter (12 Å) channels preexisting in NAFION membrane when at room temperature and are dependent on the pore size. Later, Pineri et al.[36] have taken NMR, DSC, ESR and other mechanical measurements on NAFION 1200 EW acid form. DSC experiments show the existence of exothermic or endothermic peaks for water contents larger than 8 wt% when at room temperature. The DSC heating rate influences the peaks. For NMR measurements, the NAFION membrane containing 15.2 wt% water was sealed at room temperature in a

Reproduced with permission of the copyright owner. Further reproduction prohibited without permission.

glass tube containing an excess of water, then the tube was quenched in liquid nitrogen. A rapid transfer was then realized to the NMR probe maintained at a well-defined temperature. The amplitude of the line was then recorded versus time. The experiment was repeated for several different temperature. These authors reported that there is a initial increase of the amplitude corresponding to initial heating of the sample from liquid-nitrogen temperature up to the annealing temperatures, then a systematic decrease of the amplitude versus time was observed showing a decrease of the total number of mobile protons. Both the kinetics and equilibrium values of these changes depend on the annealing temperature. Supported by other experiments, these authors attributed this change to a desorption process from the NAFION matrix to an external site where normal solid ice is formed. This desorption process was treated as a thermally activated process with an activation energy of 6 kcal/mol(0.26 eV). By this sorption-desorption process, these authors interpreted the DSC peaks as corresponding to a first order transition of water after sorption or desorption in or out of the ionic phase and therefore do not invoke a pore size effect. This description is not in agreement with the Sivashinsky's interpretation.

In electrochemical applications, the charge transport process within NAFION is very important both in NAFION coated electrodes and in solid polymer electrolytes fuel cells. The conductivity (σ) and proton self-diffusion (D) of NAFION membranes studies show that the water structure in NAFION affects the charge transport characteristic strongly. Slade et al.[37] reported their protonic conduction and ^{1}H self-diffusion coefficient in NAFION-117 (EW 1100). NAFION samples were boiled in either deionized water or aqueous nitric acid and then air dried. Conductivities were measured

Reproduced with permission of the copyright owner. Further reproduction prohibited without permission.

using ac (50 Hz to 1 MHz) admittance techniques and self-diffusion coefficients were measured by the pulsed field gradient (PFG) ^1H NMR (10 MHz) technique. Acid pretreatment enhanced conductivities by one and a half orders of magnitude, with little change in measured D values. The temperature dependence of ac conductivities show an Arrhenius form in the experimental temperature range (240 K < T < 300 K), with E_a =31.5 kJ/mol(0.33 eV) and 21.6 kJ/mol(0.22 eV) for films prepared in deionized water and dilute nitric acid pretreatment respectively. The temperature dependence of ^1H self-diffusion coefficients show non-Arrhenius behavior and lead to a D from $10^{-5.1}$ cm^2s^{-1} for 300 K down to $10^{-5.7}$ for 270 K. These D values are much greater than those appropriate to H^+, the charge diffusion $D^+ \sim 10^{-8\sim-7}$ at 298 K, which are evaluated by the Nernst-Einstein equation $\sigma = (Ne^2/kT)D^+$. These authors pointed out that the PFG technique is monitoring self-diffusion of neutral species (i.e. H_2O) while the charge transport is much slower because it could be electrostatically hindered for (H^+) by association with the ion cluster. The mechanisms for H^1 self-diffusion and H^+ transport are different, thus requiring further explanation. Uosaki et al.[38] also carried out conductivity measurements of NAFION-117, and observed a temperature-dependent change of the activation energy, 29 kJ/mol(0.30 eV) at 250~210 K and 43 kJ/mol(0.44 eV) at 210~180 K, the latter region at which a change of the water structure occurs. They concluded that the change in proton transport mechanism is correlated with the change of the water structure, giving the different activation energies in two regions. Recently, Newman and Fuller obtained the transport number of water in NAFION 117 membrane by using a concentration cell[38]. Zawodzinski et al.[13,39-41] reported the water uptake and transport properties of NAFION-117 membranes at 303 K. PFG NMR ^1H diffusion

Reproduced with permission of the copyright owner. Further reproduction prohibited without permission.

coefficient and protonic conductivity measurements were carried out as functions of water contents in the membranes. Their data of D^+ are not consistent with that of Slade, possibly due to the different pretreatment procedures not discussed by the authors. They reported that the H^+ diffusion coefficient D^+ and ^1H diffusion coefficient D are similar at low water content, differing increasingly as the water content increases, i.e. D^+ becomes larger than D. They inferred that transport of H^+ by Grotthus hopping probably becomes increasingly significant at high water contents, whereas it seems to be negligible at low water contents. They concluded that, in the extreme of low water content, H_2O and H^+ probably diffuse by an identical mechanism, i.e. that the solvated H^+ under an electric field has the same mobility as that of H_2O. Thus they identified the ^1H diffusion coefficient they measured as the intra-diffusion coefficient of H_2O in the membrane over the entire range of membrane water contents. However, this technique still does not distinguish between neutral (H_2O) and charged (H^+) species. Besides, these authors saw that the measured diffusion coefficients are independent of the value of gradient strength, which leads to a conclusion that no large "pockets" of bulk water exist in these membranes[40]. In addition to proton NMR studies of water in NAFION, ^{19}F NMR was also employed to study the backbone and pendent chain in NAFION membranes and solutions[42,43].

1-2.3. Conclusion

Although lots of studies of water in NAFION membranes have been done, as cited in the references above, the interpretation of the complicated water behavior still remains open to question. To the best of our knowledge, no one has reported water

Reproduced with permission of the copyright owner. Further reproduction prohibited without permission.

molecular rotation and anisotropic motion in the NAFION membranes, and their behavior at the conditions of low temperature; high pressure; under stretching, etc. These studies could provide very important information for investigations of water diffusion and transport in NAFION membranes.

1-3. Research Methods in This Thesis

1-3.1. Deuteron NMR

The development of high-power NMR instrumentation and implementation of the quadrupole echo pulse sequence in the last decade have led to the present popularity of deuteron NMR spectroscopy in solids[44]. Smith[45], Spiess[46] and Jelinski[44] have reviewed ^2H NMR studies in polymers comprehensively. Deuteron NMR is a powerful technique for studying structural and dynamical aspects of polymers because the nuclear quadrupole moment of the deuteron provides an illuminating probe of structure and dynamics, manifested in both spectral and relaxation effects. An advantage of deuteron NMR is its selectivity, i.e. only the deuteriated portions of the compound are observed spectroscopically. Another advantage of using ^2H is that we can interpret the water relaxation in polymer directly in terms of rotational motion since the dominant relaxation process, rotational modulation of the nuclear electric quadrupole moment, is well-defined for nuclei such as deuterium with spin $I = 1$. In contrast with other relaxation studies such as proton relaxation times (T_1, T_2, $T_{1\rho}$) reported in the literature[22,23], only broad general conclusions can be reached based on the simple determination of ^1H relaxation times since the contributions of inter and intramolecular dipolar relaxation mechanisms cannot be separated easily. The detailed characteristics of deuteron NMR will be

Reproduced with permission of the copyright owner. Further reproduction prohibited without permission.

reviewed in chapter two.

In this investigation, deuteron NMR will be a main tool to study water in NAFION-117 membranes. NAFION-127 (EW 1200) will be also considered. Samples were treated in D_2O prior to the ^2H NMR measurements. NMR studies include lineshape and spin-lattice (T_1) relaxation measurements as function of water content, temperature (particularly below room T), and pressure. The dynamics of deuteron transport can be probed by T_1 measurements, using previously reported ^1H results[22,23] as a guide. Deuteron transport and exchange on the timescale of 10^2 - 10^5 Hz will have a profound effect on the lineshape while much faster processes ($\sim 10^8$ Hz) can be probed by T_1. Spectra obtained at low temperatures and relatively low water content yield basic information about deuteron motion which would most likely be masked by rapid exchange effects at higher T and water content. The anisotropic water molecular motion due to the polymer morphology combined with motional narrowing leads to a residual anisotropic axis in the membrane, which results in a line splitting, i.e. a doublet in deuteron spectrum. The thermal activation energies for deuteron (proton) motion can be extracted from T_1 Arrhenius plots. The deuteron NMR studies were also applied to NAFION-117 containing partially deuteriated methanol (CH_3OD) for the purpose of obtaining information relevant to methanol fuel cell operation.

Although several deuteron NMR studies of water in polymers have been reported in recent years, very few people have applied deuteron NMR studies of water in NAFION. To the best of our knowledge there is one paper reporting ^2H T_1 results for NAFION-117 containing various water contents at 303 K[13] in addition to the published work originating in this thesis[47]. Nevertheless, it is useful to review the previous

Reproduced with permission of the copyright owner. Further reproduction prohibited without permission.

studies of water in polymers by deuteron NMR. Li has carried out deuteron NMR studies of water in polyimide films in Greenbaum's laboratory[48]. He observed that the doublet splitting of ^2H spectra reaches a maximum value when the plane of the films is perpendicular to the magnetic field and a minimum when the angle is about 30°. This means that the averaged quadrupole interaction axis of D_2O molecules is perpendicular to the film plan. Here the average axis represents the net quadrupole interaction axis contributed by two O-D bonds in a single D_2O molecule. Thus the water molecules are oriented perpendicular to the plane of the film. It is interesting to see the different aspects between proton and deuteron NMR spectra for same samples. Dehl studied broad line NMR of H_2O and D_2O in oriented rayon fiber[49]. Both proton and deuterium spectra showed a splitting feature. The splitting for D_2O is several times bigger than that of H_2O, and the splitting is also angularly dependent. Matsumura et al.[50-52] have done a comprehensive investigation on water in cellulose films. In cellulose acetate film, both H_2O and D_2O exhibit splitting due to dipolar and quadrupole interaction respectively. The splitting is angularly dependent and has the same behavior as that of polyimide[48]. The separation of splitting decreases as the water content increases for both H_2O and D_2O. When lower the temperature, the separation of the peaks and linewidth of the each single peak of doublet tend to increase. Angularly dependent splitting was also observed for cellulose triacetate films containing H_2O, D_2O and deuteriated methanol (CH_3OD and CD_3OH)[51].

1-3.2. Oxygen-17 NMR

Oxygen-17 NMR can shed additional light on the specific identity of the charge

Reproduced with permission of the copyright owner. Further reproduction prohibited without permission.

carriers and details concerning water molecular motion. The quadrupole coupling constant (QCC) of ^{17}O in water (ice) is 6.7 MHz[53], 30 times larger than deuteron QCC (215 kHz) in solid D_2O[54], hence the NMR signals of ^{17}O water molecules are much more sensitive to their environments, i.e. the microscopic environment of the water molecules in the polymer matrix. Since the spin for ^{17}O nucleus is 5/2, the lineshape for its NMR spectrum shows a central transition and two satellites on each side of the central line. The central transition does not broaden by the first order perturbation at room temperature while it does broaden at low temperature by the second order perturbation, from which a scale of molecular motion frequency can be evaluated. In this investigation, oxygen-17 NMR measurements for NAFION containing $H_2{}^{17}O$ (15~20% ^{17}O enriched water) or $CH_3O^{17}H$ (15% ^{17}O enriched methanol) are employed to obtain information complementary to that obtained from ^2H NMR.

1-3.3. High Pressure NMR

There is no question that temperature variations are essential in NMR studies of solid electrolytes. However, high pressure studies of ionic conductivity as well as NMR studies in solids have demonstrated that pressure is a complementary thermodynamic variable to temperature in trying to understand the mechanisms of ionic conduction and ion diffusion[55,56]. Measuring NMR parameters at elevated pressure can provide a wealth of additional information[55]. Since many macroscopic properties of solid polymers are a direct result of diffusion of ions, molecular motions of polymer chains and segments, experimental and theoretical efforts to elucidate the dynamics of motion in polymeric materials are great basic and practical significance. The mechanical motions

Reproduced with permission of the copyright owner. Further reproduction prohibited without permission.

necessarily produce volume fluctuations that can be probed by changing the conjugate variable, pressure. The motional parameter K, which could be a motional correlation time τ, or thermally activated motion ω, or diffusion D, can be represented by an exponential expression[57,58]:

$$K \sim exp\ (-G/RT). \tag{1.1}$$

where G is the free energy. We may break G down into temperature and pressure derivatives near any point on the equilibrium surface, by writing

$$G = Q\text{-}ST+pV \tag{1.2}$$

with $S = -(\delta G/\delta T)_p$ and $V = (\delta G/\delta p)_T$.

In NMR measurements in the fast motion approximation, the longitudinal relaxation $1/T_1$ is proportional to τ[59], thus from equation 1.1, we then have

$$\Delta V = (\frac{\delta G}{\delta p})_T = -RT(\frac{\delta(\ln 1/T_1)}{\delta p})_T . \tag{1.3}$$

ΔV is the activation volume for a spin-lattice relaxation process. It need not be related directly to any physical volume. It may be regarded as the physical expansion of the system at the saddle-point configuration ($\alpha'' = -\Delta V/RT$)[57] or simply as the pressure dependence of the activation energy[58].

A detailed review of wide range of problems which can be successfully studied by high pressure NMR can be found at High Pressure NMR edited by Jonas et al.[60]. For high pressure NMR studies of polymers, Conradi and co-workers have studied hydrostatic pressure dependence of molecular motions in polycarbonates[58], Liu and Jonas carried out high pressure NMR study of molecular motions and glass transition in natural rubber, synthetic *cis*-1,4-polyisoprene, *cis*-1,4-polybutadience and natural rubber

Reproduced with permission of the copyright owner. Further reproduction prohibited without permission.

gum stock over a range of pressures from 1 bar to 3 kbar[61]. Greenbaum et al. reported high pressure conductivity and NMR investigation of siloxane-based polymer electrolytes[62].

In this thesis, high pressure proton, deuteron and oxygen-17 NMR measurements on NAFION were performed. The spin-lattice relaxation time (T_1) was measured as a function of pressure in the range from 1 bar to 2.5 kbar. Activation volumes were extracted from the T_1 pressure dependence.

Reproduced with permission of the copyright owner. Further reproduction prohibited without permission.

Chapter 2. NMR Background

2-1. Basic Theory of NMR

There are two approaches to explain nuclear magnetic resonance (NMR): quantum and classical treatment. The quantum treatment is characterized by the spin quantum number I and the magnetic quantum number m, while the main benefit of the classical treatment is that it gives us a vivid physical picture.

According to quantum principles, a particular nuclear spin **I** has an associated magnetic moment μ, expressed as

$$\mu = \gamma \hbar I \tag{2.1}$$

where $\hbar$ is Planck's constant h divided by 2π and γ is called the gyromagnetic ratio. This magnetic moment μ will interact with an applied magnetic field $\mathbf{H}_0$ with a simple Hamiltonian

$$\mathcal{H} = -\mu \cdot H_o \tag{2.2}$$

Taking the field along Z-direction, the energy states can be characterized by the magnetic quantum number m:

$$E_m = -\mu_z H_o = -\gamma \hbar H_o m\,, \qquad m = I, I\text{-}1, \cdots, -I \tag{2.3}$$

Figure 2.1 displays the so-called Zeeman energy levels of ^{1}H(I=1/2) and ^{2}H(I=1).

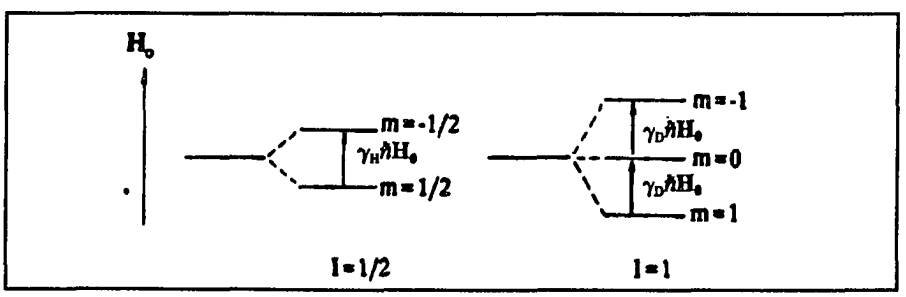

Figure 2.1: Zeeman energy levels for spin-1/2 and spin-1 cases.

Reproduced with permission of the copyright owner. Further reproduction prohibited without permission.

where γ_H and γ_D are the gyromagnetic ratios for ^1H and ^2H, respectively. The separation of two adjacent energy levels is

$$\Delta E = \gamma \hbar H_o \tag{2.4}$$

and the transition between two levels could be induced by applying a radio-frequency (rf) magnetic field $\mathbf{H}_1$ ($|\mathbf{H}_1| \ll |\mathbf{H}_o|$, $\mathbf{H}_1 = \mathbf{e}_x 2H_1 \cos 2\pi\nu t$) perpendicular to the static field $\mathbf{H}_o$. The Hamiltonian for this interaction is $\mathcal{H} = -\mu \cdot \mathbf{H}_1$, if $\mathbf{H}_1$ is so small that time-dependent perturbation theory applies, then the transition probability per unit time is given by the Golden rule:

$$P_{mm'} = \gamma^2 H_1^2 |\langle m|I_x|m'\rangle|^2 \delta(\nu_{mm'} - \nu) \tag{2.5}$$

where

$$\nu_{mm'} = \frac{\Delta E_{mm'}}{h} = \frac{\gamma H_o |m' - m|}{2\pi} \tag{2.6}$$

from Equation 2.5 and 2.6, several conclusions can be summarized:

1) the transition probability is proportional to γ^2 and H_1^2.

2) from $\langle m'|I_x|m\rangle$, only transitions where $|m'-m| = 1$ can occur.

3) $\mathbf{H}_1$ must be perpendicular to the static field $\mathbf{H}_o$ otherwise no transition occurs because the transition matrix would be $\langle m'|I_z|m\rangle = m\hbar\delta_{mm'}$.

4) from $\delta(\nu_{mm'} - \nu)$, in order to induce transitions, the rf frequency ν should be equal to $\nu_{mm'}$, or the rf angular frequency ω equals $2\pi\nu_{mm'} = \gamma H_o$, i.e., known as the condition of resonance:

$$\omega_o = \gamma H_o \tag{2.7}$$

where ω_o is called the Larmor frequency.

Reproduced with permission of the copyright owner. Further reproduction prohibited without permission.

Now consider a spin system in thermal equilibrium with the surroundings (which we will call the lattice), the ratio of the population for two states will be given by the Boltzmann relation: $N_b/N_a = \exp(-\Delta E/kT)$, where T is the temperature of the lattice. Suppose the spin system is disturbed by an rf field so that the population of the upper state increased and that of the lower state decreased. We can change the definition of T to T_s (spin temperature) to keep the Boltzmann relation correct. If the rf field increased the spin temperature T_s, then T_s will approach T by giving up thermal energy at a rate characterized by $1/T_1$. Here T_1 is the spin-lattice relaxation time and will be discussed later. The phenomenon described above is called nuclear magnetic resonance (NMR).

The classical treatment may be more suitable for visualizing pulse NMR. A macroscopic magnetization **M** is defined as

$$\boldsymbol{M} = \Sigma \boldsymbol{\mu}_i \quad , \tag{2.8}$$

the sum of all the individual magnetic moments per unit volume. The equation of motion of **M** in an external field **H** is given by

$$\frac{d\boldsymbol{M}}{dt} = \gamma \boldsymbol{M} \times \boldsymbol{H} \quad . \tag{2.9}$$

M will precess about the direction of **H** and Equation 2.9 can be easily solved in a rotating frame (x',y',z') rotating with frequency ω with respect to the laboratory frame (X,Y,Z). The transformed eqution is

$$\frac{d\boldsymbol{M}}{dt}\Big|_{rot} = \frac{d\boldsymbol{M}}{dt}\Big|_{lab} - \omega \times \boldsymbol{M} = \gamma(\boldsymbol{M} \times \boldsymbol{H}) - \omega \times \boldsymbol{M} = \gamma \boldsymbol{M} \times (\boldsymbol{H} + \frac{\omega}{\gamma}) \tag{2.10}$$

Remember that **H** consists of a static field $\mathbf{H}_0$ in the Z-direction and an rf field $\mathbf{H}_1$ in the X-direction in the form $\mathbf{H} = \mathbf{e}_z H_0 + \mathbf{e}_x 2H_1 \cos\omega t$. Taking the direction of z' to coincide

Reproduced with permission of the copyright owner. Further reproduction prohibited without permission.

with Z direction, and decomposing $\mathbf{H}_1 = (2H_1\cos\omega t, 0)$ into two counter-rotating vectors $\mathbf{H}_L+\mathbf{H}_R = (H_1\cos\omega t, -H_1\sin\omega t)+(H_1\cos\omega t, H_1\sin\omega t)$, then in the rotating frame, one component ($\mathbf{H}_L$) is static with amplitude of H_1 while the other is rotating at 2ω which can be ignored. Equation 10 becomes

$$\frac{dM}{dt}|_{rot} = \gamma M \times [(H_o + \frac{\omega}{\gamma})e_{z'} + H_1 e_{x'}] = M \times \gamma H_{eff} \qquad (2.11)$$

When $\omega = -\gamma H_o$, then $\mathbf{H}_{eff} = H_1 e_{x'}$, a static field aligned on x'-axis. **M** will precess about the x'-axis with frequency γH_1. This makes the **M** tip in longitudinal direction. The tipping angle θ of **M** is given by

$$\theta = \gamma H_1 t_p \qquad (2.12)$$

where t_p is the duration of H_1. Making t_p such a 90° pulse so that $\theta = 90°$, as illustrated in Figure 2.2, the **M** will align on the x'-y' plane and precess about Z-axis with Larmor frequency ω_o in the laboratory frame. If the spin system was placed into an rf-coil, then a voltage will be induced in the coil.

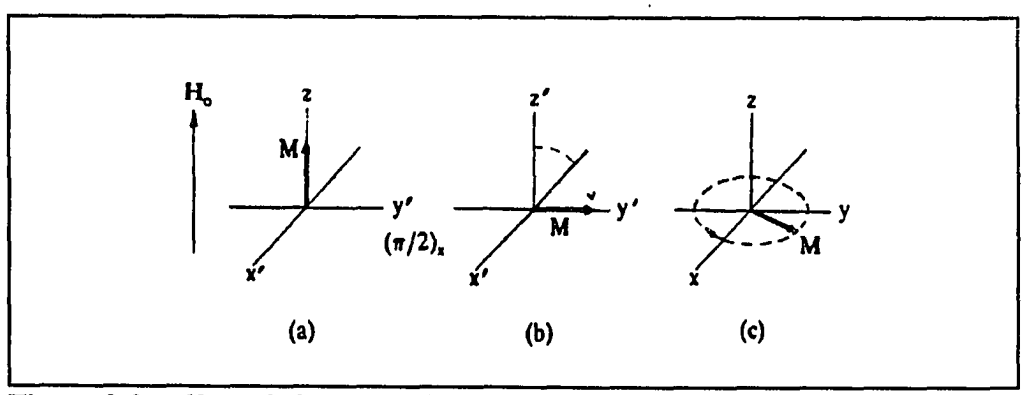

Figure 2.2: Effect of rf pulse, a) initially, **M** is aligned along $\mathbf{H}_o$; b) at the end of 90° pulse applied on x'-axis, **M** lies in y'-axis; c) after pulse, **M** precesses in X-Y plane at Larmor frequency.

Reproduced with permission of the copyright owner. Further reproduction prohibited without permission.

This induced voltage is a measure of the magnetization in the horizontal plane after the rf pulse and will decay due to spin-spin interaction and inhomogeneity of the static field $\mathbf{H}_0$. We call it the free induction decay (FID) since the spins are precessing freely without the rf field. The FID can be Fourier transformed from time domain f(t) to frequency domain spectrum $F(\omega)$ to obtain the absorption spectrum[63].

2-2. Interactions in a Solid State System and Their Effects on Spectra

The interactions in a spin system can be studied by NMR. For instance, the main terms of interactions for a solid state system can be written in a total Hamiltonian $\mathcal{H}$

$$\mathcal{H} = \mathcal{H}_Z + \mathcal{H}_Q + \mathcal{H}_D + \mathcal{H}_{CS} \tag{2.13}$$

where $\mathcal{H}_Z$ is the Zeeman term; $\mathcal{H}_Q$ is nuclear electrical quadrupole interaction term; $\mathcal{H}_D$ is nuclear magnetic dipole-dipole coupling and $\mathcal{H}_{CS}$, chemical-shift. We now evaluate the order of magnitude of these terms for the case of deuterium NMR, on which this thesis is heavily focused. The strength of the interaction can be expressed as a frequency because of the relation $E = \hbar\omega$. Here $\mathcal{H}_Z$ is 47 MHz corresponding to a 7 tesla magnetic field; $\mathcal{H}_Q$ is approximately 220 kHz; $\mathcal{H}_D$ is about 5 kHz and $\mathcal{H}_{CS}$ is around 0.5 kHz[44]. Therefore, deuterium solid-state NMR spectra are dominated completely by the quadrupole interaction while the chemical-shift is negligible. Both $\mathcal{H}_D$ and $\mathcal{H}_Q$ can cause perturbations on the Zeeman splitting. First, we describe quadrupole effects in NMR.

A Nucleus with spin 1 or greater possesses electric quadrupole moment due to its non-spherical charge distribution. This quadrupole moment will interact with the electric field gradient (EFG) where the nucleus resides and may have a very strong effect on NMR spectrum. The Hamiltonian of quadrupole interaction is given as[64]:

Reproduced with permission of the copyright owner. Further reproduction prohibited without permission.

$$\mathcal{H}_Q = \frac{eQ}{6I(2I-1)} \sum_{ij} V_{ij} \left[\frac{3}{2}(I_i I_j + I_j I_i) - \delta_{ij} I^2 \right] \tag{2.14}$$

where eQ is the quadrupole moment of the nucleus. V_{ij} are the components of the EFG tensor, which reflects the electronic charge distribution, therefore, the chemical bonds. If we choose a coordinate system, the so-called principal axis system of EFG tensor, so that the V_{ij} is diagonal and $|V_{zz}| \geq |V_{yy}| \geq |V_{xx}|$, $\mathcal{H}_Q$ is reduced to a simpler form:

$$\mathcal{H}_Q = \frac{e^2 qQ}{4I(2I-1)} \left[3I_z^2 - I^2 + \eta (I_x^2 - I_y^2) \right] \tag{2.15}$$

where $eq = V_{zz}$, η is called asymmetry parameter defined as

$$\eta = \frac{V_{xx} - V_{yy}}{V_{zz}} \tag{2.16}$$

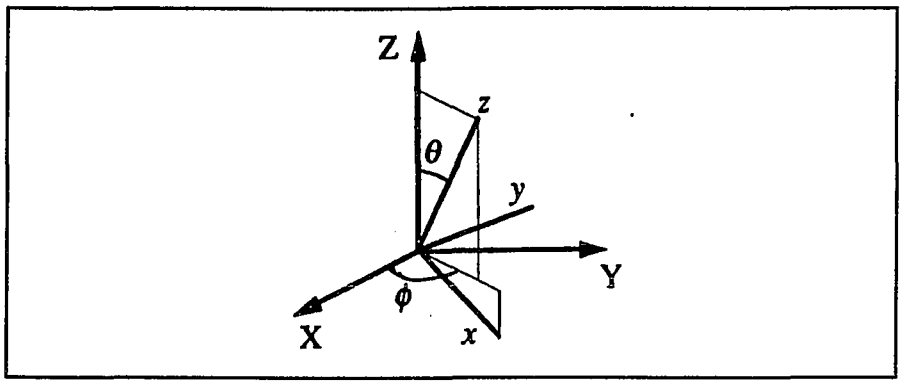

Figure 2.3: The orientation of the principal axis frame of the EFG (x,y,z) relative to laboratory frame (X,Y,Z). The V_{zz} is aligned on z-axis.

The relationship between the EFG principal axis system (x,y,z) and the laboratory frame (X,Y,Z) is shown in Figure 2.3, then for an axially symmetric EFG (η=0) case, Equation 2.15 in the laboratory frame will be:

Reproduced with permission of the copyright owner. Further reproduction prohibited without permission.

$$\mathcal{H}_Q = \frac{e^2qQ}{4I(2I-1)}\left[3I_Z^2\cos^2\theta + 3I_X^2\sin^2\theta + 3(I_ZI_X + I_XI_Z)\sin\theta\cos\theta - I^2\right] \quad (2.17)$$

Treating $\mathcal{H}_Q$ as a perturbation of the Zeeman levels, the first order perturbation energy shift will be

$$E_m = \frac{e^2qQ}{8I(2I-1)}(3\cos^2\theta - 1)\left[3m^2 - I(I+1)\right] \quad . \quad (2.18)$$

As an example, the effect of the quadrupole interaction for deuterium ($I=1, \eta \approx 0$) is shown in Figure 2.4.

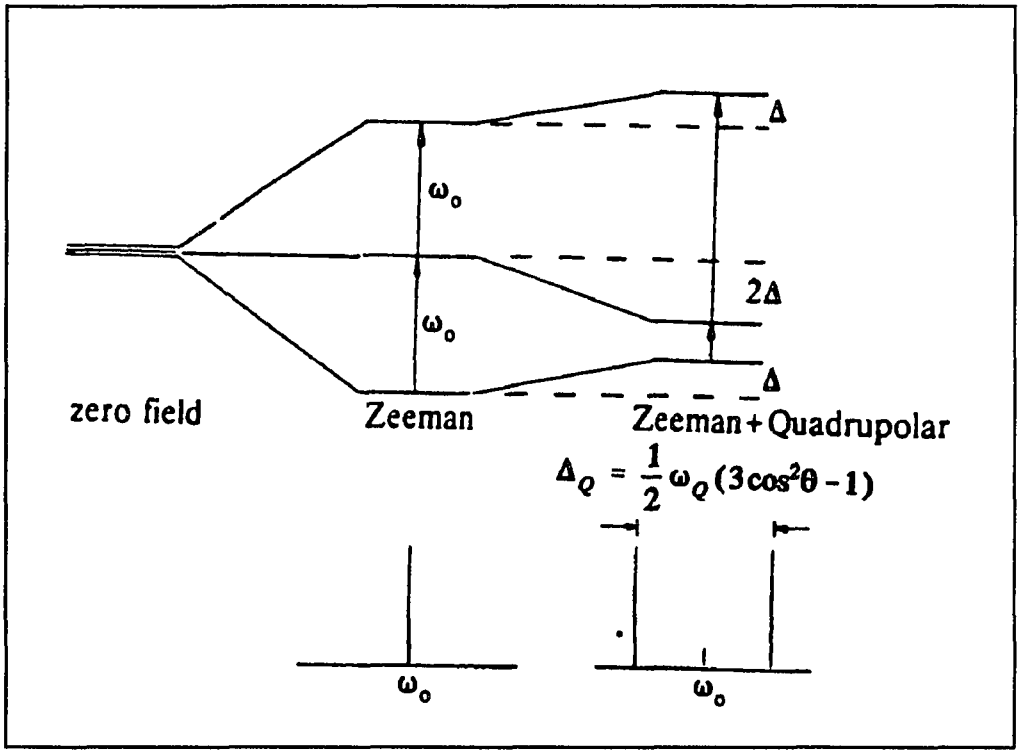

Figure 2.4: The energy levels and spectra for a nucleus of spin I = 1 subject to a quadrupolar interaction.

Conventionally, we define the quadrupole coupling constant (QCC) = $e^2qQ/\hbar$, a measure of how strong the interaction is between the quadrupole moment and the EFG; and it is

Reproduced with permission of the copyright owner. Further reproduction prohibited without permission.

usual to define a quadrupole frequency $\omega_Q = 3e^2qQ/2I(2I-1)\hbar$. Hence, in Figure 4, $\Delta = (1/12)\omega_Q(3\cos^2\theta-1)$, and the quadrupole splitting Δ_Q is, in frequency units,

$$\Delta_Q = \frac{1}{2}\omega_Q(3\cos^2\theta - 1) \quad . \tag{2.19}$$

In the case of asymmetric field ($\eta \neq 0$), the energy shift E_m has the form[59]

$$E_m = \frac{e^2qQ}{8I(2I-1)}(3\cos^2\theta - 1 + \eta\sin^2\theta\cos 2\phi)\left[3m^2 - I(I+1)\right] \quad . \tag{2.20}$$

and the quadrupole splitting will be

$$\Delta_Q = \frac{1}{2}\omega_Q[(3\cos^2\theta-1)+\eta\sin^2\theta\cos 2\phi] \tag{2.21}$$

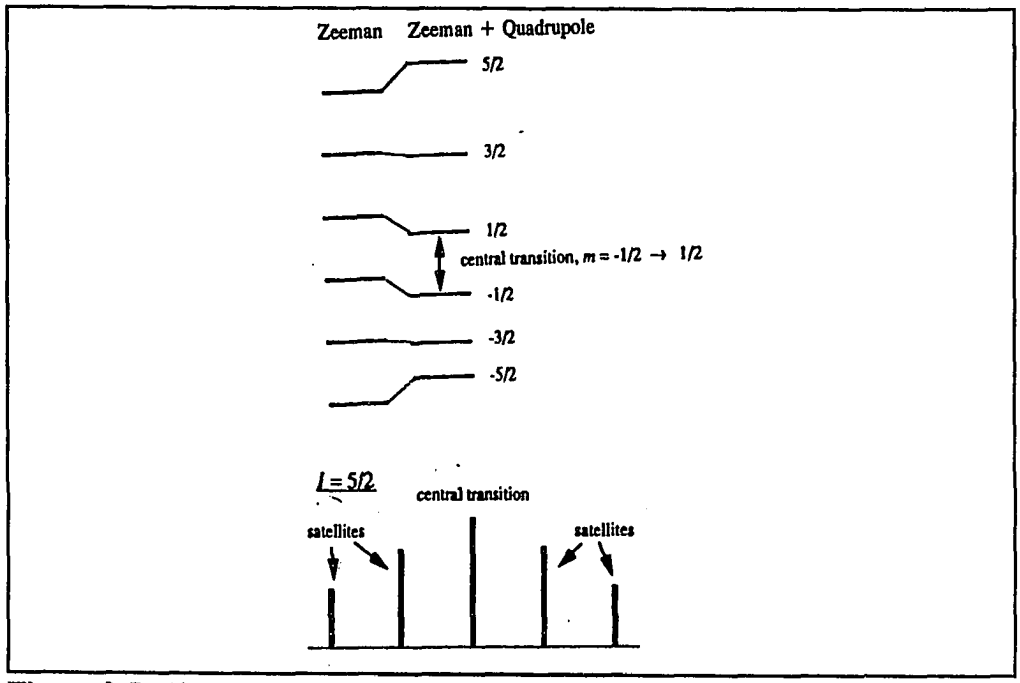

Figure 2.5: The energy levels (top) and spectra (bottom) for spin I = 5/2 nucleus subject to a quadrupole interaction.

Reproduced with permission of the copyright owner. Further reproduction prohibited without permission.

Another example is oxygen-17 (I=5/2). Figure 2.5 shows the spin 5/2 energy levels and the corresponding spectra. It could be seen that there are 2I = 5 lines, the central transition -1/2 ⇔ 1/2 is not shifted in first order by checking Equation 18 or 20, the transitions on either side of the central one are called satellite lines and are equally separated by the quadrupole splitting Δ_Q.

It is interesting to point out that the dipole-dipole coupling for two like spins has an equivalent form to the quadrupole interaction: $\mathcal{H}_{D/Q} = a_{D/Q}\hbar I_z^2(3\cos^2\theta-1)$. The anisotropic orientation factor $(3\cos^2\theta-1)$ is common to both $\mathcal{H}_D$ and $\mathcal{H}_Q$. This causes an inhomogeneous broadening of the spectra. For example: in a rigid D_2O water molecule, we assume that V_{zz} is along the O-D bond for each deuteron, an average V_{zz} axis lies along the bisector of the two O-D bonds, thus the splitting depends on the molecule's orientation. In the liquid state, the angular factor will be averaged to zero by rapid isotropic motion of the molecules, thus no splitting is observed. In solid samples, for example, a solid powder sample, the orientation effect contributed by nuclei from all the isotropically distributed microcrystallites results in a special lineshape, the so called Pake's pattern. For a sample that is partially ordered, the splitting could be seen but the separation may be reduced due to averaging by molecular motion. If this motion is anisotropic then there will be a residual orientation present. So, the orientation-dependent information could be used to determine the orientation of a specific functional group in a solid sample as well as the degree of motion of molecules. Figure 2.6 shows the theoretical deuteron spectra for several different cases.

Reproduced with permission of the copyright owner. Further reproduction prohibited without permission.

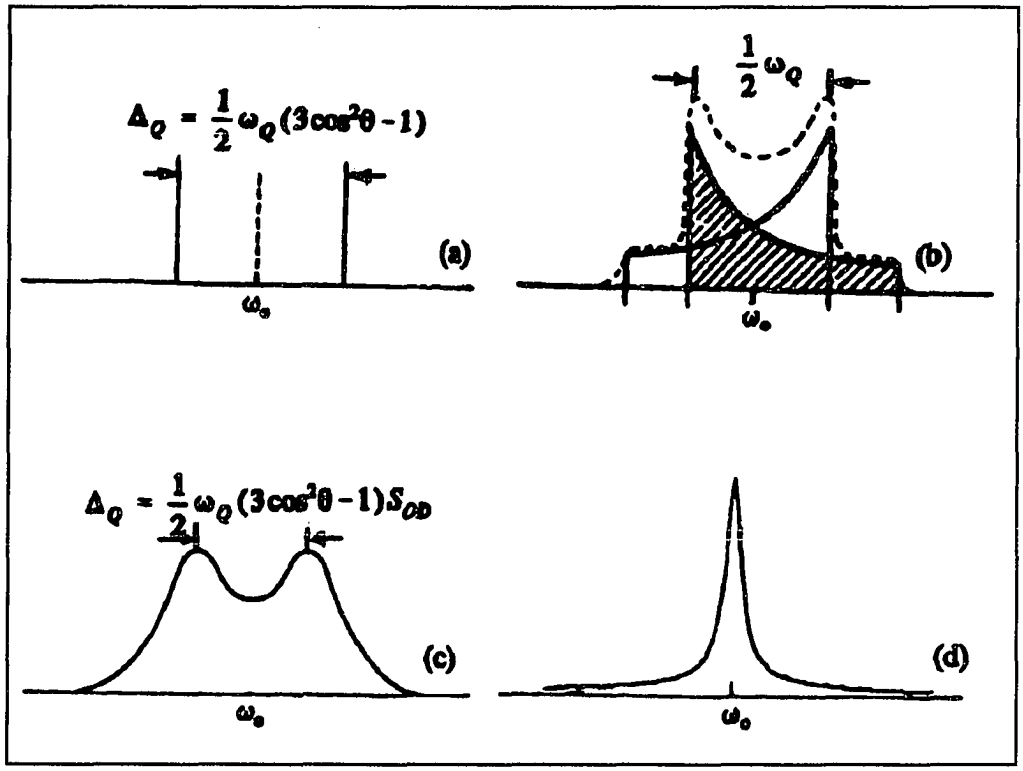

Figure 2.6: Effect of quadrupole interaction: (a) an isolated deuteron, (b) Pake's pattern, (c) Many deuterons undergoing partially oriented motions, (d) Motional narrowing.

To describe the degree of molecular orientation, an order parameter S_{OD} ($0 \leq S_{OD} \leq 1$) is introduced, then the splitting Δ_Q will be

$$\Delta_Q = \frac{1}{2}\omega_Q(3\cos^2\theta - 1)S_{OD} \quad . \tag{2.22}$$

2-3. Relaxation

As mentioned before, after being disturbed by an rf field, the raised spin temperature of a spin system T_s will recover to equilibrium temperature T by giving up energy to the lattice, i.e., making a transition from an upper level state to a lower level state. The process by which the spins in an upper state return nonradiatively to a lower

Reproduced with permission of the copyright owner. Further reproduction prohibited without permission.

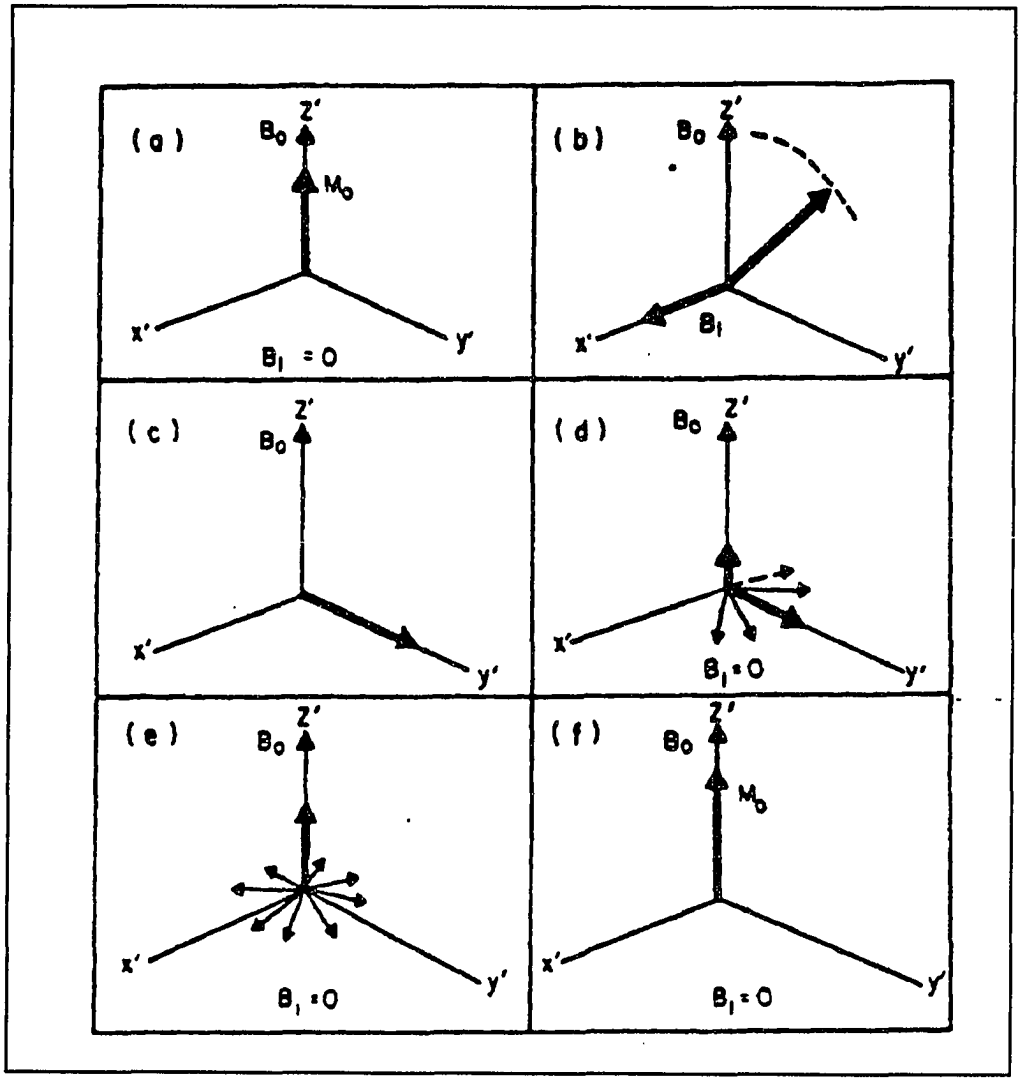

Figure 2.7: Rotating frame digrams describing relaxations: (a) The net $\mathbf{M}_0$ is aligned with $\mathbf{B}_0$ ($\mathbf{H}_0$); (b) & (c) A 90° rf field $\mathbf{B}_1$ ($\mathbf{H}_1$) tips $\mathbf{M}_0$ to y'-axis; (d) & (e) The spins begin to relax in the x'-y' plane by spin-spin (T_2) process and in z' direction by spin-lattice (T_1) process; (f) the equilibrium $\mathbf{M}_0$ is reestablished along $\mathbf{B}_0$.

state is called relaxation. The spin-lattice relaxation is often termed longitudinal relaxation because it involves changes of energy and therefore involves the components of the nuclear moments along the direction of the applied magnetic field. The spin-lattice relaxation time T_1 is a measure of the rate of transfer of energy from spins to lattice. The spin-spin relaxation is termed transverse relaxation because it is a process in which the

Reproduced with permission of the copyright owner. Further reproduction prohibited without permission.

magnetization in X-Y plane decays due to dephasing, e.g., precessing at unequal rates, as a result of the energy coupling within the spin system. Figure 2.7 exhibits the processes of both spin-lattice and spin-spin relaxation. In order to undergo a transition, the nucleus needs to see fields fluctuating at its Larmor frequency. In our work, there are two randomly fluctuating fields effective in NMR relaxation. One is a time varying magnetic field which can interact with the nuclear magnetic dipole moments and the other is a fluctuating EFG which can interact with the quadrupole moment of the nucleus. Each one gives rise to a specific spin-lattice relaxation mechanism. Since the spin-lattice relaxation processes usually depend on the existence of molecular motion to generate a randomly fluctuating magnetic field or EFG, we can get valuable information about these motions from the T_1 measurements. At NMR time-scales, normally the motions of the molecule in a solid sample that are most effective in NMR relaxation are hindered rotations and translations, since small amplitude vibrations are not as effective because their frequency is usually much higher than the Larmor frequency[65]. A random motion can have associated with it a special form of an autocorrelation function G(t), expressed in terms of a scalar product of the local field **h**(t) and the same local field at an earlier time **h**(o), which is a measure of how rapidly the local field changes in magnitude and direction. To a good approximation, the autocorrelation function

$$G(t) \propto \boldsymbol{h}(t)\cdot\boldsymbol{h}(0) \propto \exp(-t/\tau_c) \qquad (2.23)$$

is exponential and is independent of the time origin, where τ_c is called the correlation time for the motion and is a measure of the time between the field fluctuations or the average time between molecular collisions. The spectral density $J(\omega)$ is the frequency spectrum corresponding to the autocorrelation function G(t). i.e., it is its Fourier

Reproduced with permission of the copyright owner. Further reproduction prohibited without permission.

transform:

$$J(\omega) = \int_{-\infty}^{\infty} G(t)\exp(-i\omega t)dt = G(0)\frac{2\tau_c}{1+\omega^2\tau_c^2} \qquad (2.24)$$

The relationship between T_1 and T_2 and $J(\omega)$ can be derived through time dependent perturbation theory as was done originally by Bloembergen, Purcell, and Pound (BPP). Here we list the results in the case for a model of random molecular rotation from reference[59].

For spin $\bar{1} = 1$, the relaxation rate $1/T_{1Q}$ contributed by quadrupole interaction with fluctuating EFG is

$$\frac{1}{T_{1Q}} = \frac{3}{40}\left(1+\frac{\eta^2}{3}\right)\left(\frac{e^2qQ}{\hbar}\right)^2\left[\frac{\tau_c}{1+\omega^2\tau_c^2} + \frac{4\tau_c}{1+4\omega^2\tau_c^2}\right] \qquad (2.25)$$

In the extreme narrowing case, $\omega\tau_c \ll 1$, Equation 2.25 becomes

$$\frac{1}{T_{1Q}} = \frac{3}{8}\left(1+\frac{\eta^2}{3}\right)\left(\frac{e^2qQ}{\hbar}\right)^2\tau_c \qquad (2.26)$$

The relaxation rate $1/T_{1D}$ contributed by dipole interaction with the fluctuating local field is

$$\frac{1}{T_{1D}} = \frac{2}{5}\frac{\gamma_D^4\hbar^2}{r^6}I(I+1)\left[\frac{\tau_c}{1+\omega^2\tau_c^2} + \frac{4\tau_c}{1+4\omega^2\tau_c^2}\right] \qquad (2.27)$$

The total relaxation rate for deuteron pair in D_2O is approximately written as

Reproduced with permission of the copyright owner. Further reproduction prohibited without permission.

$$\frac{1}{T_1}(^2H) = \frac{1}{T_{1Q}} + \frac{1}{T_{1D}} \tag{2.28}$$

Since our work concentrates on T_1 as opposed to T_2 measurements, the form of spin-spin relaxation rate is not presented here and it can be found in reference [59]. The relation for T_1 vs. correlation time τ_c at a fixed frequency is plotted in Figure 2.8. The curve shows a minimum value of T_1 at $\omega\tau_c \approx 1$, this means that the frequency of molecular motion is comparable with Larmor frequency at that temperature so that the relaxation is most efficient and leads to the minimum of T_1.

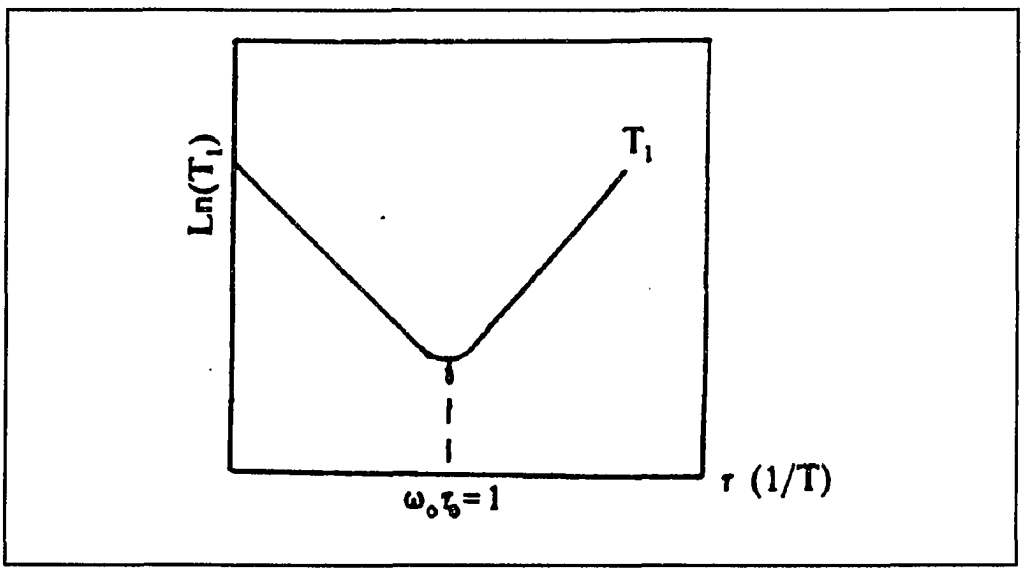

Figure 2.8: Spin-lattice relaxation time (T_1) as a function of correlation time (τ_c) or reciprocal of temperature (1/T).

In the higher temperature region (left side of T_1 minimum), the frequency of molecular motion is too fast to relax efficiently at the Larmor frequency and results in a longer T_1. On the right side of T_1 minimum, as the temperature decreases, the molecules move slower and slower than the Larmor frequency, the contribution to relaxation is also small and results in an increase in T_1.

Reproduced with permission of the copyright owner. Further reproduction prohibited without permission.

2-4. Pulse NMR and Pulse Sequences

In our work, a single pulse, an inversion recovery sequence, and a quadrupole echo sequence are usually employed. A single pulse is used to acquire the FID, (recall Figure 2.2, in which the FID signal is acquired after a 90° pulse), and Fourier transformation then yields the NMR absorption spectrum. The inversion recovery sequence is used to measure T_1. It consists of a $180°_x$ pulse followed by a $90°_x$ pulse separated by time τ. The equilibrium magnetization M_0 is inverted by the first pulse then relaxes back towards Z-axis during the interval time τ and finally tips to x'-y' plane by the second pulse, which samples the magnetization recovery after time τ. Specifically, the magnetization after waiting a time τ is given by

$$M(\tau) = M_0(1-2e^{-\tau/T_1}) \quad . \tag{2.29}$$

By varying the value of τ, we can get a set of $M(\tau)$ data which can be fitted to the above equation to obtain T_1. A classical picture of inversion recovery is illustrated in Figure 9.

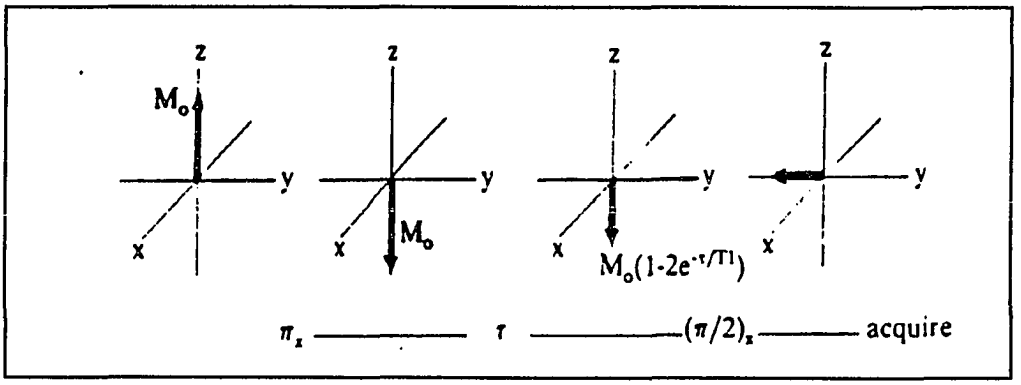

Figure 2.9: The inversion recovery sequence method for T_1 measurements.

The quadrupole echo sequence, or solid echo sequence, is used when the signal decays very rapidly because of quadrupole broadening, for instance, at low temperature. In that case, the time for decay is too short so that lineshape investigations in solids are limited

Reproduced with permission of the copyright owner. Further reproduction prohibited without permission.

by the "deadtime" of the spectrometer. This sequence enables us to get a refocused signal. It contains a $90°_x$ pulse followed by a $90°_y$ pulse separated by τ and the acquisition of signal starts at $t = 2\tau$. Unfortunately, there is no classical picture to describe this process. However, we can use quantum density matrix methods to calculate a 2τ echo. Here, we present the case of a 2τ echo for deuteron ($I = 1$) following the method given by references [59,66,67].

For the complex amplitude of the free induction decay (FID) following the second rf pulse, we can write

$$S(t) = Tr[\rho(t)I_+] \quad , \tag{2.30}$$

where $\rho(t)$ is the density matrix and I_+ is the raising operator.

For quadrupole perturbation, $\mathcal{H}_Q = a\hbar I_z^2$+constant.

The time evolution of the density matrix is given by Liouville-Von Neumann equation

$$\frac{d\rho(t)}{dt} = \frac{1}{i\hbar}[\mathcal{H}(t),\rho(t)] \quad , \tag{2.31}$$

Since $\mathcal{H}(t) = \mathcal{H}_Q$ is not explicitly dependent on time, the solution of the above equation is

$$\rho(t) = e^{-iaI_z^2 t}\rho(0)e^{iaI_z^2 t} \quad , \tag{2.32}$$

at $t = \tau$, immediately after the second β degree pulse with shift ϕ degree around z'-axis with respect to the first pulse,

$$\rho'(\tau) = R_1^{-1}e^{-iaI_z^2\tau}\rho(0)e^{iaI_z^2\tau}R_1 \quad , \tag{2.33}$$

where R_1 is the rotation operator,

Reproduced with permission of the copyright owner. Further reproduction prohibited without permission.

$$R_1 = e^{i\phi I_z} R e^{-i\phi I_z}, \qquad R = e^{-i\beta I_y} \quad , \tag{2.34}$$

for t > τ, at t - τ, the density matrix becomes

$$\rho(t-\tau) = e^{-iaI_z^2(t-\tau)} R_1^{-1} e^{-iaI_z^2\tau} \rho(0) e^{iaI_z^2\tau} R_1 e^{iaI_z^2(t-\tau)} \quad , \tag{2.35}$$

the FID in Equation 2.30 becomes

$$\begin{aligned} S(t) &= \sum_{m=-I}^{I-1} \langle m|\rho(t-\tau)I_+|m\rangle \\ &= \sum_{m,m',m''}^{I-1} \langle m|R^{-1}|m''\rangle\langle m'|R|m+1\rangle\langle m''|\rho(0)|m'\rangle F(m) e^{i\phi(m'-m''-1)} e^{ia[(2m+1)(t-\tau)-(m''^2-m'^2)\tau]} , \end{aligned} \tag{2.36}$$

where F(m) = [I(I+1)-m(m+1)]$^{1/2}$, which comes from $I_+|I,m\rangle = F(m)\hbar|I,m+1\rangle$. Equation 2.36 satisfies every value of the spin I because it is a result of quadrupole perturbation $\mathcal{H} = a\hbar I_z^2$+constant in general cases.

For half-integer spin I, when 2m+1 = 0 and m"^{2}-m'^{2} = 0, the signal is independent of time, which corresponds to a central transition.

For spin I = 1, such as deuteron, no central transition exists.

Now, if for particular values of t, S(t) is independent of a, signals of all the nuclei are "in phase" and we get an echo. From Equation 2.36 we see that this happens for t > τ

$$\frac{t-\tau}{\tau} = \frac{m''^2 - m^2}{2m+1} = k \quad . \tag{2.37}$$

For spin = 1, a 2τ echo occurs when k = 1, we have such combinations in the summation: (m = 0, m" = $\pm$1, m' = 0),

(m =-1, m" = 0, m' = $\pm$1),

the case of m = 1 is excluded because F(1) = 0.

Reproduced with permission of the copyright owner. Further reproduction prohibited without permission.

The matrix elements containing the rotation operator are Wigner coefficients $d^{\mu}_{m'm}(\beta)$. For spin = 1, $<m'|R|m> = d^{1}_{m'm}(\beta)$, and has the property[68]:

$$d^{1}_{m'm}(-\beta) = d^{1}_{mm'}(\beta).$$

$d^{1}_{m'm}(\beta)$ for every possible m' and m can be written as

m' \ m	+1	0	-1
+1	$(1+\cos\beta)/2$	$(1/2)^{1/2}\sin\beta$	$(1-\cos\beta)/2$
0	$-(1/2)^{1/2}\sin\beta$	$\cos\beta$	$(1/2)^{1/2}\sin\beta$
-1	$(1-\cos\beta)/2$	$-(1/2)^{1/2}\sin\beta$	$(1+\cos\beta)/2$

Now let us check the $\rho(0)$;

before the first pulse, the system is in equilibrium and the density matrix has the form

$$\rho_{eq} \propto \exp(-\gamma\hbar H_o I_z/kT),$$

at high T approximation, $\rho_{eq} \propto 1-\gamma\hbar H_o I_z/kT \propto I_z$.

After the first $90°_y$ pulse, in the approximation $\gamma H_1 \gg a$, the initial density matrix is proportional to I_x.

Thus $<m''|\rho(0)|m'> \propto <m''|I_x|m'> \propto 1/2[<m''|I_+|m'> + <m''|I_-|m'>]$, a non-zero factor occurs at $|m''-m'| = \pm 1$.

Substituting all the possible elements in Equation 2.36, finally we get

$$S(t) = \sin^2\beta \cos[a(t-2\tau)](1-e^{-i2\phi}) \quad . \qquad (2.38)$$

From the above equation, we can see the maximum S(t) occurs at $t = 2\tau$ and the second pulse $\beta=90°$ and the shift $\phi = 90°$. This is in good agreement with experiment.

Reproduced with permission of the copyright owner. Further reproduction prohibited without permission.

Chapter 3. Experiment

3-1. Sample Preparation

3-1.1. Pretreatment of Samples

Samples of NAFION-117 were obtained from E.I.du Pont Co. and pretreated by boiling in dilute aqueous H_2SO_4 (20:1) solution for 1 hour, rinsing in distilled water, and storing in distilled water[40]. Some early NMR results were obtained from a non-pretreatment sample, the NMR data obtained from the acid-treated and non-acid-treated samples have been examined the difference listed in Chapter 4, no significant difference was observed between acid-treated and non-acid-treated samples.

3-1.2. The Choice of Reference State of Dry Samples

The amount of water present in the polymer is a very important parameter. Since the water incorporated in the NAFION will be retained after hydration, a dry reference state of sample should be addressed. Different authors used their own methods to dry samples in early studies, in which NAFION membrane was usually placed in vacuo at various high temperatures for several days. Bunce et al.[69] stated that the absolute water contents in those various arbitrary "standard states" are unknown, they therefore suggested a fixed choice of a reference state, in which the NAFION-H was dried in vacuo to constant weight at room temperature instead of various high temperature. Constant weight was achieved in 10 h for $\sim 10^{-5}$ torr or 340 h for ~ 1 torr. Rehydration from the reference state was relatively slow, and samples could be handled at ambient conditions. However, there is an alternative reference state[40]; Zawodzinski et al. dried

Reproduced with permission of the copyright owner. Further reproduction prohibited without permission.

the membrane sample by suspending it over P_2O_5 in a sealed jar for several days. The former leads to a water content of $\lambda = 1$ (λ = the number of water molecules per sulfonate), while the latter results in a "near zero" water content ($\lambda < 1$), which is equivalent to those obtained via the 105 ^{0}C under vacuum treatment. For the acid form polymer, the room temperature drying method is preferred since exposure of polymer samples to elevated temperature generally leads to some charring of the polymer, with unknown effects on, for example, the ion-exchange capacity of the polymer. In this thesis, both of these methods were used. Sample were removed from the storage jar, dried by absorbent paper, then put in a vacuo (about 10^{-3} torr) at room temperature for 2 days to reach the reference state, alternately, samples were suspended above the P_2O_5 in a glass desiccator for at least one day. In any case the maximum residual water content, corresponding to $\lambda = 1$, is less than 2% by weight. The effect of this residual water in determination of the percentage uptake of water in the treated samples is negligible.

3-1.3. Samples for NMR Measurements

The membranes were cut into 5 by 15 mm rectangular pieces, the direction of cut was chosen so that the angle between alignments on the as-received sample and external magnetic field can vary from 0° to 360°. The samples were then assembled into a stack and loaded into open-ended 7.5 mm outer diameter pyrex tubes, each tube contains about 25 layers membranes, 0.7 gram in total weight . After the samples were dehydrated to reference state, they were treated in D_2O or 20% ^{17}O enriched H_2O vapor (or other solvent such as CH_3OD, ^{17}O enriched CH_3OH) in a sealed bottle for several days, with

Reproduced with permission of the copyright owner. Further reproduction prohibited without permission.

various water content of the NAFION achieved by adjusting the relative humidity in the bottle through suitable choices of saturated salt solutions. Stretched NAFION samples were also prepared by gradually (over a period of several minutes) increasing the tension of a film clamped at both ends, to a maximum elongation of about 20%, and maintaining this position for 2 days. The tension was then increased until an additional 15% elongation was achieved, and the sample was clamped in this position for 4 days. The films were then released and were found to relax to about 118% of the original length after 2 days, maintaining this length for about 1 week before further contraction was observed. The stretched film was then treated in the same manner as the unstretched samples. The direction of stretching is along the alignment showing on the as-received membranes, this is a attempt to enlarge the orientation effect, which originally exists in the polymer. The orientation of the stacked films with respect to the external magnetic field is shown in Figure 3.1.

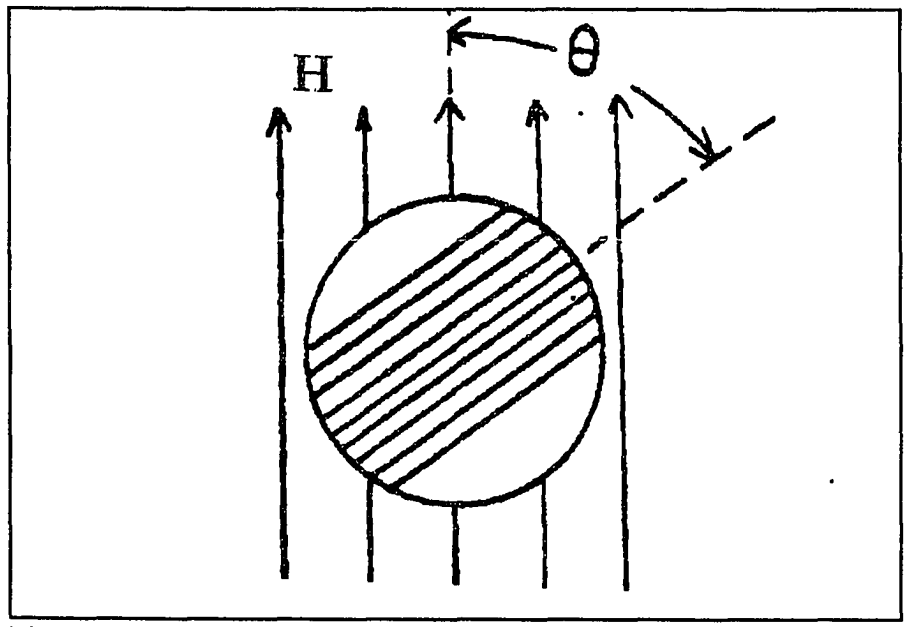

Figure 3.1: Orientation of film stack in magnetic field **H**. For stretched films, the dotted line corresponds to the elongation axis.

Reproduced with permission of the copyright owner. Further reproduction prohibited without permission.

3-1.4. Water Content Control

Since we control the water content by exposing the samples to water vapor, the relative humidity (RH) generated by different saturated salt solutions should be addressed. Table 3.1 lists the relative humidities of various saturated salt solutions at 25 °C.

Table 3.1: Solutions for maintaining constant humidity at 25 °C

Saturated salt solution	Relative humidity (%RH)
Heavy water [D_2O]	100
Sodium chloride [NaCl]	75
Potassium nitrite [KNO_2]	45

Various water contents can be achieved by placing the dry sample in a sealed bottle containing appropriate relative humidity above the salt solutions. Different water content can be determined by the absolute water weight relative to the dry membrane weight (reference state).

Table 3.2: D_2O uptake in NAFION-117 at room temperature

Relative humidity (%)	Water content (wt%)	n (water molecules/sulfonate)
100	16~18	8.8~9.9
75	8~10	4.4~5.5
45	3~4	1.7~2.2

Reproduced with permission of the copyright owner. Further reproduction prohibited without permission.

A microbalance with 10^{-5} gram accuracy is used for measuring weight changes. Also we can convert the water weight percentage to the number of water molecules per sulfonate. An example for the amounts of D_2O gained by NAFION-117 at different RH is presented in Table 3.2.

3-2. NMR Experiment

3-2.1. NMR Facilities

All the measurements were performed on a Novex broad line NMR spectrometer interfaced to a microcomputer and a LeCroy 9400 digital oscilloscope with built in Fourier transform function. The power amplifier of the spectrometer has a maximum output of 1 kilowatt in the frequency range from 10 to 100 MHz. A cryomagnet system with field strength 7.2 tesla superconducting magnet produces the static field. The linewidth broadening of liquid sample due to the field inhomogeneity is about 40 Hz for bulk D_2O in 8 mm tube. Referring to the linewidth of spectra in NAFION sample, this inhomogeneity broadening is negligible. Both single pulse and quadrupole echo sequences are employed, the latter primarily for measurements of broad spectra at low temperature. Variable temperature control ($\pm$2K) is achieved by regulating the flow rate of N_2 through a copper heat exchanger immersed in liquid N_2. The variable temperature range of this study is from room temperature down to 110 K. In addition to 7.2 tesla, a 4.5 tesla static magnetic field is also utilized. The Larmor frequency is 47 MHz for deuteron and 42 MHz for oxygen-17 at 7.2 tesla, 29 MHz for deuteron and 26 MHz for oxygen-17 at 4.5 tesla, respectively. In addition, a Varian electromagnet was utilized for ^1H measurements at 42 MHz. A block diagram of the spectrometer and accessories is shown in Figure 3.2.

Reproduced with permission of the copyright owner. Further reproduction prohibited without permission.

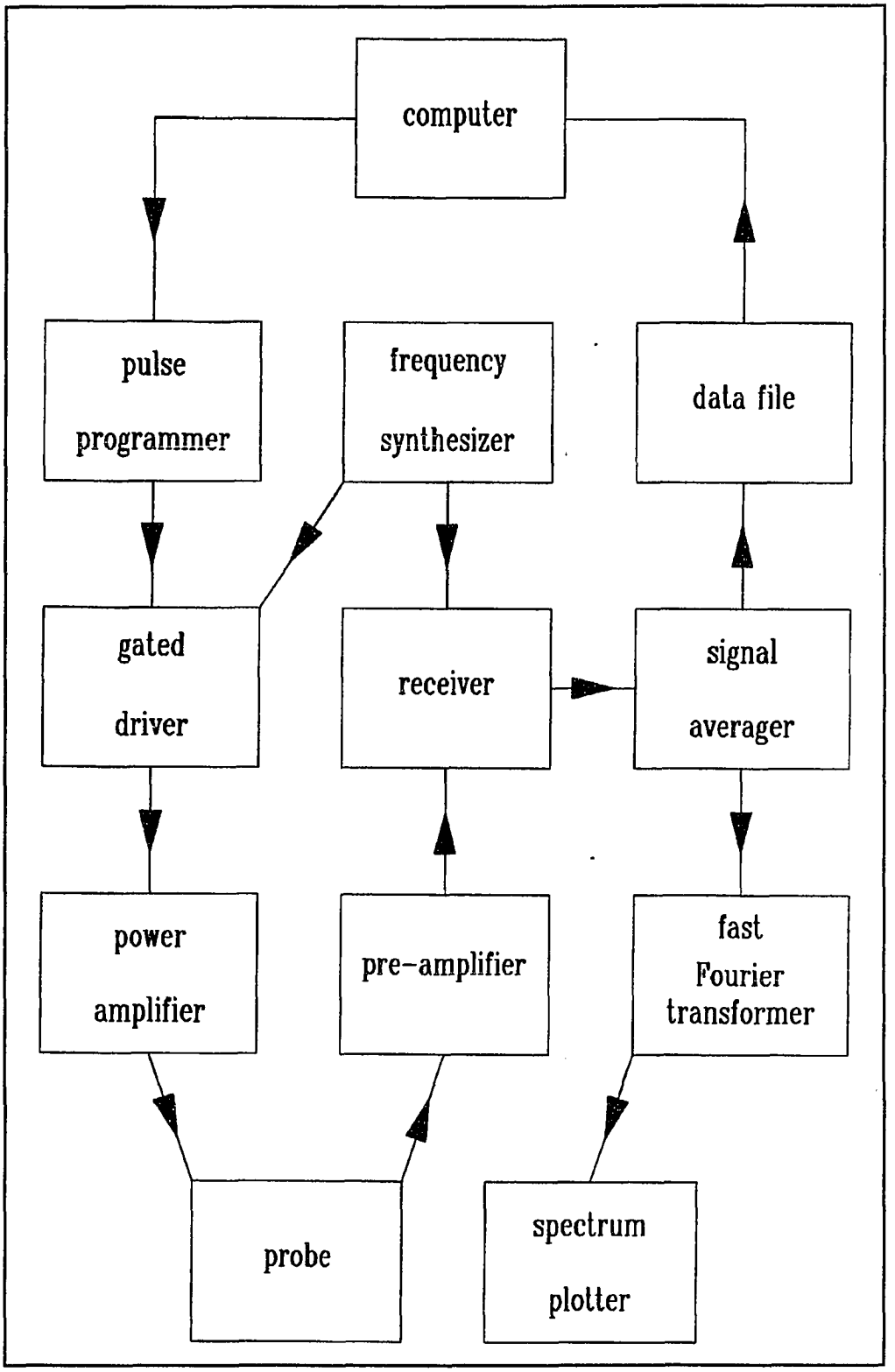

Figure 3.2: Block diagram of Novex NMR spectrometer and its accessaries.

Reproduced with permission of the copyright owner. Further reproduction prohibited without permission.

The matching network for transmitter and receiver in the probe is shown in Figure 3.3. It consists of a matching capacitor C_1, a tuning capacitor C_2, and a solenoid rf-coil. Both C_1 and C_2 are high-voltage (2000 V) variable capacitance (0.8-10 pf) capacitors obtained from Polyflon company. The home made coil has 0.5 μH and its quality factor is 250.

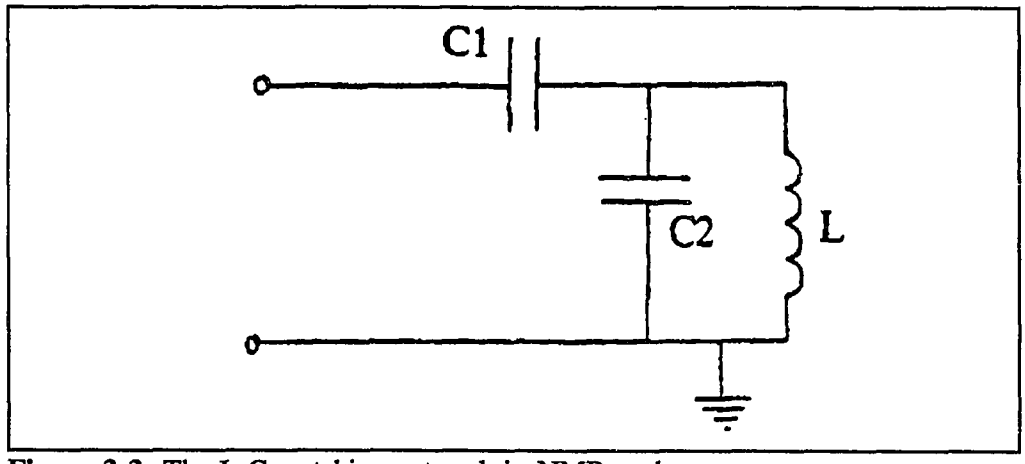

Figure 3.3: The L-C matching network in NMR probe.

3-2.2. High Pressure Apparatus

A home-built NMR probe was adapted for use at pressures up to 2.5 kbar. Typical dimensions of the solenoidal rf-coil were 7 mm in diameter and 10 mm in length, just large enough to hold the samples. The samples were wrapped by teflon tape (or rubber for deuteron and oxygen-17 measurements) to isolated them from the pressure-transmitting fluid. The teflon tape was checked for absence of proton signal. The coil assembly was housed in a stainless steel cylindrical pressure cell fitted with a plug with a single electrical feed-through, the cell serving as electrical ground. A new two-electrical feed-through plug was also employed, the insulating material surrounding the two leads made from machinable ceramic. The intrinsic capacitance of the new plug is

Reproduced with permission of the copyright owner. Further reproduction prohibited without permission.

very small and has virtually no pressure dependence which leads a good tuning at the elevated pressure. Elevated hydrostatic pressures were achieved using a hydraulic Enerpac 11-4000 manual pump; hydrogen-free Fluorinert FC-77 (3M) was employed as the pressure-transmitting fluid. Pressures were monitored with a Heise 12" circular gauge. The structural diagram of high pressure cell and plug is shown in Figure 3.4.

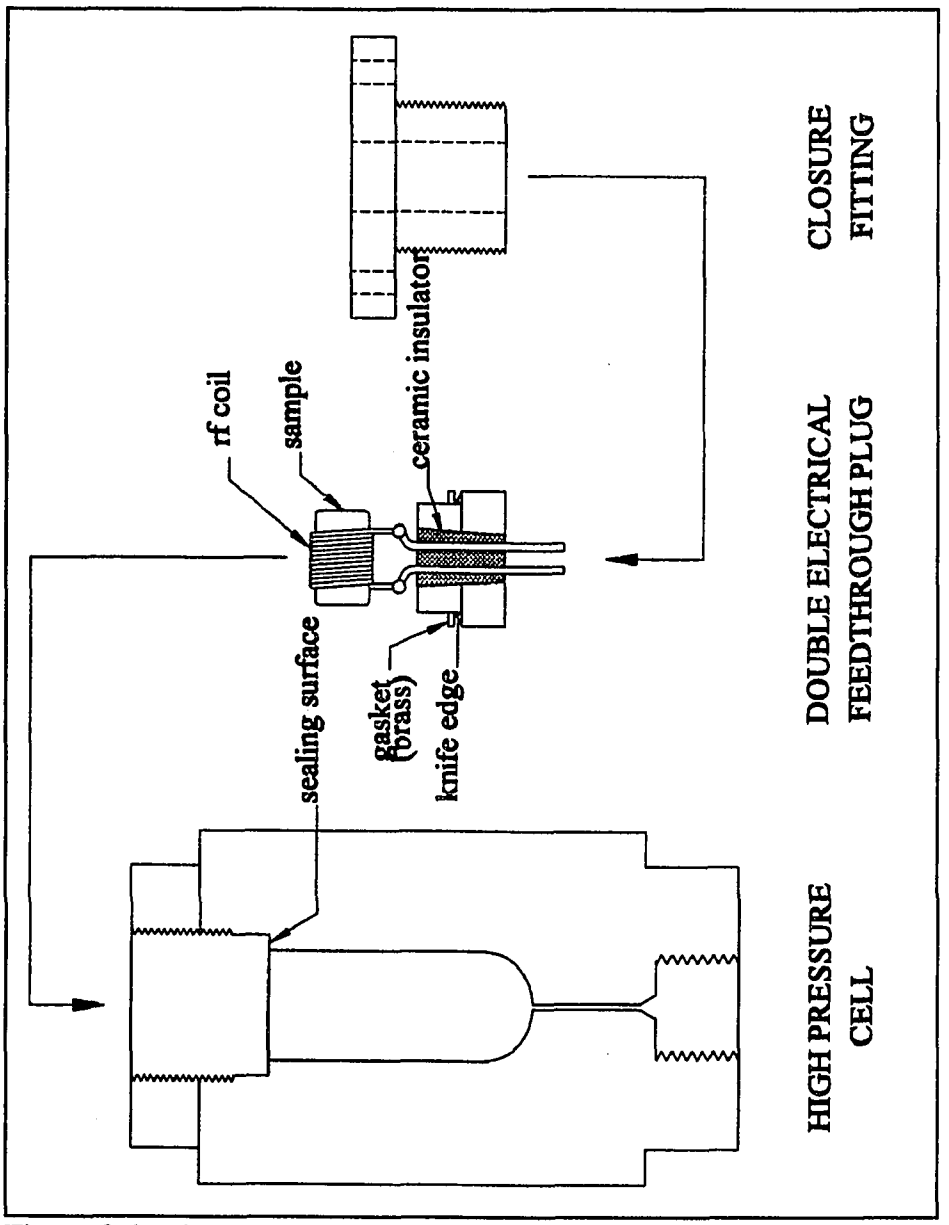

Figure 3.4: Diagram of High pressure cell and plug structure.

Reproduced with permission of the copyright owner. Further reproduction prohibited without permission.

3-2.3. Fourier Transform

The NMR signals, the free induction decay (FID) or echoes, were recorded by the digitizer in the LeCroy oscilloscope. The spectra are the corresponding Fourier transforms. LeCroy supports only a single channel Fourier transform, which has no phase correction, this restricts the adjustment of the line symmetry of the absorption spectrum. A way to solve this problem is using the magnitude mode spectrum. In this thesis, all of the spectra are in magnitude mode. Assuming the FID signal f(t) is an exponential decay:

$$f(t) = A_o \exp^{-t/T_2^*} \quad , \tag{3.1}$$

the spectrum is its Fourier transform:

$$F(\omega) = \int_{-\infty}^{\infty} f(t)\, e^{-i\omega t} dt = v - iu \quad , \tag{3.2}$$

it is of Lorentzian shape:

$$v = \frac{A_o T_2^*}{1 + \omega^2 T_2^{*2}} \quad , \qquad u = \frac{A_o T_2^{*2} \omega}{1 + \omega^2 T_2^{*2}} \quad . \tag{3.3}$$

where v is the absorption spectrum and u is the dispersion spectrum. The magnitude spectrum is:

$$M = (v^2 + u^2)^{1/2} \quad . \tag{3.4}$$

The full width at half magnitude or the linewidth $\Delta\nu$ for a Lorentzian absorption spectrum v is:

Reproduced with permission of the copyright owner. Further reproduction prohibited without permission.

$$\Delta \nu_{\nu} = \frac{1}{\pi T_2^*} \quad . \tag{3.5}$$

The linewidth of the magnitude mode spectrum M is:

$$\Delta \nu_M = \frac{\sqrt{3}}{\pi T_2^*} = \sqrt{3}\,\Delta \nu_{\nu} \quad . \tag{3.6}$$

It is easy to see that the ratio of the linewidth between absorption mode and magnitude mode is $1:3^{1/2}$, thus we can evaluate the absorption spectrum linewidth from that of magnitude by dividing the latter by $3^{1/2}$. Figure 3.5 shows a free induction decay, its spectrum in un-phase corrected absorption mode and magnitude mode dumped from LeCroy screen.

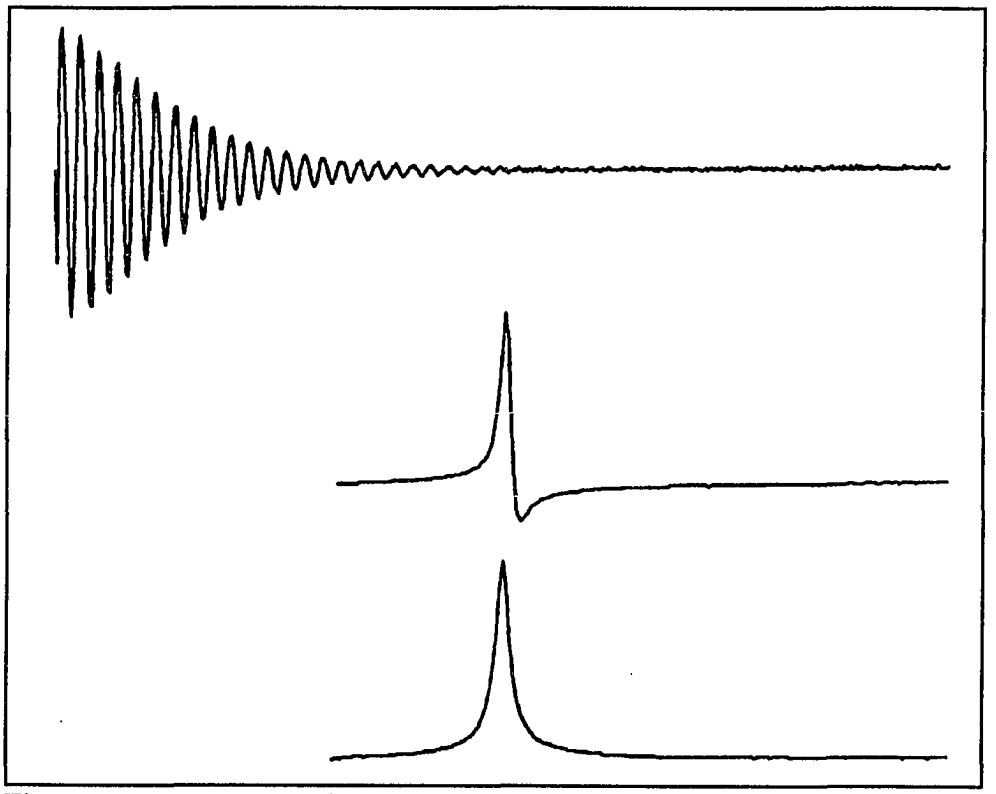

Figure 3.5: A FID and its spectrum. top: FID, middle: un-phase corrected absorption spectrum, bottom: magnitude spectrum.

Reproduced with permission of the copyright owner. Further reproduction prohibited without permission.

Chapter 4. NMR Results and Discussion

In this chapter, deuteron, oxygen-17, and proton NMR results are presented. The first section contains the values of spin-lattice relaxation times (T_1) of bulk solvents including H_2O, D_2O, ^{17}O enriched H_2O, and CH_3OD. Section 2 includes deuteron spectra and T_1 results for NAFION-117 containing D_2O, and a detailed investigation of spectra of stretched samples. A comparison of NMR results of acid-treated and non-acid-treated NAFION is also included. Oxygen-17 spectra and T_1 results for NAFION-117 containing 20% ^{17}O enriched H_2O form Section 3. High pressure proton, deuteron, and oxygen-17 NMR T_1 results are presented in section 4. A cluster model described the water organization in NAFION is discussed in Section 5. Section 6 compiles deuteron and oxygen-17 NMR spectra and T_1 for NAFION containing either CH_3OD or 15% ^{17}O enriched CH_3OH. Section 7 is the NMR results of NAFION-127 (EW 1200) containing D_2O and ^{17}O enriched H_2O. The last section is the conclusions.

4-1. Spin-lattice Relaxation Times of Bulk Solvents

In order to study the behavior of water or other solvents in NAFION membranes, it is necessary to review both spectra and spin-lattice relaxation times (T_1) of the bulk solvents. As mentioned in section 2.4, motional narrowing results in a very narrow and featureless line typical of liquid-state NMR. However, the measurements of T_1 for several bulk solvents were carried out. Assuming a single exponential profile of inversion recovery, T_1 was determined by a PC software package *Peakfit* in which T_1 could be obtained using a two-parameter fitting routine. Examples of inversion recovery for D_2O

Reproduced with permission of the copyright owner. Further reproduction prohibited without permission.

and $H_2{}^{17}O$ are displayed in Figures 4.1 and 4.2.

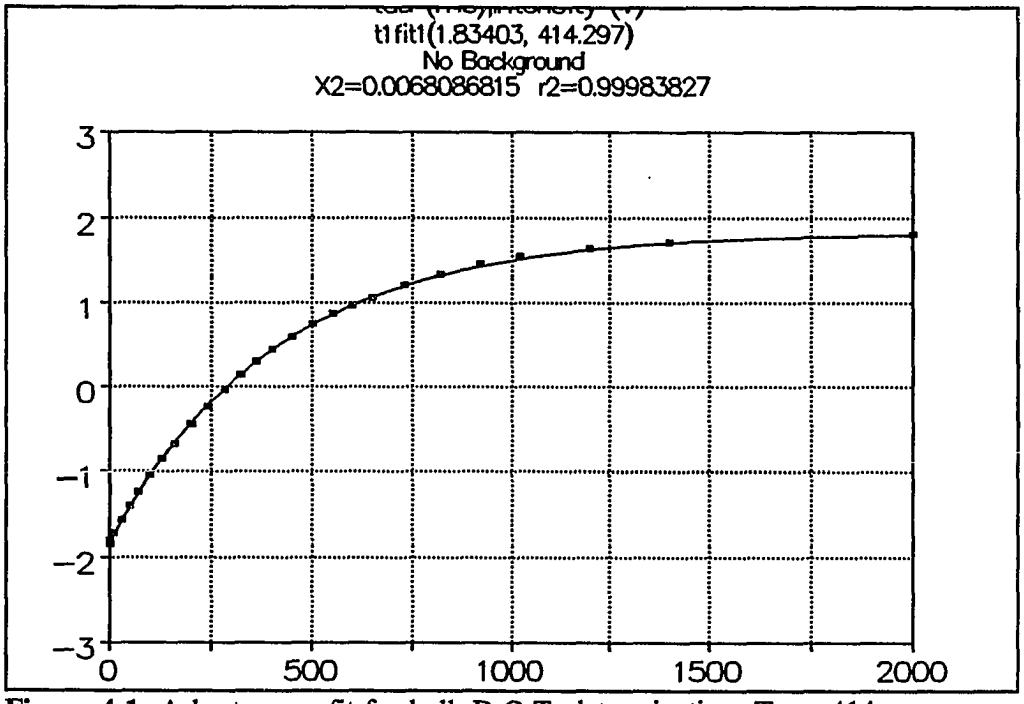

Figure 4.1: A best curve fit for bulk D_2O T_1 determination, T_1 = 414 ms.

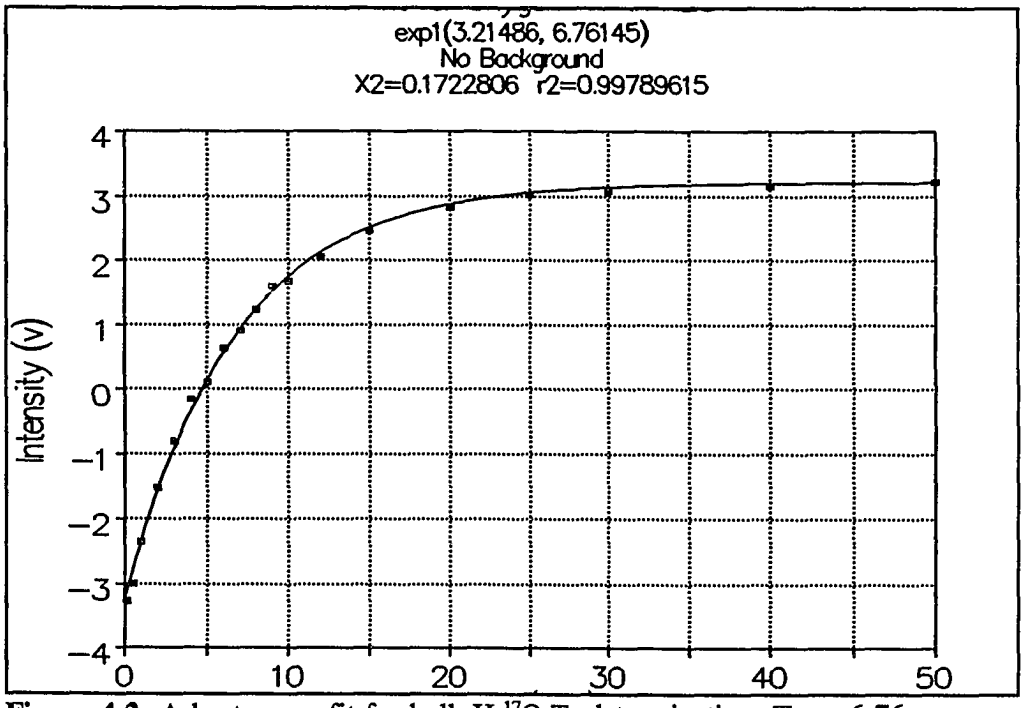

Figure 4.2: A best curve fit for bulk $H_2{}^{17}O$ T_1 determination, T_1 = 6.76 ms.

Reproduced with permission of the copyright owner. Further reproduction prohibited without permission.

Table 4.1 lists the spin-lattice relaxation times (T_1) of several solvents utilized in this investigation, which includes the results obtained by our measurements and from the associated references as well.

Table 4.1: Spin-lattice relaxation times for bulk solvents at room temperature.

Bulk solvents	T_1 (obtained in this Lab)	T_1 (from literature)
H_2O	3.6 (s)	3.5 (s)[70]
D_2O	0.414 (s)	0.40 (s)[71]
CH_3OD	0.29 (s)	0.29 (s)[72]
$H_2{}^{17}O$	6.76 (ms)	6.7 (ms)[53]

As we can see, the values of T_1 obtained from our measurements agree with those of the literature quite well. T_1 values at other than room temperature can be found in the references cited in table 4.1. The relaxation of bulk H_2O and D_2O under elevated pressure can be found in reference[73], in which the T_1 value for bulk D_2O reveals a very weak pressure dependence at room temperature in the range of pressure from 1 bar to 9 kbar.

It is also useful to list the quadrupole coupling constant (QCC) and the rotational correlation time τ_c of those bulk solvents, because coupling between quadrupole interaction and molecular rotation dominates the mechanism of the relaxation. Table 4.2 lists the QCC and τ_c of D_2O, $H_2{}^{17}O$, and CH_3OD, from which we can see that the QCC of oxygen-17 is 30 times of that of deuteron in water. The rotational correlation time of the OD bond of methanol molecule is larger than that of water, which means the speed of rotation of methanol molecule is slower than that of the water molecule.

Reproduced with permission of the copyright owner. Further reproduction prohibited without permission.

Table 4.2: Quadrupole coupling constant and rotational correlation time τ_c of D_2O, $H_2{}^{17}O$, and CH_3OD.

	Solvents	QCC	τ_c (s)
D_2O	(Gas)	315 (kHz)[54]	-
	(solid)	215 (kHz)[54]	-
	(Liquid)	222 (kHz)[74]	2.0×10^{-12} (25 °C)[71]
$H_2{}^{17}O$	(Gas)	10.2 (MHz)[53]	-
	(solid)	6.7 (MHz)[53]	-
	(Liquid)	6.7 (MHz)[53]	2.4×10^{-12} (27 °C)[74]
CH_3OD	(Liquid)	192 (kHz)[72]	5.4×10^{-12} (25 °C)[72]

4-2. D_2O in NAFION-117

In this section, deuterium NMR results for the NAFION-117 containing various amount of D_2O are presented. Samples of NAFION were assembled in both rolled and stacked films. The former is for suppressing the splitting effects. The latter is for checking the anisotropic motion of water molecules in NAFION membranes, which we will call the orientation effect. Studies of T_1 and spectra yield information about (1) water concentration effect at room temperature, (2) low temperature behavior, (3) orientation effect, (4) sample stretching effect, and (5) acid-treated and non-acid-treated effect.

4-2.1. Water Concentration Effect

The NMR results of D_2O in membranes show a large departure of that of the bulk water. Figure 4.3 displays the linewidth (a) and T_1 (b) as a function of water content at 295 K. As can be seen, the linewidth decreases speedily from 480 Hz as the water

Reproduced with permission of the copyright owner. Further reproduction prohibited without permission.

content increases when the water content is less than 10%; at water content above 10%, there is a small decrease in the linewidth, approaching the spectrometer limit of 40 Hz as the membrane becomes saturated. This trend is consistent with the proton results reported by Duplessix[32]. T_1 is 29 ms for 3.0% water content and increases as water content increases up to 157 ms for 18% water content, approaching the value for free D_2O (414 ms). Our T_1 results are in good agreement with deuteron T_1 values reported by Zawodzinski[13]. Deuteron lineshapes vs. water content are displayed in Figure 4.4. The NAFION membrane surface plane is parallel to the external field $\mathbf{H}_0$, where the largest quadrupolar splitting occurs, resulting in a doublet. The splitting decreases as the water content increases. The splitting is no longer observed when the water content is 14%. These data are consistent with the expectation that some fraction of the total water in the membrane approaches an isotropically free state, and that rapid exchange, on the NMR time-scale, between these nearly free water molecules and those that are more motionally restricted (by interaction with the polymer host) yield an averaged response. Such behavior is commonly observed in organic membranes containing large amounts ($\geq$ 10%) of water[51].

Reproduced with permission of the copyright owner. Further reproduction prohibited without permission.

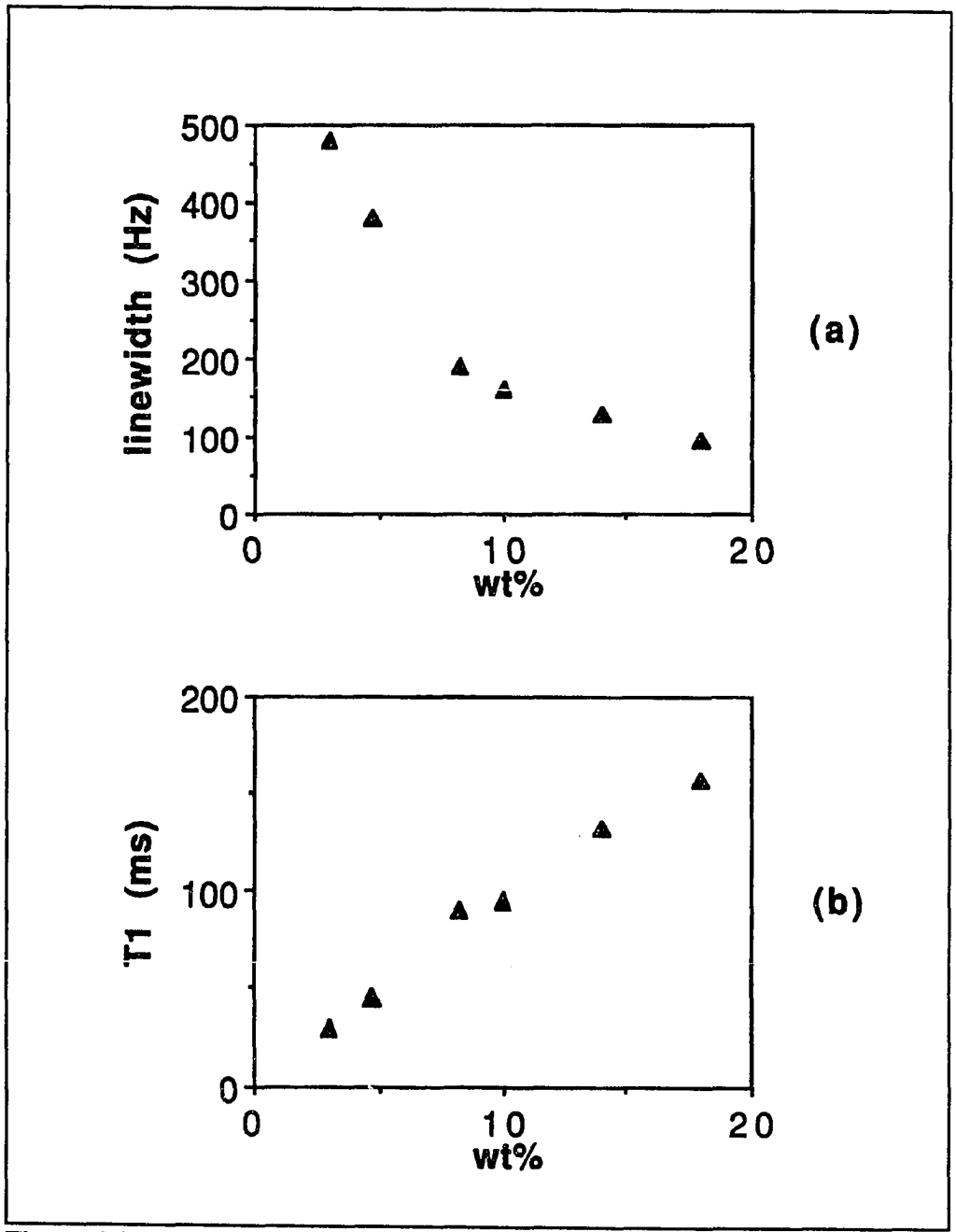

Figure 4.3: The deuteron NMR as a function of D_2O content in NAFION-117 at 295 K. (a) The linewidth vs. water content, (b) The T_1 vs. water content.

Reproduced with permission of the copyright owner. Further reproduction prohibited without permission.

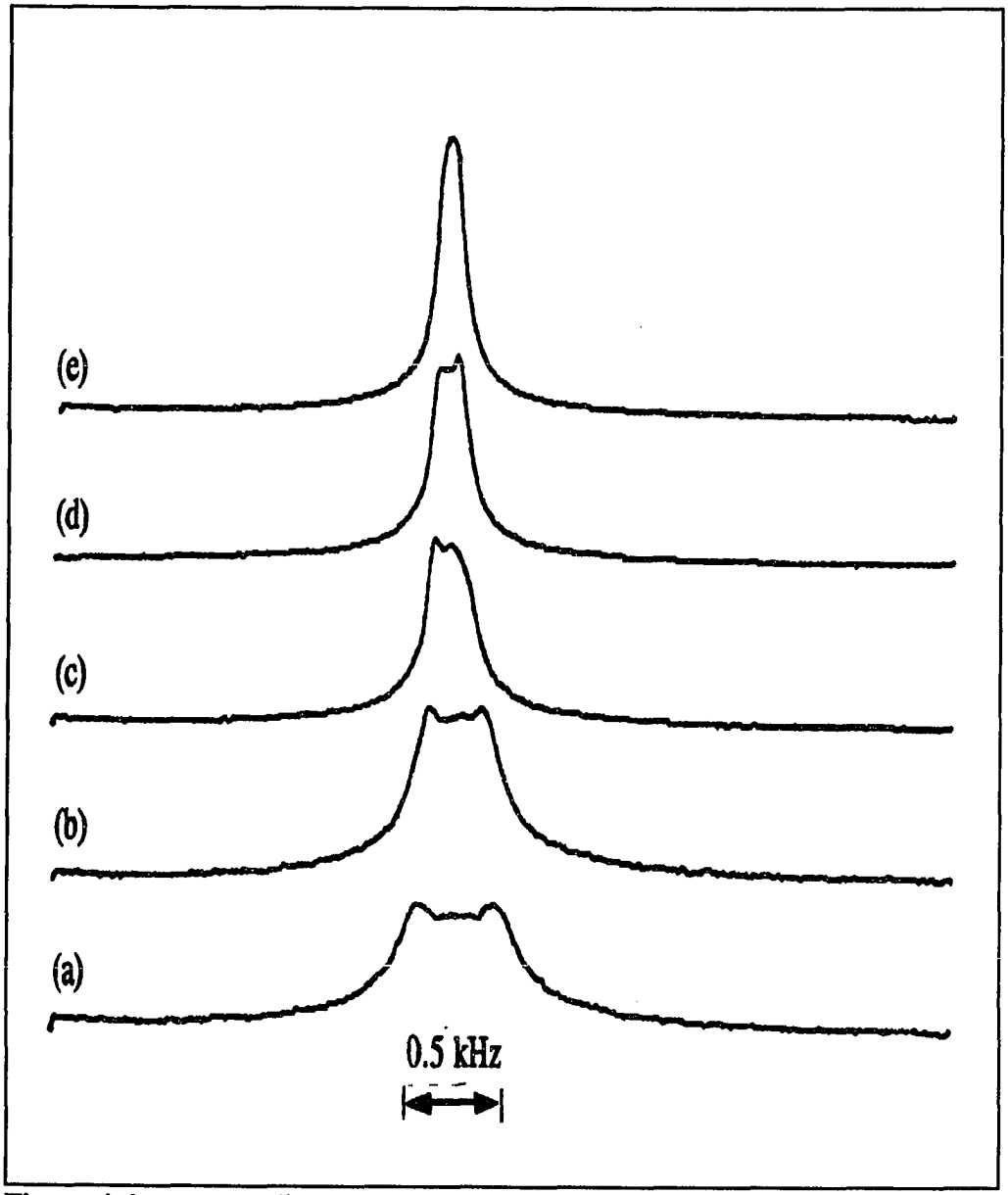

Figure 4.4: Deuteron lineshapes vs. water content in NAFION-117, (a) 3.0 wt%, (b) 4.7 wt%, (c) 8.2 wt%, (d) 10 wt%, (e) 14 wt%.

Reproduced with permission of the copyright owner. Further reproduction prohibited without permission.

4-2.2. Low Temperature Behavior

Variable temperature measurements of both spectra and T_1 were carried out in the temperature range from room temperature down to 115 K. For all samples the linewidth increases as the temperature decreases, as shown in Figure 4.5. For NAFION containing 13% D_2O, the linewidth increases from about 230 Hz at room temperature to 26 kHz at 184 K, for NAFION containing 18% D_2O, the linewidth increases from about 100 Hz at room temperature to about 70 kHz at 160 K. This trend is also found in proton NMR by Duplessix[32], and reflects the decreasing mobility of the water molecules with decreasing temperature. For NAFION containing water less than 13%, the doublet splitting of the spectra makes it difficult to define a linewidth. However, we can observe lineshape changes at variable temperature. Figure 4.6 and 4.7 display the temperature dependence of lineshape. As can be seen, for NAFION containing 7.1% D_2O, the doublet disappears at 205 K because of broadening. Above this temperature the splitting shows very little change, and each component peak broadens gradually as the temperature decreases, which means that the mobility of the water molecules still is comparable of that at room temperature. Below 205 K, the linewidth increases to 88 kHz at 166 K rapidly (not shown), which implies that the water molecules become more rigid at such low T. For 18% D_2O concentration sample, it is a relative large amount water, the large fraction of isotropic water molecular motion narrows the line, thus no splitting was observed in the whole temperature range. The temperature dependence of linewidth for the 18% sample is shown in Figure 4.5, and it has same trend as that of lower water content. Although the previous investigators[27,29] reported the presence of two or three water environments associated with a void volume containing a small amount of water

Reproduced with permission of the copyright owner. Further reproduction prohibited without permission.

and an ion cluster region in the membrane, our spectrum shows only a single frequency, which does not exhibit behavior consistent with isotropically free water contained in voids.

Deuteron spin-lattice relaxation times (T_1) at various temperature were measured by inversion recovery. Recovery profiles were observed to be exponential from room T down to ~ 190 K, Figure 4.8 shows several recovery curves at different temperatures. Below this temperature the recoveries do not fit exponential well. Previously reported proton data[22] shows non-exponential relaxation near the low side of 193 K for NAFION-115 membranes. Thus there is a transition around 190-193 K seen by both ^2H and ^1H. T_1 data for samples at different water content are presented as a function of temperature in Figure 4.9. The T_1 minima occur at ca. 205 K for all the water contents with approximately the same value, 3 ms. By employing the relation $\omega\tau \sim 1$, one can find the correlation time τ_c, which is about 3.4×10^{-9} s. At room temperature, T_1 has the value ca. 100 ms, by applying Equation 2.26, assuming the relaxation mechanism is due to the quadrupole interaction only, one can find the rotational correlation time τ_c = 1.4×10^{-11} s at room temperature. Although the magnetic dipole-dipole interactions also contribute to the relaxation rate, the dipole-dipole relaxation rate in pure D_2O due to dipolar interactions is expected to be lower than the relaxation rate for protons in pure H_2O by a factor of 665[75], which is the result from $(\gamma_H/\gamma_D)^4$, thus it is negligible.

Arrhenius plots of deuteron T_1 in NAFION at four different water concentrations (4.7, 10, 14 and 18%) are shown in Figure 4.10. Activation energies for deuteron motion have been extracted from the high T (with respect to the T_1 minimum) data in Figure 4.10 and are listed in Table 4.3. Calculation of activation energy assumes a BPP

Reproduced with permission of the copyright owner. Further reproduction prohibited without permission.

relaxation process along with the fast motion approximation $\omega\tau_c \ll 1$, which yields

$$\frac{1}{T_1} \propto \tau_c = \tau_0 e^{-E_A/kT} \qquad (4.1)$$

here ω is the NMR frequency, τ_c is the motional correlation time and E_A is the activation energy[59]. Although the true relaxation process is undoubtedly more complex than given by the BPP approximation, the rational for using Equation 4.1 is that comparisons are being made between samples in which only one parameter (water content) is varied. Thus it is the relative change in activation energy that is physically significant. From the Table 4.3, we see that E_A increases with increasing water content. The values in Table 4.3 are somewhat larger than the corresponding activation energy for free molecular rotation in bulk D_2O (0.14 eV)[71]. This observation is consistent with earlier proton NMR results which suggested that thermally activated motion of water molecules is somewhat impeded by interactions with the host polymer[34].

Table 4.3: Activation Energies From Figure 4.9.

Water content (wt%)	E_A (ev) $\pm$ 0.01eV
4.7	0.20
10.2	0.22
14.1	0.25
18.3	0.27

Glassy behavior at low temperatures, reported by previous investigators[76], can be inferred from the deuteron NMR lineshape. Figure 4.11 displays spectra for both D_2O ice at 233 K and NAFION-117 containing 18 wt% D_2O at 109 K. The ice spectrum

Reproduced with permission of the copyright owner. Further reproduction prohibited without permission.

exhibits the well-known divergences associated with a spin-1 powder pattern[44]. The NAFION spectrum, while being of comparable width to the ice spectrum, shows no clear divergences. Although averaging due to molecular motion (though much restricted at this low T) is partly responsible for this effect, the NAFION lineshape is also attributed to a glassy arrangement of water molecules, in which the associated distribution of deuteron quadrupole coupling parameters smears out the divergences. It is also observed that the temperature where the glassy behavior occurs shifts to lower T as the water content increases.

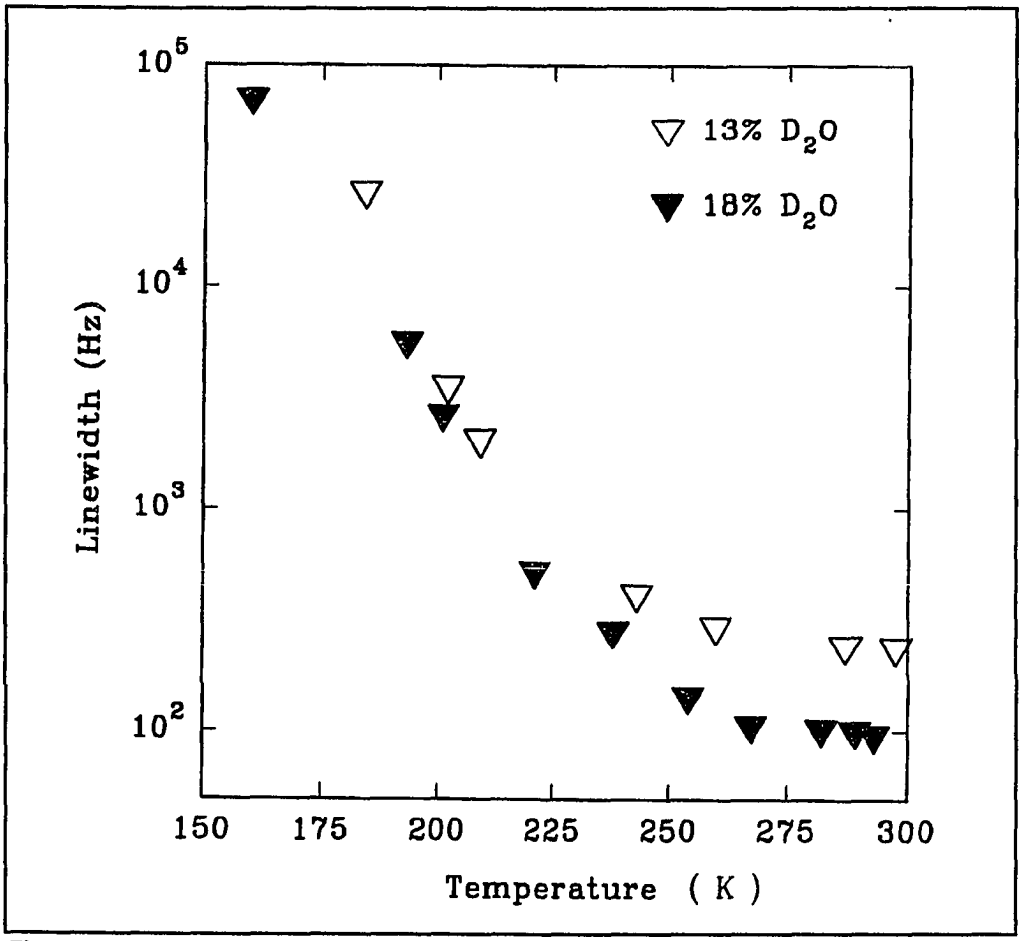

Figure 4.5: Deuteron NMR linewidth temperature dependence for NAFION-117 containing different content of D_2O.

Reproduced with permission of the copyright owner. Further reproduction prohibited without permission.

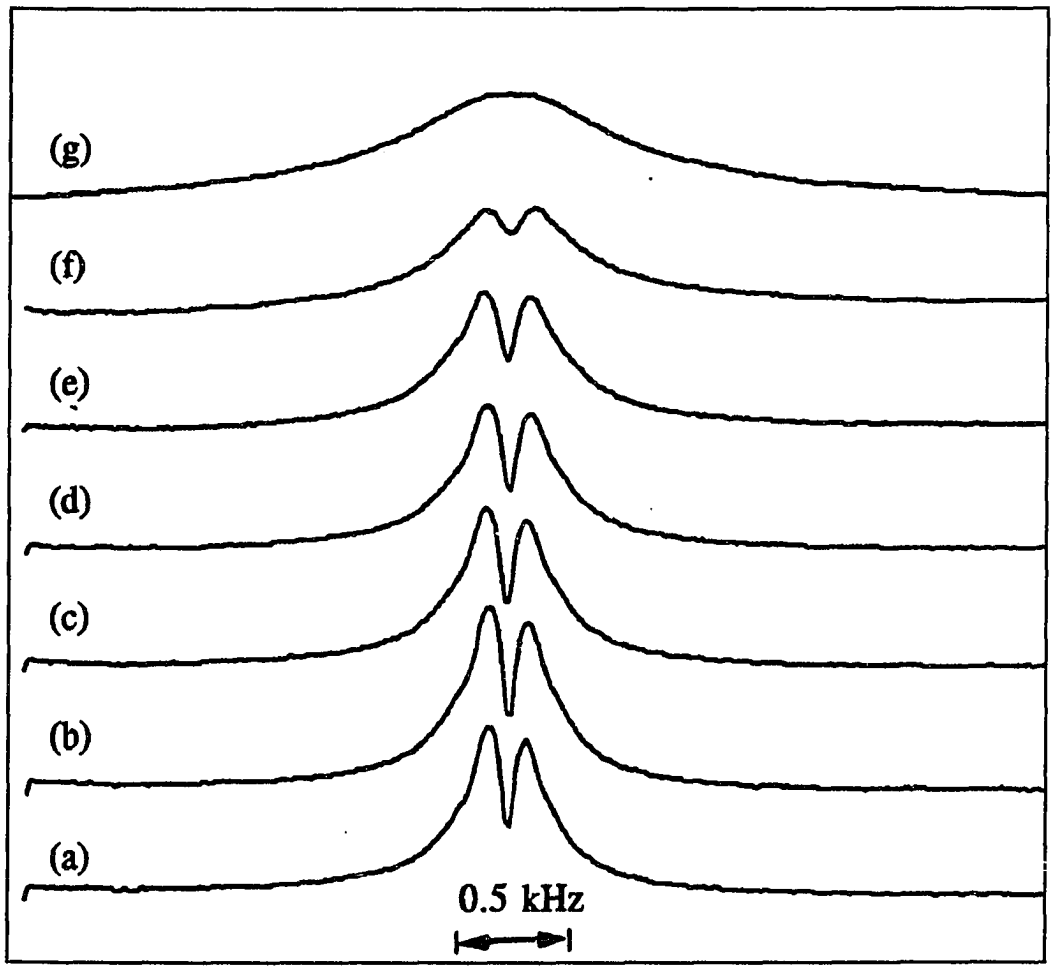

Figure 4.6: Temperature dependence of deuteron lineshape for NAFION-117 containing 7.1% D_2O. (a) 25 °C, (b) 15 °C, (C) 4 °C, (d) -10 °C, (e) -21 °C, (f) -45 °C, (g) -68 °C.

Reproduced with permission of the copyright owner. Further reproduction prohibited without permission.

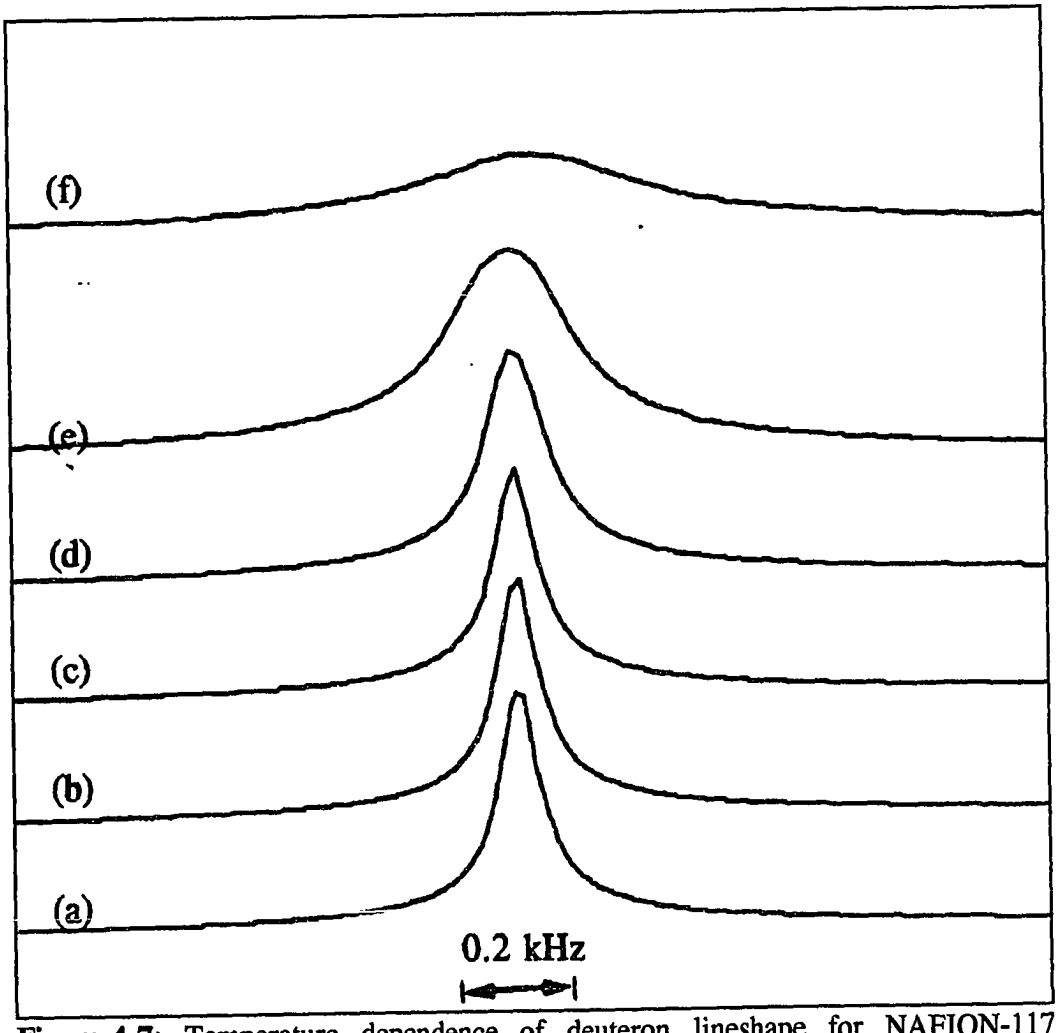

Figure 4.7: Temperature dependence of deuteron lineshape for NAFION-117 containing 18% D_2O. (a) 20 °C, (b) 9 °C, (C) -6 °C, (d) -19 °C, (e) -35 °C, (f) -52 °C.

Reproduced with permission of the copyright owner. Further reproduction prohibited without permission.

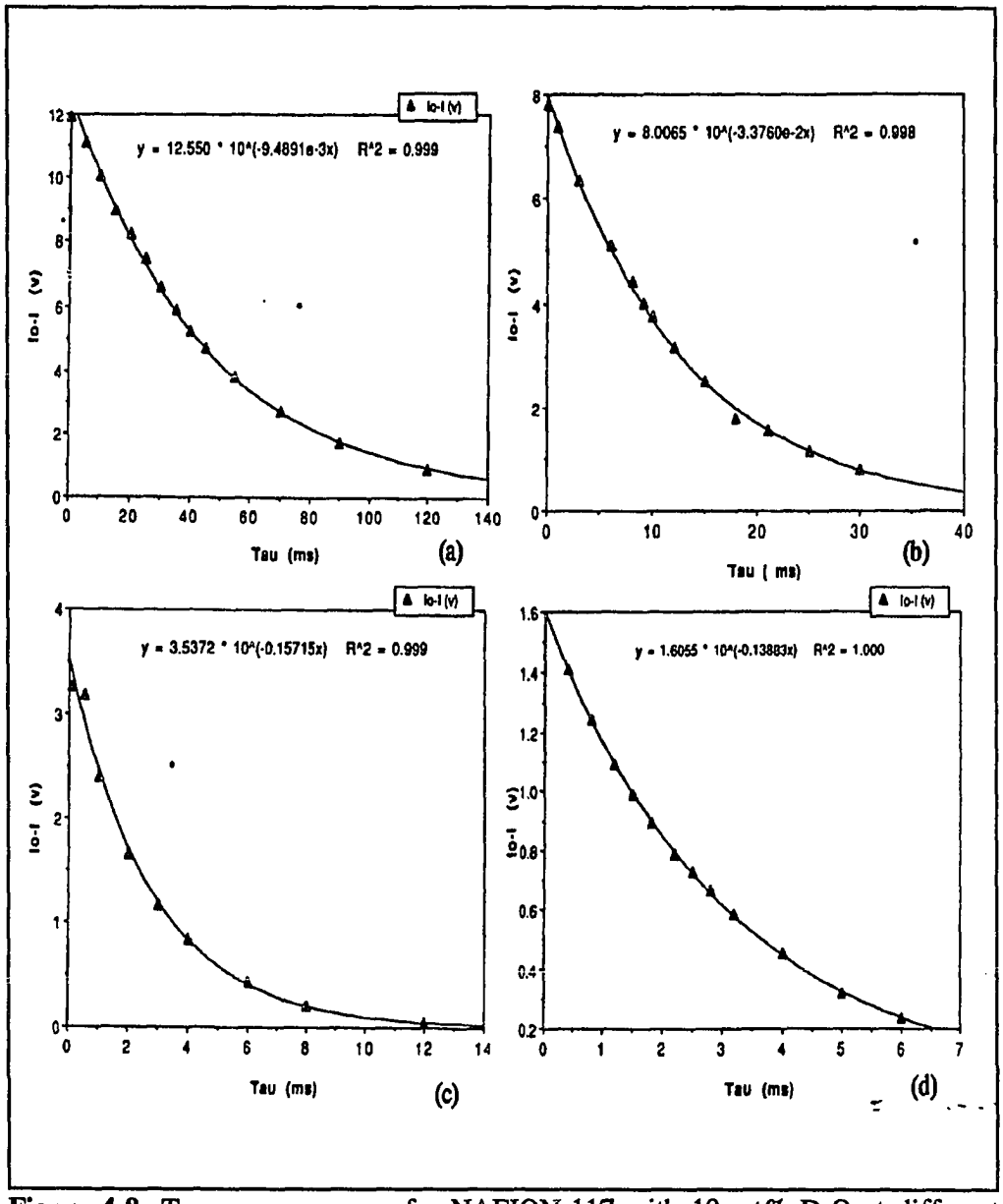

Figure 4.8: T_1 recovery curves for NAFION-117 with 10 wt% D_2O at different temperature (a) T = 268 K, (b) T = 243 K, (c) T = 213 K, (d) T = 193 K. It can be easily seen that the data fits an exponential relation very well.

Reproduced with permission of the copyright owner. Further reproduction prohibited without permission.

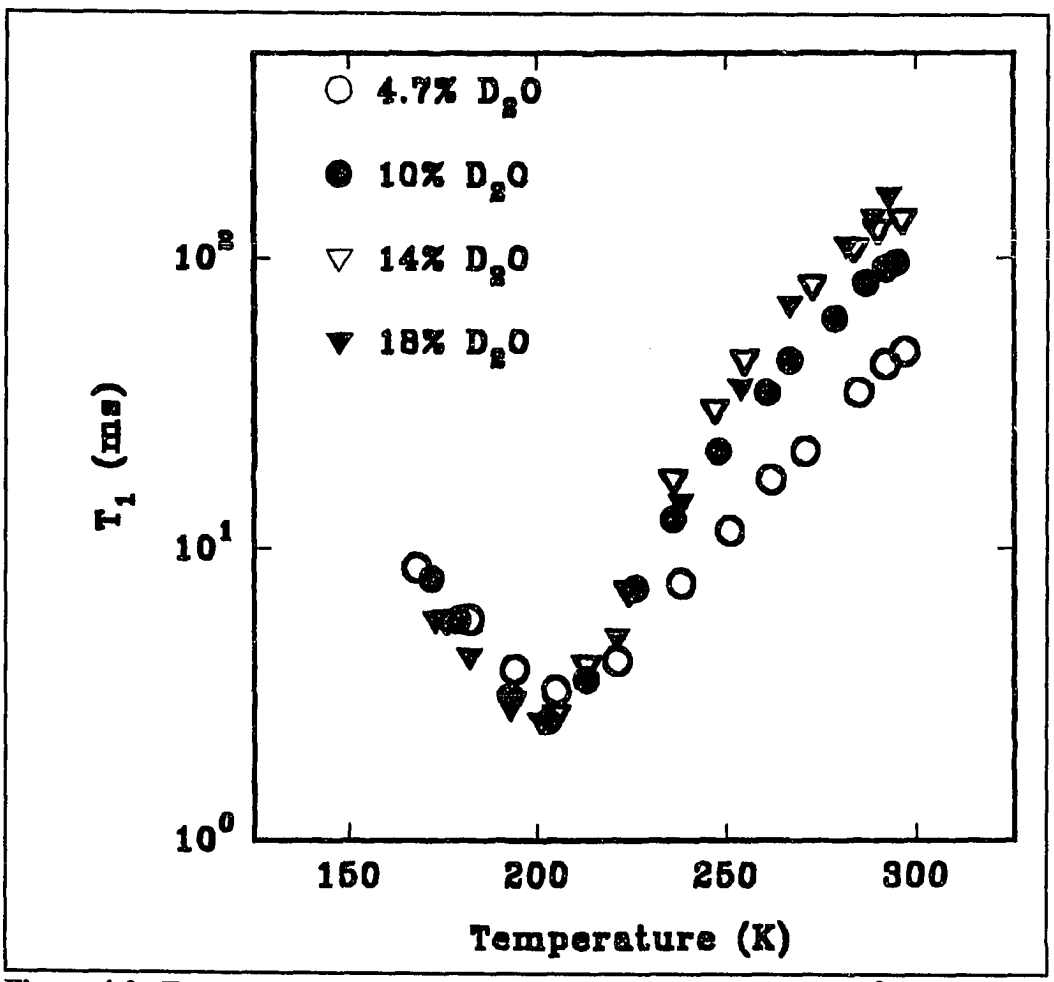

Figure 4.9: Temperature dependence of spin lattice relaxation time (^{2}H NMR) for NAFION-117 containing various D_2O contents.

Reproduced with permission of the copyright owner. Further reproduction prohibited without permission.

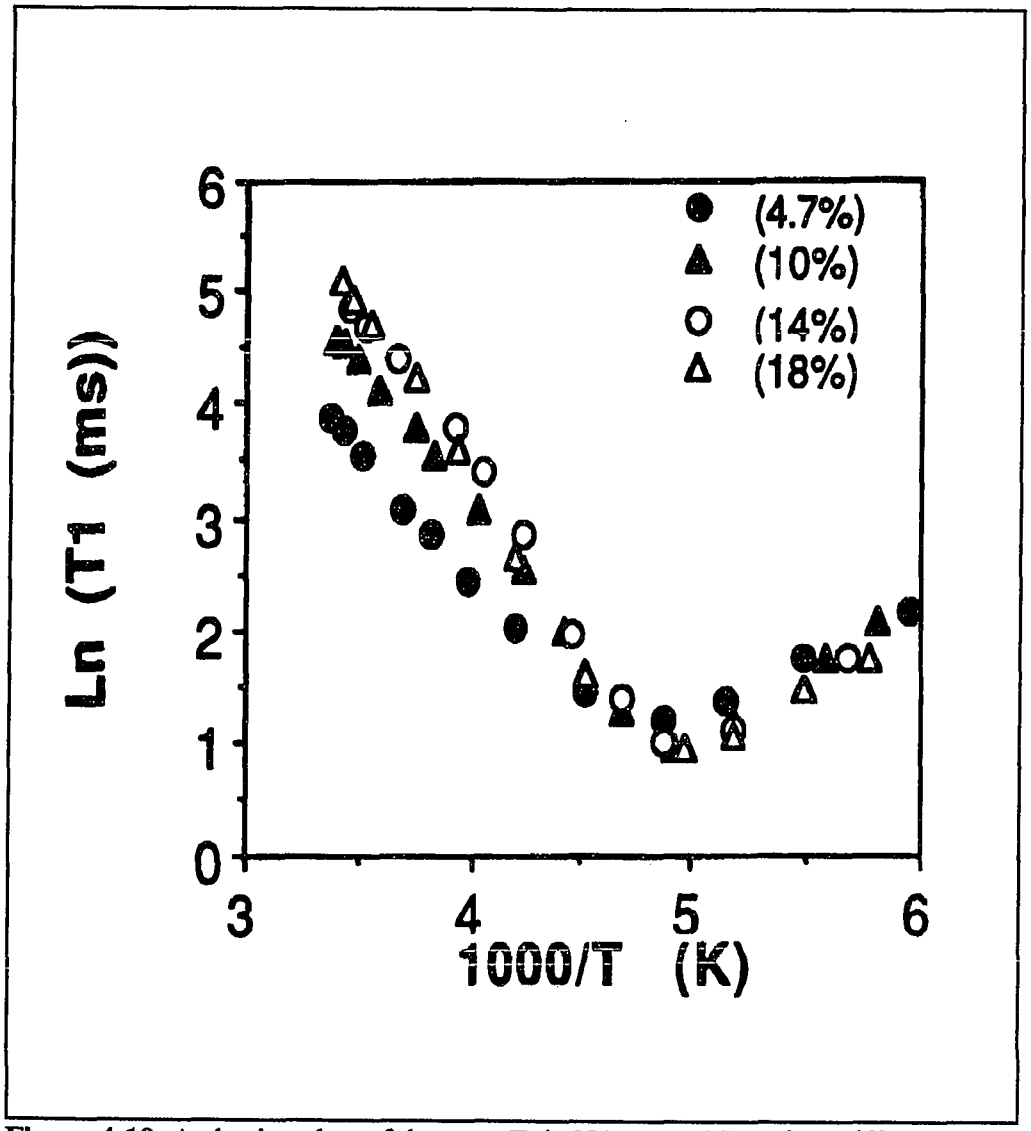

Figure 4.10: Arrhenius plots of deuteron T_1 in NAFION-117 at four different water concentrations (4.7,10,14 and 18%). The activation energies extracted from the high T (left side) data are listed in Table 4.3.

Reproduced with permission of the copyright owner. Further reproduction prohibited without permission.

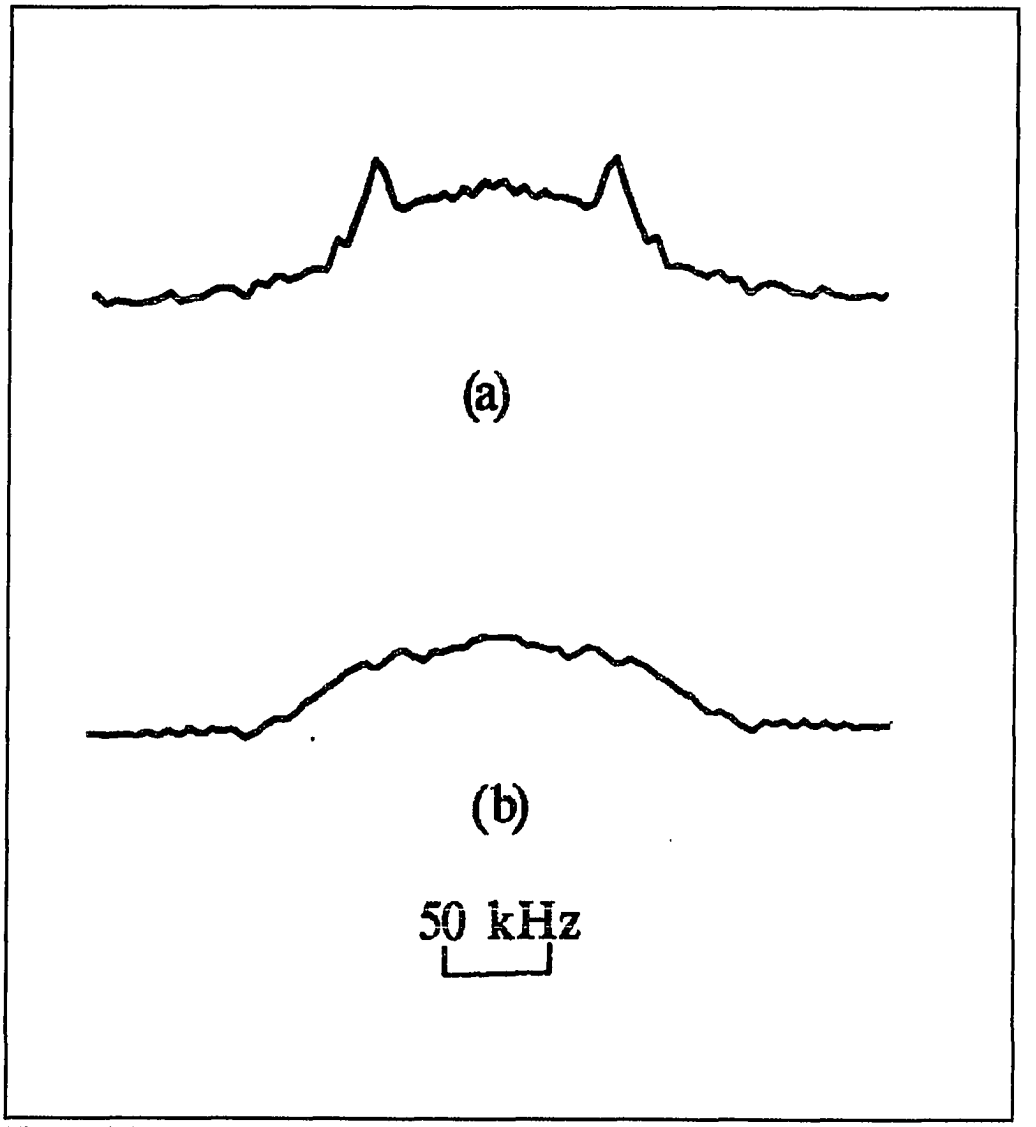

Figure 4.11: Deuteron powder pattern shows glassy behavior at low temperature, (a) D_2O ice at 233 K. (b) NAFION-117 containing 18 wt% D_2O at 109 K.

Reproduced with permission of the copyright owner. Further reproduction prohibited without permission.

4-2.3. Orientation Effect

Deuteron NMR spectra of oriented stacks of NAFION membranes containing various amount of D_2O at 295 K and at various angles between the membrane plane and the static magnetic field are displayed in Figure 4.12 to 4.17. The observed angular dependence follows the $3\cos^2\theta - 1$ dependence of the quadrupole splitting, which indicates that the deuteron motion, while rapid on the NMR time-scale, is anisotropic. That is, although much of the quadrupole interaction is averaged out by molecular motion, the residual molecular orientation persists approximately in the plane of the membrane[51]. This conclusion is most evident by observing that the splitting reaches a minimum at the 55° orientation, which is close to the angle at which the quadrupole splitting vanishes. (The actual value of the angle displayed in the figures has an uncertainty of about ± 3°). Recall the quadrupole splitting Equation 2.22:

$$\Delta_Q = \frac{1}{2}\omega_Q(3\cos^2\theta - 1)S_{OD} \quad , \tag{4.2}$$

the order parameter S_{OD} can be evaluated from the doublet splitting in the spectra. The order parameters for NAFION containing various water content are listed in Table 4.4.

Table 4.4: Order parameter for NAFION-117 containing various D_2O contents.

Water content wt%	Order parameter
3.0	3.6×10^{-3}
4.7	2.5×10^{-3}
7.1	1.5×10^{-3}
8.2	7.5×10^{-4}
10	6.2×10^{-4}
14	unresolved

Reproduced with permission of the copyright owner. Further reproduction prohibited without permission.

From the data in Table 4.4, one can see that the order parameter decreases as the water content increases, which indicates the larger of the water content, the more isotropic motion of the deuterons. This trend also has been observed in cellulose triacetate film and cellulose acetate film containing several percent D_2O[51], those order parameters are of the same order of manitude as that of NAFION membranes. In polyimide films, the order parameter is about one to two orders of magnitude larger than that of NAFION[48].

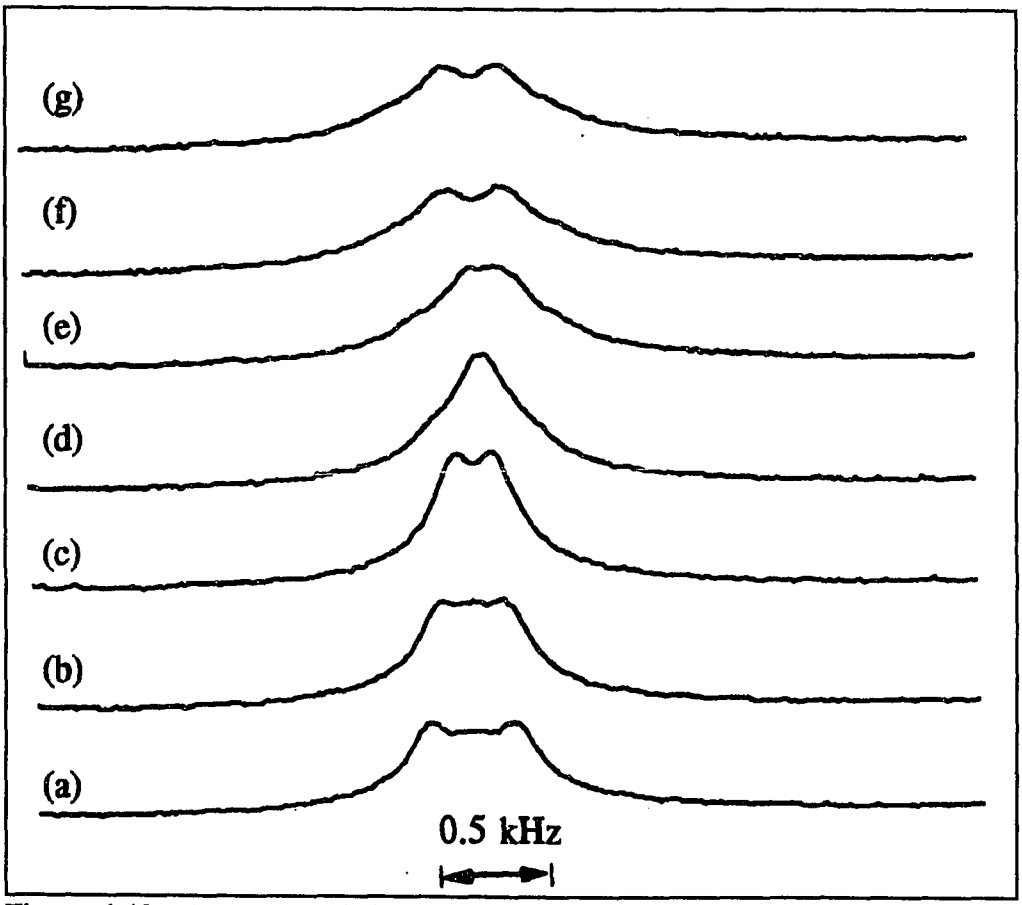

Figure 4.12: Angular variation of deuteron NMR spectra for NAFION-117 containing 3.0 wt% D_2O. (a)-(g), θ = 0°, 15°, 30°, 45°, 60°, 75°, 90°.

Reproduced with permission of the copyright owner. Further reproduction prohibited without permission.

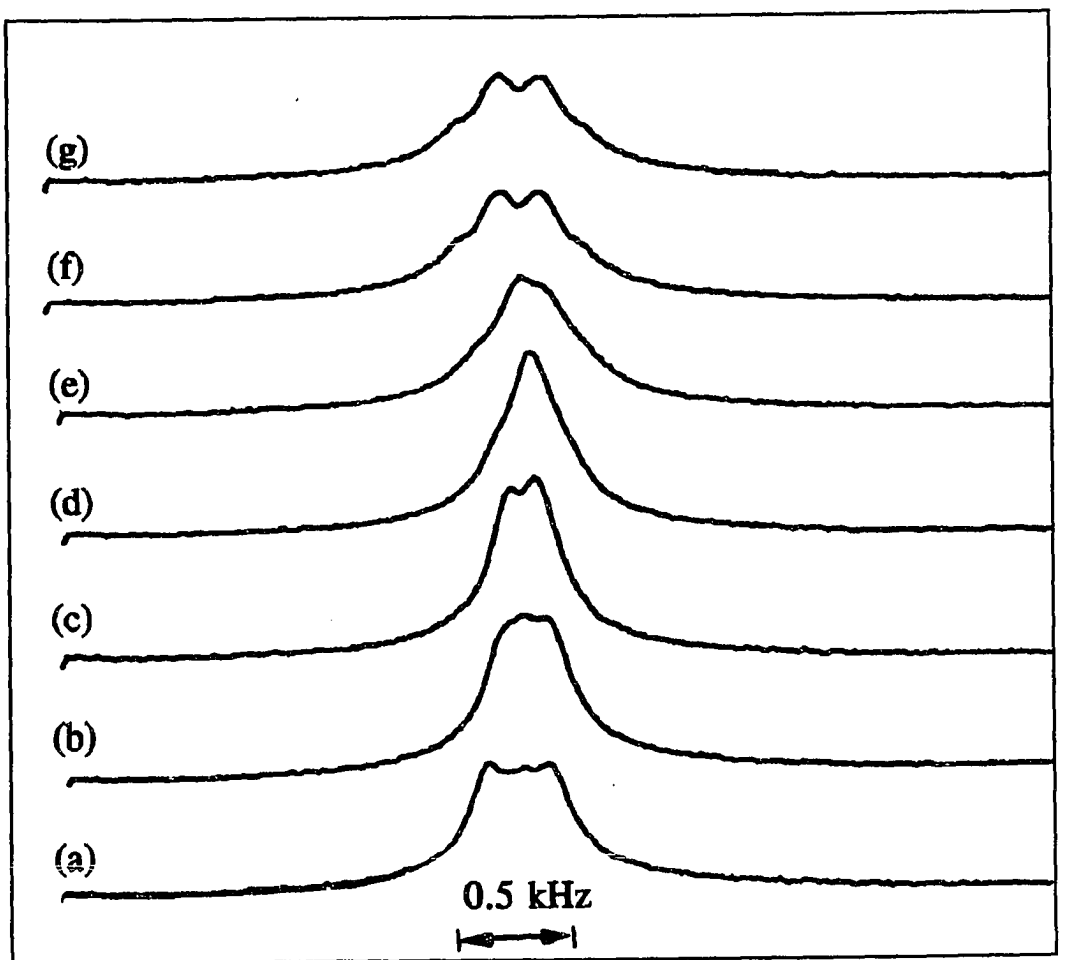

Figure 4.13: Angular variation of deuteron NMR spectra for NAFION-117 containing 4.7 wt% D_2O. (a)-(g), θ = 0°, 15°, 30°, 45°, 60°, 75°, 90°.

Reproduced with permission of the copyright owner. Further reproduction prohibited without permission.

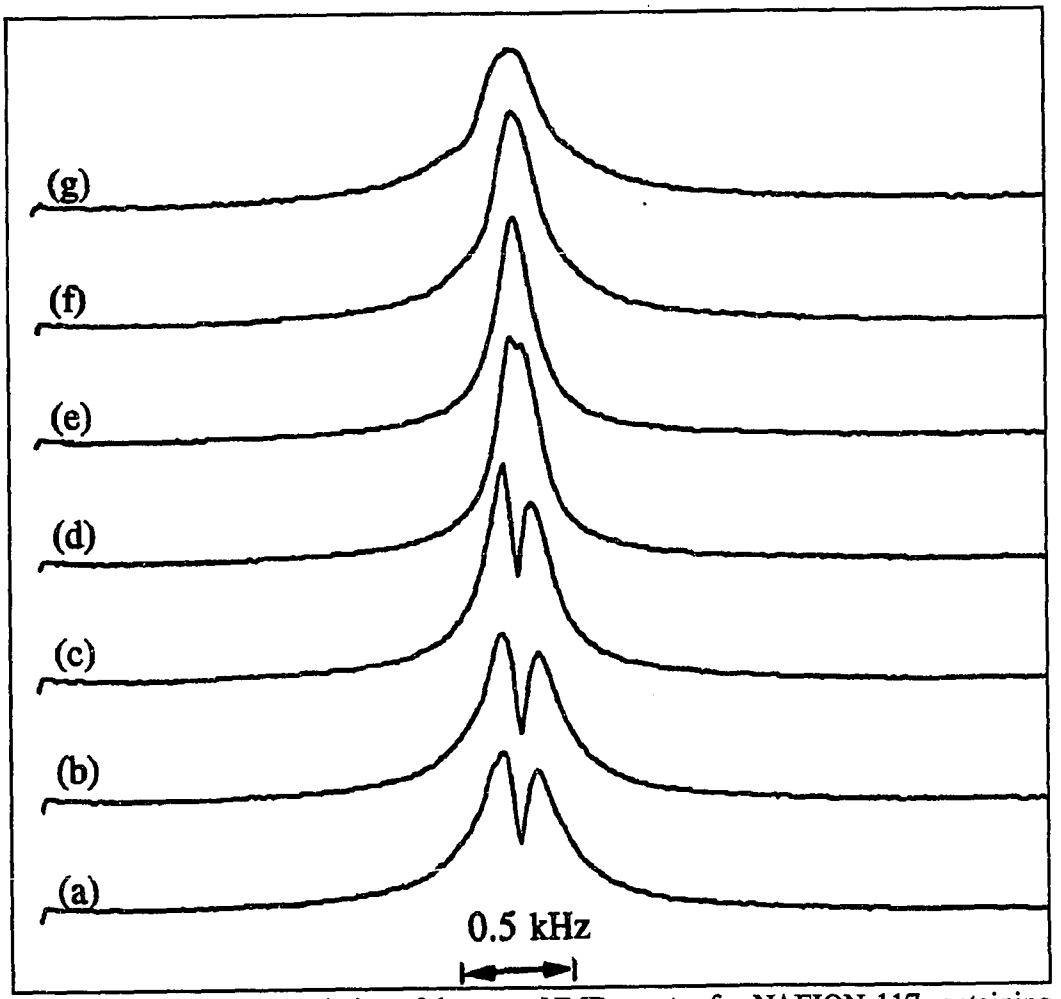

Figure 4.14: Angular variation of deuteron NMR spectra for NAFION-117 containing 7.1 wt% D_2O. (a)-(g), θ = 0°, 15°, 30°, 45°, 60°, 75°, 90°.

Reproduced with permission of the copyright owner. Further reproduction prohibited without permission.

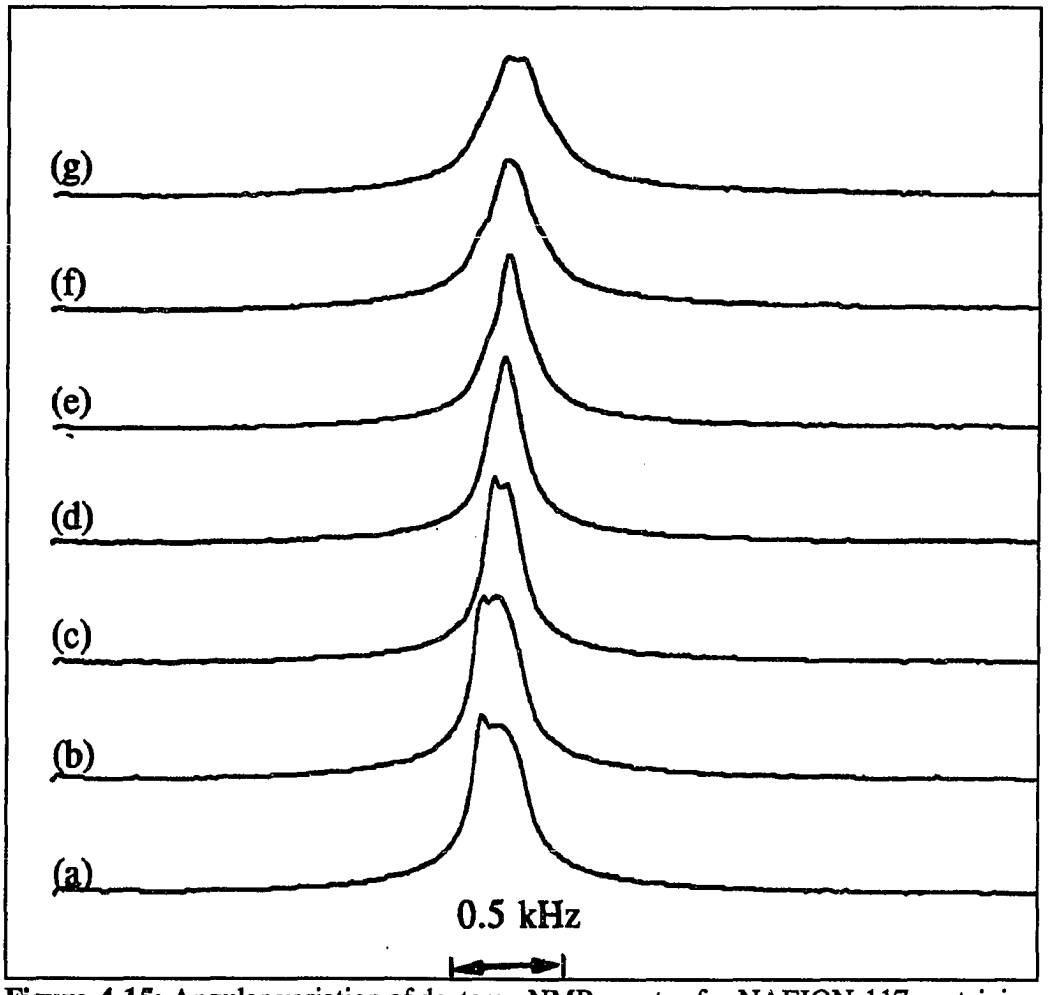

Figure 4.15: Angular variation of deuteron NMR spectra for NAFION-117 containing 8.2 wt% D_2O. (a)-(g), θ = 0°, 15°, 30°, 45°, 60°, 75°, 90°.

Reproduced with permission of the copyright owner. Further reproduction prohibited without permission.

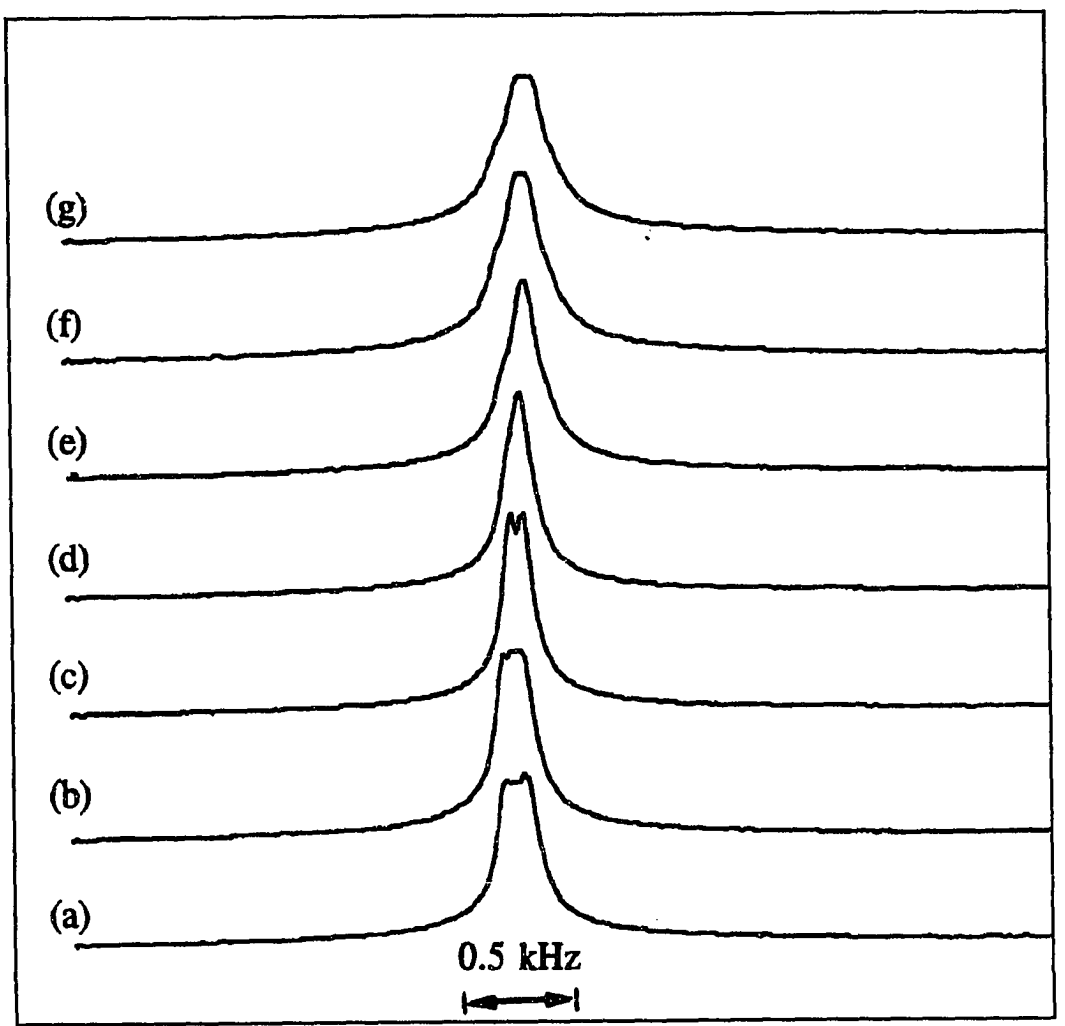

Figure 4.16: Angular variation of deuteron NMR spectra for NAFION-117 containing 10 wt% D_2O. (a)-(g), θ = 0°, 15°, 30°, 45°, 60°, 75°, 90°.

Reproduced with permission of the copyright owner. Further reproduction prohibited without permission.

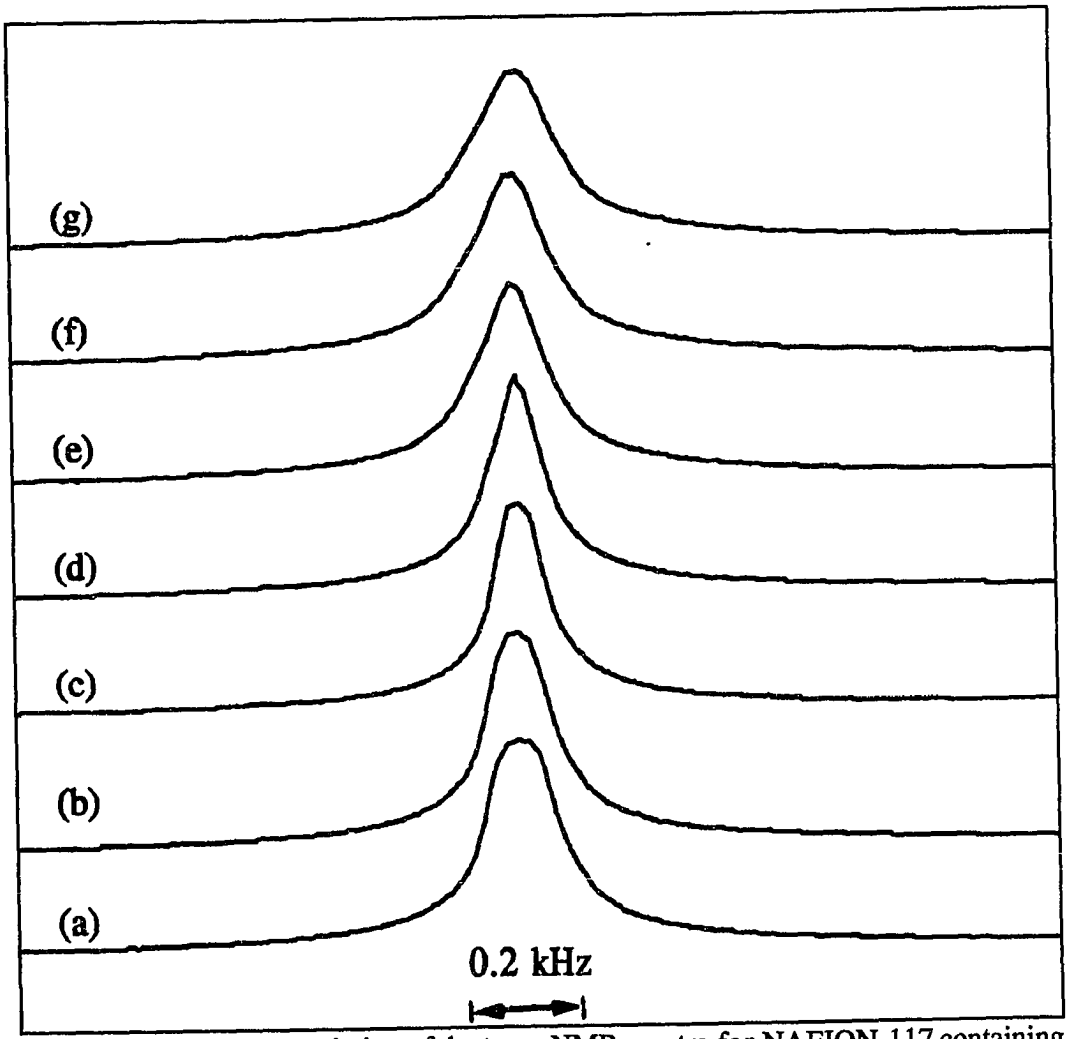

Figure 4.17: Angular variation of deuteron NMR spectra for NAFION-117 containing 14 wt% D_2O. (a)-(g), θ = 0°, 15°, 30°, 45°, 60°, 75°, 90°.

Reproduced with permission of the copyright owner. Further reproduction prohibited without permission.

4-2.4. Sample Stretching Effect

The orientation results in the previous section arise from anisotropy in the polymer chain morphology, which, in turn, may be related to manufacturing processes. Because NAFION fabrication is proprietary, explanations of the anisotropy are necessarily speculative. However, we can introduce additional anisotropy in a controlled manner by stretching. We already have seen that the deuteron motion in the unstretched NAFION presents an anisotropic response, yielding an angular dependence splitting in the deuteron spectra. We now demonstrate that this quadrupole splitting of the spectra can be enhanced significantly by stretching the membranes. Consequently, the order parameter can be increased by stretching the membranes. Figure 4.18 to 4.22 display the deuteron spectra angular dependence for membranes of various D_2O contents that were stretched by 13% elongation. The largest splitting occurs when the static magnetic field is parallel to the stretched direction, this splitting represents a spectral width nearly a factor of seven greater than that of the unstretched sample. This is apparent in Figure 4.23, where the deuteron spectra of stretched and the unstretched samples are replotted together for an comparison. An examination of $3\cos^2\theta - 1$ dependence of the splitting for a stretched sample containing 8.2 wt% is plotted in Figure 4.24. The value of $3\cos^2\theta - 1$ becomes negative when $\theta > 54.7°$, nevertheless, the appearance of the spectra still shows a doublet although the peaks assigned to individual transition are exchanged. The splitting plotted in Figure 4.24 fits Equation 4.2 very well. Thus the average principal axis of the electric field gradient (EFG) is along the stretch direction[51].

Reproduced with permission of the copyright owner. Further reproduction prohibited without permission.

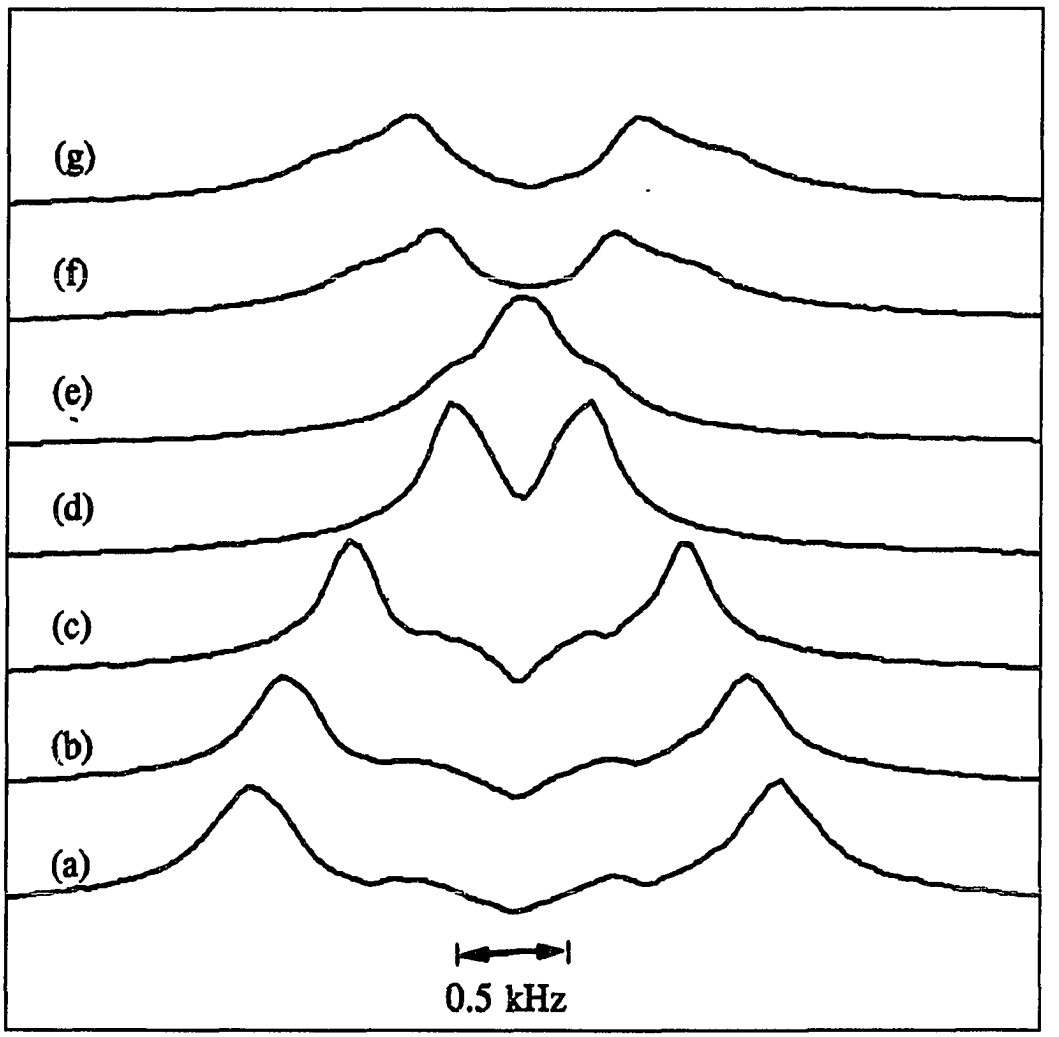

Figure 4.18: Angular variation of deuteron NMR spectra for 13% stretched NAFION-117 containing 3.7 wt% D_2O. (a)-(g), θ = 0°, 15°, 30°, 45°, 60°, 75°, 90°.

Reproduced with permission of the copyright owner. Further reproduction prohibited without permission.

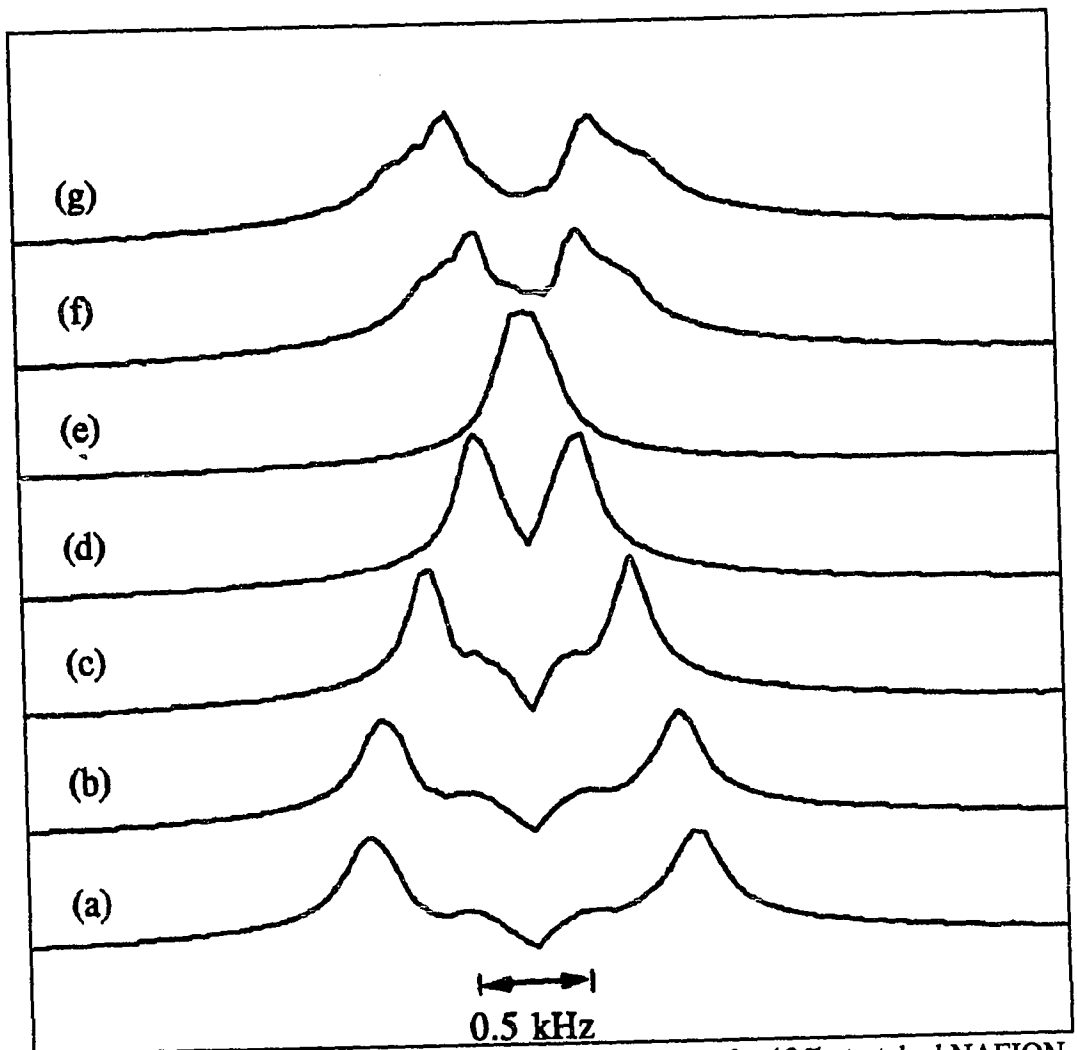

Figure 4.19: Angular variation of deuteron NMR spectra for 13% stretched NAFION-117 containing 6.1 wt% D_2O. (a)-(g), θ = 0°, 15°, 30°, 45°, 60°, 75°, 90°.

Reproduced with permission of the copyright owner. Further reproduction prohibited without permission.

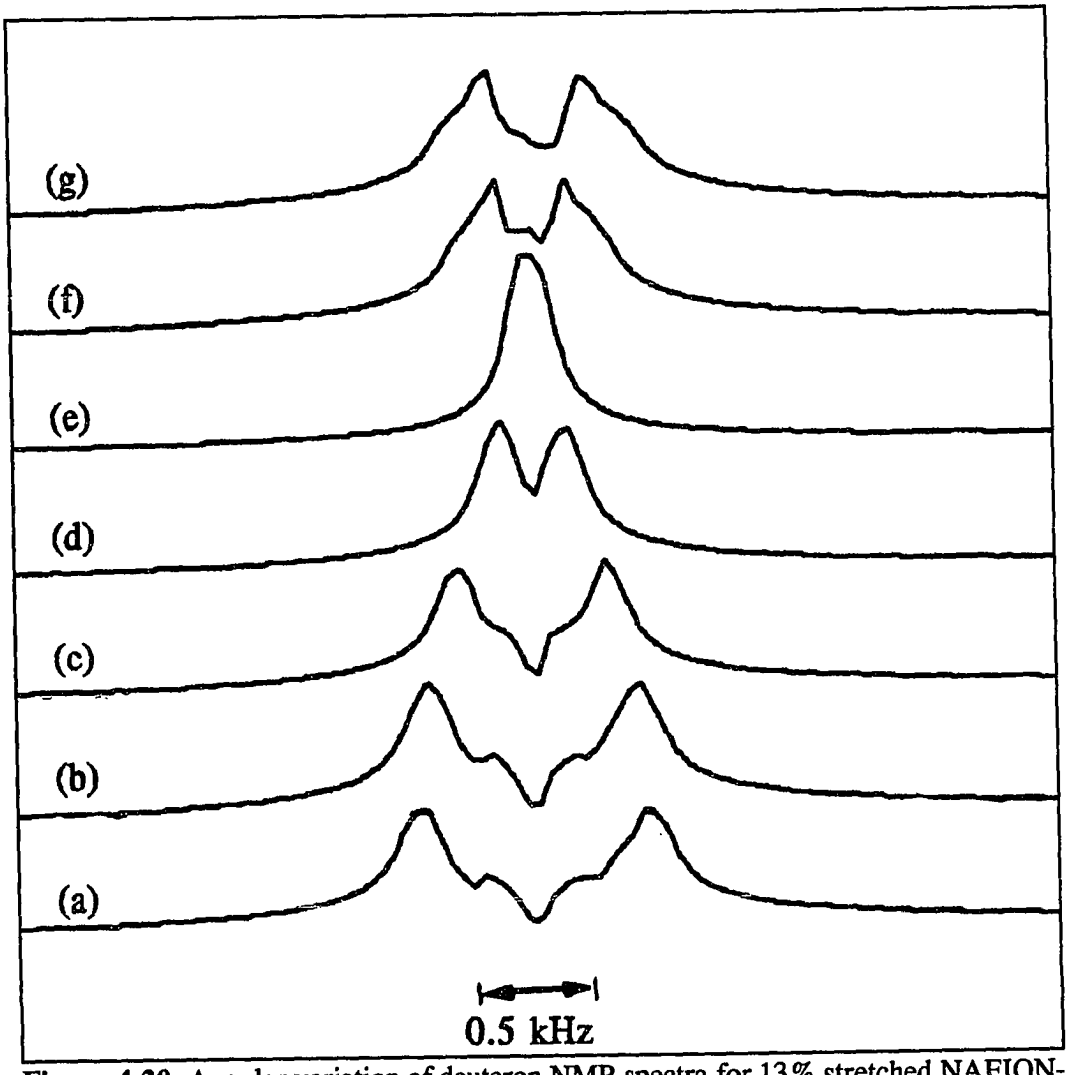

Figure 4.20: Angular variation of deuteron NMR spectra for 13% stretched NAFION-117 containing 8.2 wt% D_2O. (a)-(g), θ = 0°, 15°, 30°, 45°, 60°, 75°, 90°.

Reproduced with permission of the copyright owner. Further reproduction prohibited without permission.

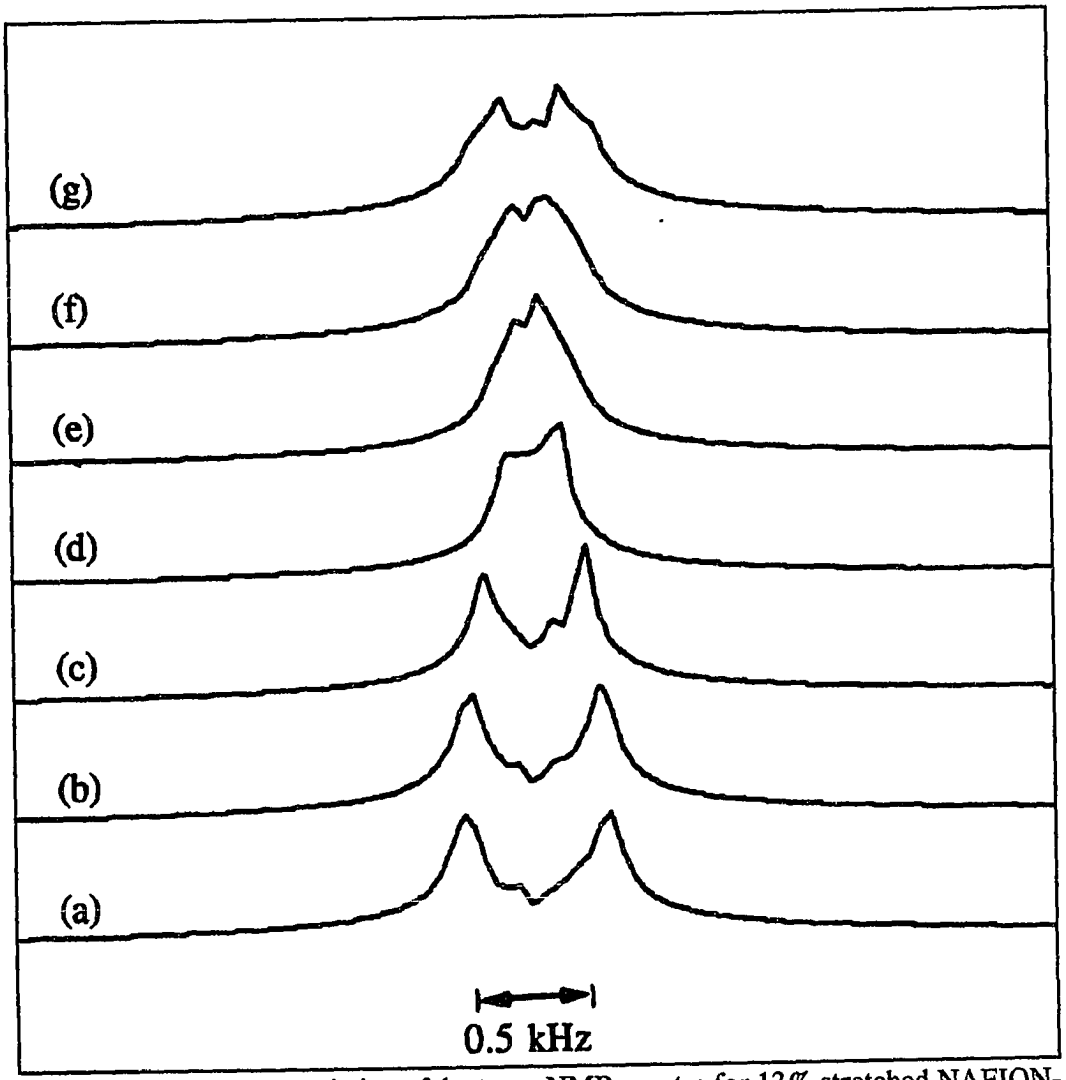

Figure 4.21: Angular variation of deuteron NMR spectra for 13% stretched NAFION-117 containing 10.5 wt% D_2O. (a)-(g), θ = 0°, 15°, 30°, 45°, 60°, 75°, 90°.

Reproduced with permission of the copyright owner. Further reproduction prohibited without permission.

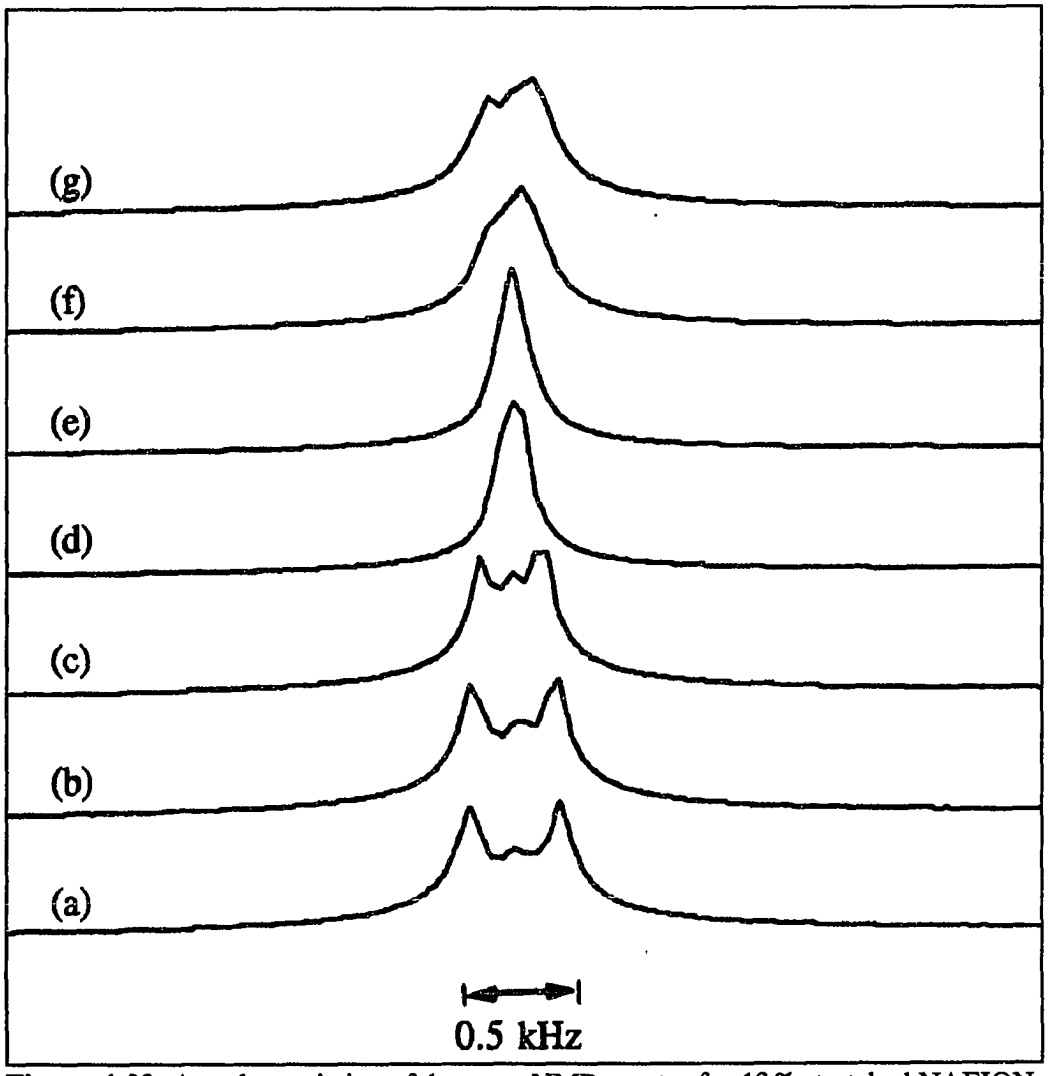

Figure 4.22: Angular variation of deuteron NMR spectra for 13% stretched NAFION-117 containing 14 wt% D_2O. (a)-(g), θ = 0°, 15°, 30°, 45°, 60°, 75°, 90°.

Reproduced with permission of the copyright owner. Further reproduction prohibited without permission.

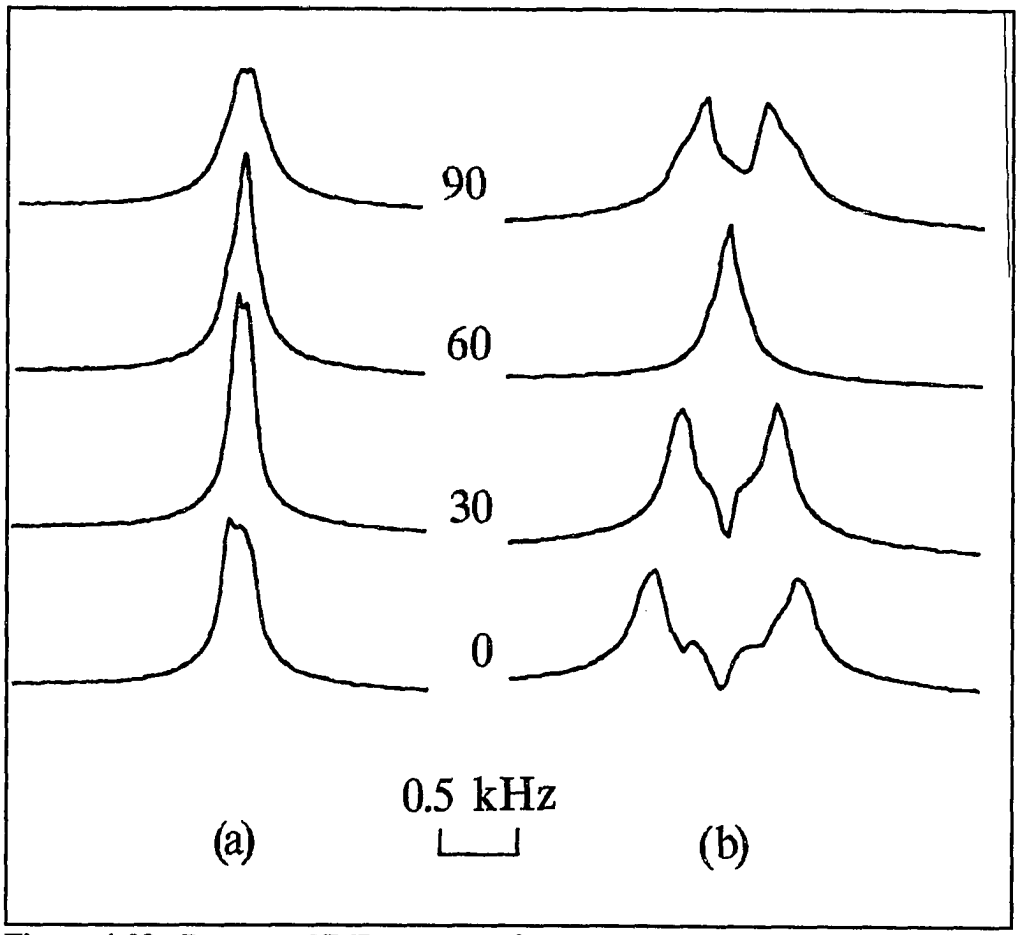

Figure 4.23: Deuteron NMR spectra of NAFION-117 with 8.2 wt% D_2O at θ=0°,30°,60°,90°.(a) unstretched, (b) stretched to 13% elongation.

Reproduced with permission of the copyright owner. Further reproduction prohibited without permission.

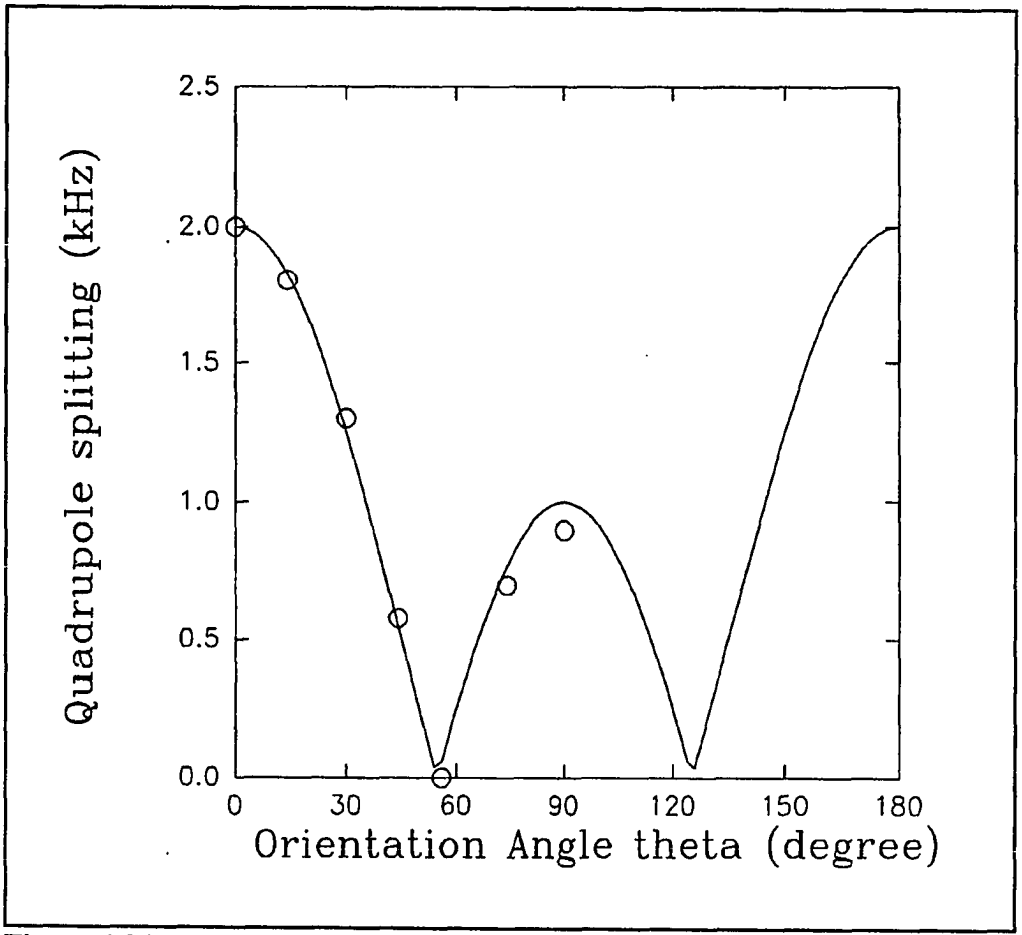

Figure 4.24: The angular dependence of deuteron quadrupole splitting in stretched NAFION-117 containing 8.2 wt% D_2O. The solid line represents the function $3\cos^2\theta$-1.

Reproduced with permission of the copyright owner. Further reproduction prohibited without permission.

The 0° spectra in Figures 4.18-22 suggest the presence of two inequivalent deuteron sites in the stretched samples. Further investigation has been done to check if the lower intensity inner peak has the orientation effect. Two 18% stretched samples containing 15 wt% D_2O were treated identically except for the cutting directions. Sample B is cut along the stretching direction while sample A is cut perpendicular to the stretching direction. Sample B is assembled in such way so that the stretching direction is always perpendicular to the external static magnetic field, i.e. the rotation axis lies along the stretching direction. In sample A the rotation axis is orthogonal to the stretching direction as in the previous measurements (Figures 4.18-22). Evidence that the inner peaks also have an angular dependence is shown in Figure 4.25 (a) and (b). From 4.25-a, we see the outer peaks followed same angular dependence as we have seen before, although the intensity of inner peaks is not as strong as that of the previous spectra, they do exist and exhibit no variations as θ changes. The reason for the low intensity of the inner peaks is probably due to the higher water content of the films, relative to those in Fig 4.19, 4.20. In Figure 4.25-b, the outer peaks remain at the same splitting because the angle θ between the stretching direction and the external field is always 90°, however, the inner peak splitting varies as the angle Ω between sample plane (orthogonal to the stretching direction) and the external field changes. The minimum splitting of the inner peaks occur at the Ω about 0°, resulting in a spectral broadening in the center of the spectrum. The maximum splitting occurs at $\Omega = 60°$, where the two sets of peaks overlap and make the spectral components narrower than at the other angles. Suppose there is a second average EFG axis oriented about 60° to the sample plane, it is easily to see that the splitting variation of the inner peaks also follows

Reproduced with permission of the copyright owner. Further reproduction prohibited without permission.

the relation of $3\cos^2\theta - 1$, when the $\Omega = 0°$, the corresponding angle θ is 60°, leading to a minimum splitting, when the $\Omega = 60°$, the corresponding angle θ is 0°, leading to a maximum splitting. These data confirm the assumption that there are two different deuteron sites in the stretched NAFION membrane. The outer peak of the spectrum is more intense and thus represents most of the deuteron in the sample, which show residual orientation along the stretch direction. The second site is apparently oriented about 60° with respect to the stretched direction. Curiously the ^{17}O results are consistent with only one residual orientation of the EFG tensor (along the stretch direction). The exhibited two sites of deuterons are possibly generated by the sample stretching, and resulting deformation of the water cluster. The clusters are discussed in more detail in Section 4-5.

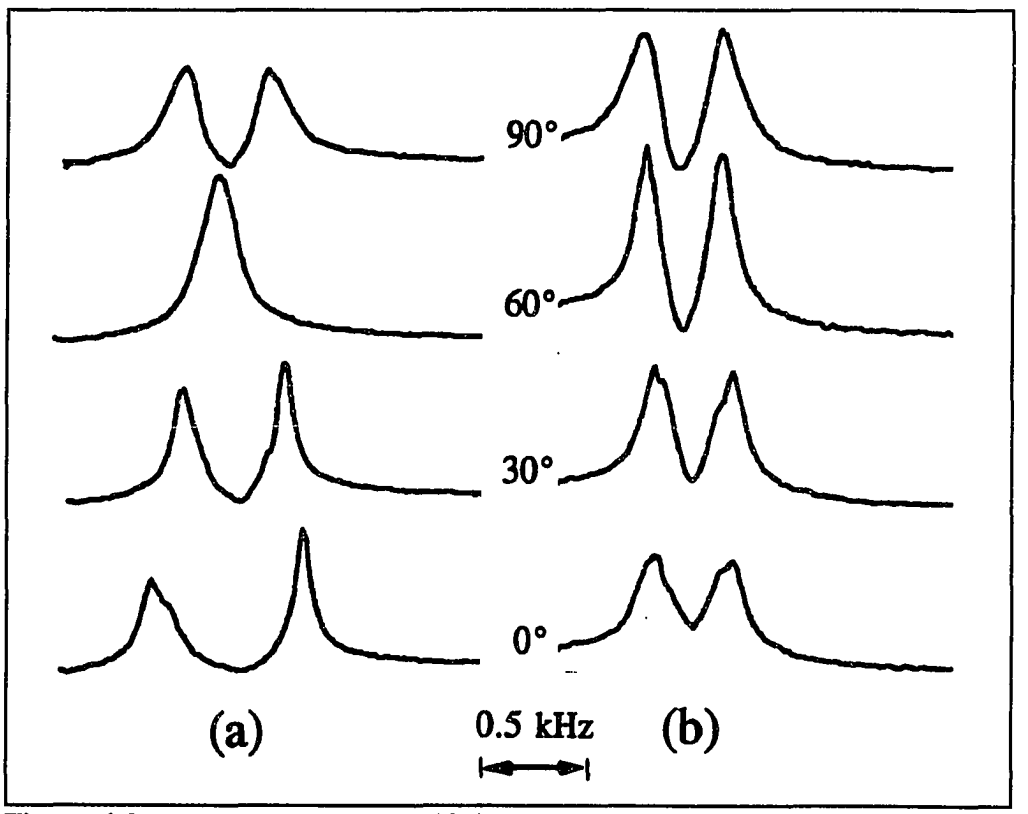

Figure 4.25: Deuteron spectra for 18% stretched NAFION-117 containing 15 wt% D_2O. (a) the rotation axis is orthogonal to the stretch direction, (b) the rotation axis lies along the stretch direction.

Reproduced with permission of the copyright owner. Further reproduction prohibited without permission.

4-2.5. Acid-treated and Non-acid-treated Effect

It is necessary to examine the difference of NMR results for acid-treated and non-treated NAFION-117. Previous studies of NAFION 117 report a large difference in conductivity measurements due to acid treatment. Slade[37] boiled samples in aqueous nitric acid and found that the protonic conductivity has been remarkable enhanced by one and half orders of magnitude compared with that the sample treated by placing it in boiled deionized water. However, the NMR measurement shows that the ^1H self-diffusion coefficients are enhanced by a factor < 3 on acid (as opposed to water) pretreatment. Pineri[36] found that the swelling water properties of the boiled acid NAFION 1200 EW are the same as those of the unboiled sample within one percent, he concluded that a minor effect could therefore be expected between the boiled water pretreatment and unboiled sample. Indeed, our data shows no significant difference between the acid-treated and non-treated NAFION. From Figure 4.26., we can see that the linewidth is slightly narrower for the acid-treated sample than for the non-treated sample. The T_1 values also show small but non-systematic variations for acid-treated sample compared to the non-treated sample. However, the slight differences noted are well within the uncertainty of the variation in water content between the two samples; i.e. small changes in water content ($\sim$ 0.5 wt%) can produce comparable T_1 and linewidth effects. Considering the very wide temperature range represented in Figure 4.26, we conclude that there is essentially no difference between treated and non-treated samples.

Reproduced with permission of the copyright owner. Further reproduction prohibited without permission.

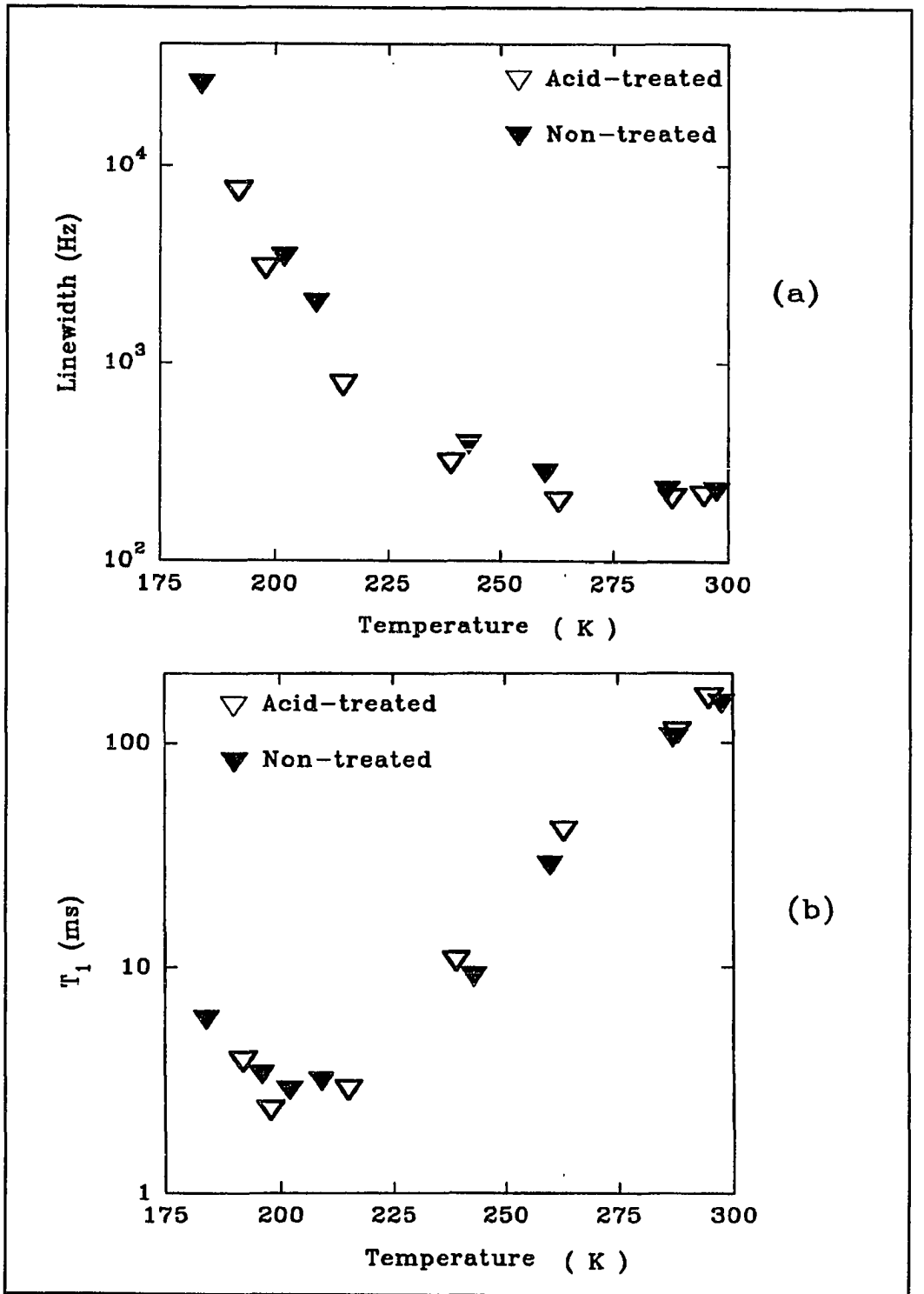

Figure 4.26: Comparisons of deuteron spectra linewidth and T_1 for acid-treated and non-treated NAFION-117 containing 13 wt% D_2O. Temperature dependence of (a) linewidth, (b) T_1.

Reproduced with permission of the copyright owner. Further reproduction prohibited without permission.

4-3. $H_2{}^{17}O$ in NAFION-117

Deuteron NMR studies shed light on the transport of ions (i.e. deuterons) as well as the motion of water molecules, while oxygen-17 NMR probes the details concerning only water molecular motion. In this section, ^{17}O NMR studies of NAFION-117 containing various ^{17}O enriched H_2O contents are presented in a similar manner as in the ^2H NMR results; comparisons of ^{17}O NMR and ^2H NMR results are included.

4-3.1. Water Concentration Effect

^{17}O T_1 measurements show some different features from that of deuteron. Since ^{17}O has a central as well as satellite transitions (with different relaxation times) while ^2H has only a single effective resonance frequency, the recovery profiles were observed to be exponential only at large water content and high temperature, where the high rate molecular motion averages the quadrupole interaction. Figure 4.27 shows several recovery plots with curve fitting. As we can see, the recovery profiles are exponential when the temperature is not so low (287 K, 270 K), the experimental curves can no longer be fit by a single exponential when T is lower (201 K and 183 K).

Reproduced with permission of the copyright owner. Further reproduction prohibited without permission.

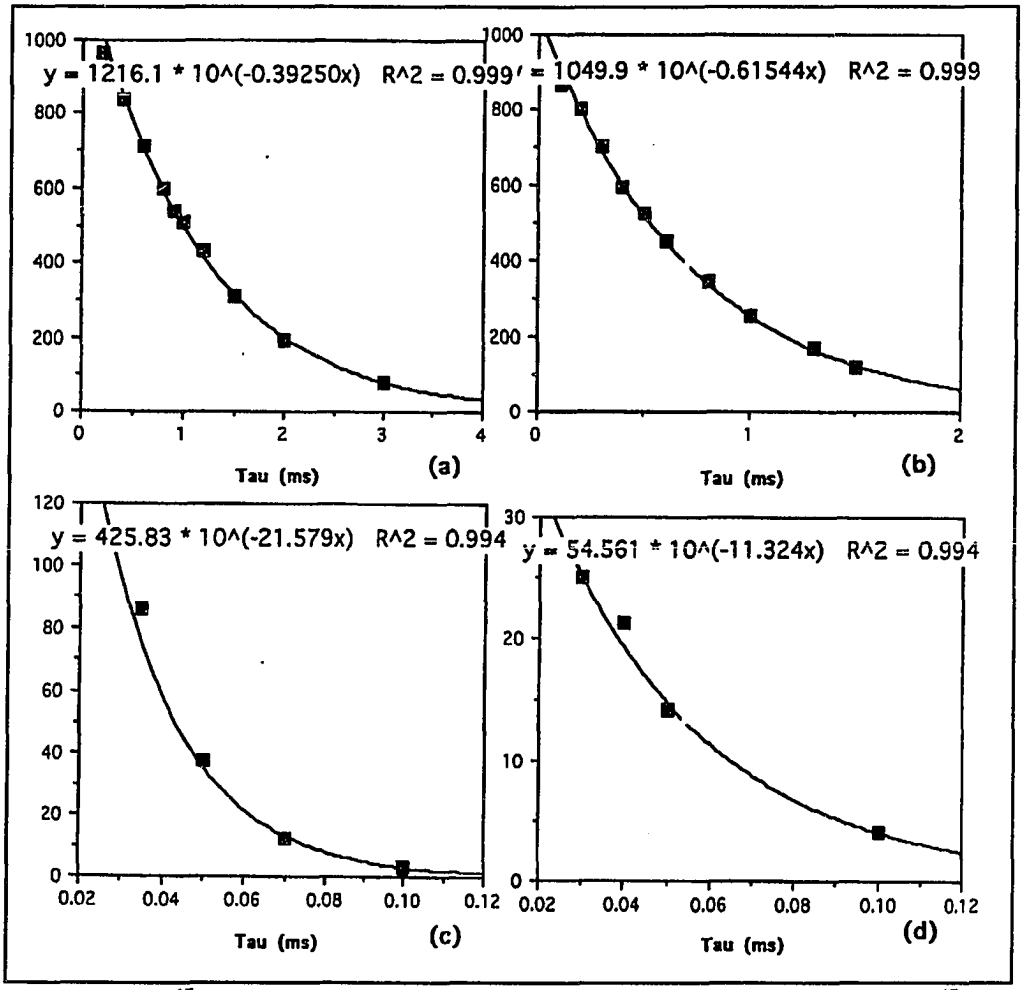

Figure 4.27: ^{17}O T_1 recovery profiles for NAFION-117 with 13.2 wt% $H_2{}^{17}O$ at several different temperature, (a) T = 287 K, (b) T = 270 K, (c) T = 201 K, (d) T = 183 K.

Oxygen-17 spin-lattice relaxation times (T_1) as a function of water content are plotted in Figure 4.28. Since the recovery profiles were not always exponential, determination of T_1 becomes complicated. Therefore two sets of data were plotted, the circles correspond to exponential curve fitting while the triangles were obtained from the relation $T_1 = \tau_0/\ln 2$, where τ_0 is the time separation between the two pulses in the inversion recovery sequence corresponding to a null signal. It can be seen, at the high

Reproduced with permission of the copyright owner. Further reproduction prohibited without permission.

water content (> 10 wt%), the T_1 data obtained by both methods are in good agreement, which means that the large fraction of the "free" water averages the quadrupole interaction. At low water content there are some deviations because of non-exponential profiles. The T_1 value of 0.26 ms for 6.0 wt% increases to 1.8 ms for 15.7 wt%, following the trends observed for deuteron T_1, i.e. the larger water content, the larger the T_1.

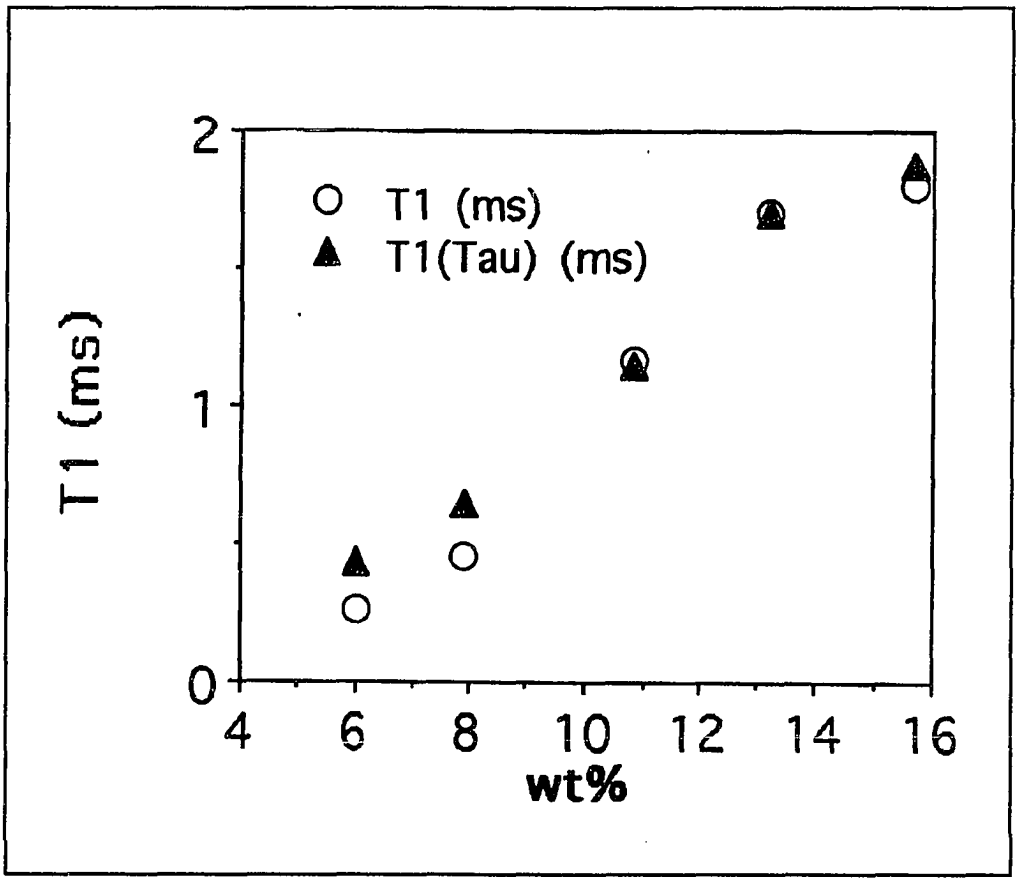

Figure 4.28: Oxygen-17 T_1 as a function of water content in NAFION-117 membranes.

Oxygen-17 lineshapes vs. water content are displayed in Figure 4.29. The plane of NAFION membranes is parallel to the external field H_0. The spectra show a central

Reproduced with permission of the copyright owner. Further reproduction prohibited without permission.

transition peak and two inner satellites when the water content is low. The outer satellites are unresolved.

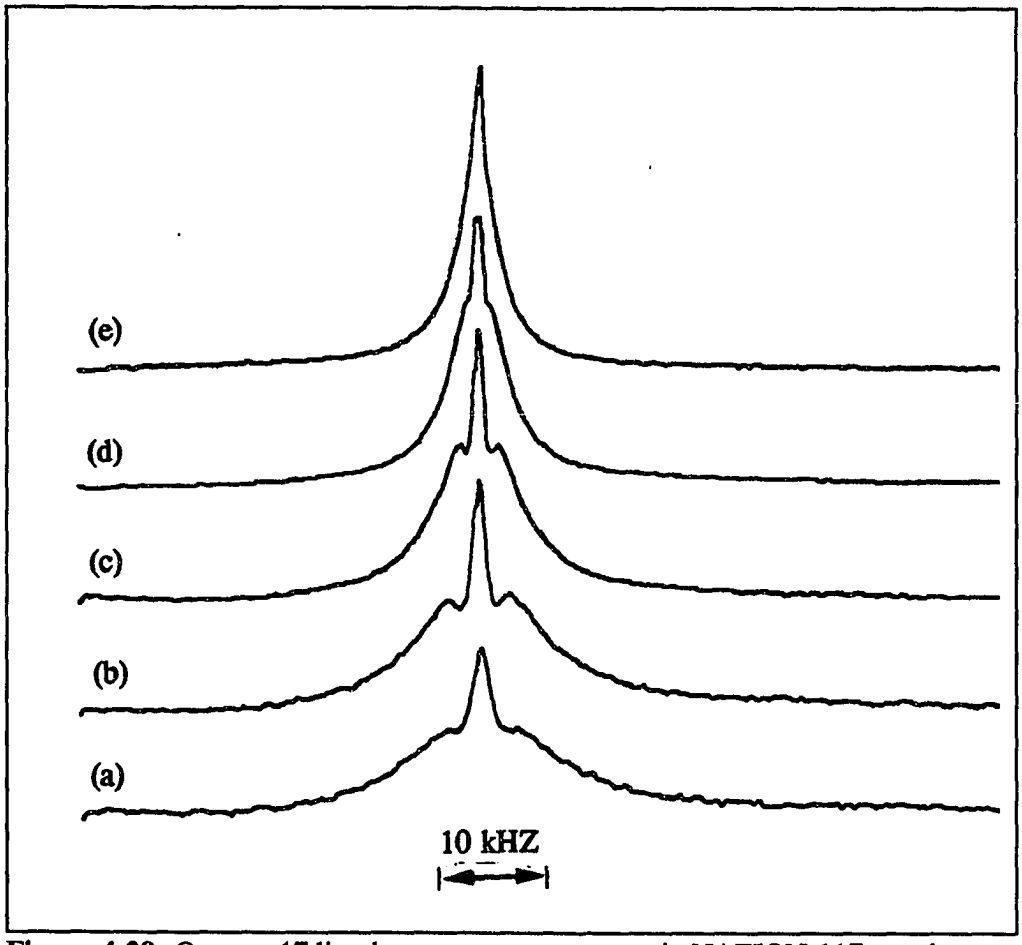

Figure 4.29: Oxygen-17 lineshapes vs. water content in NAFION-117 membranes. (a) 6.0 wt%, (b) 7.9 wt%, (c) 10.9 wt%, (d) 13.2 wt%, (e) 15.7 wt%.

In order to have a quantitative description of the spectra as a function of water content, we define a Δf, the separation of two peaks of satellites, and ΔF, the linewidth of the satellites, when the samples are at 0° degree orientation; the overall linewidth $\Delta\nu$ is determined when the samples are at 54.7° orientation, where the satellites vanish. Figure 4.30 displays the definitions.

Reproduced with permission of the copyright owner. Further reproduction prohibited without permission.

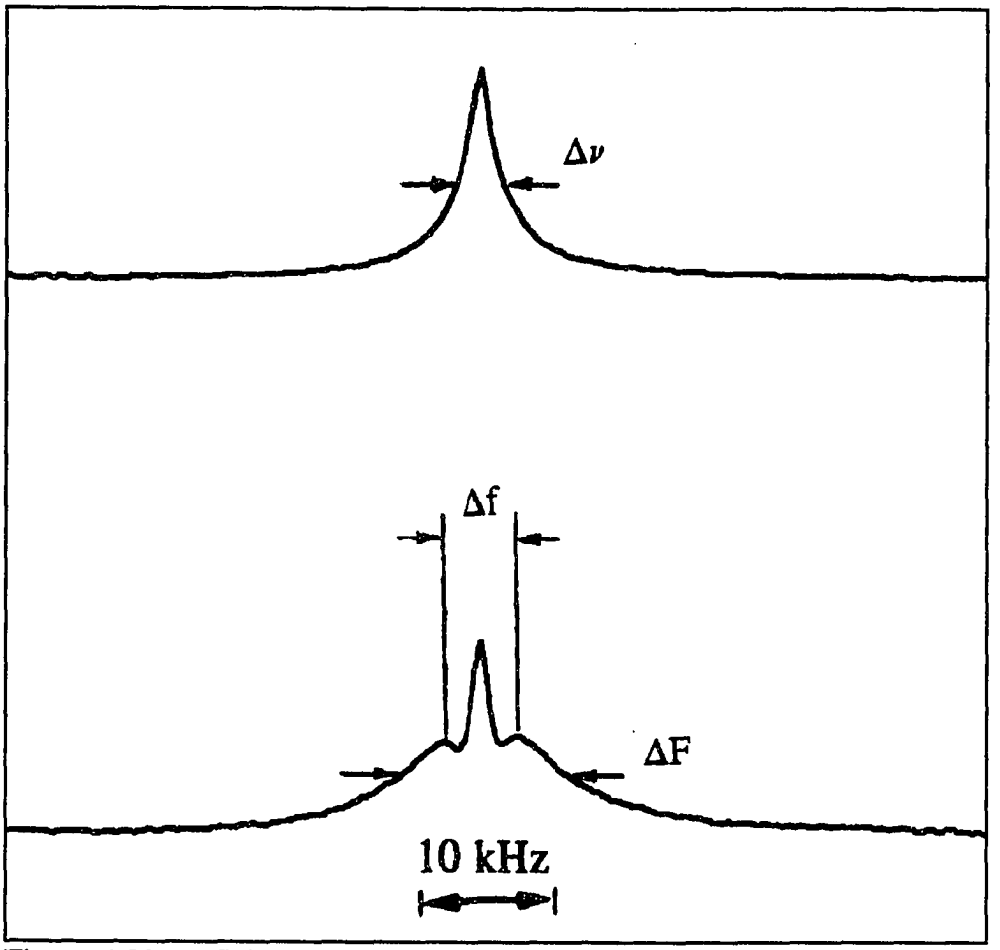

Figure 4.30: Definitions of Δf, ΔF, and Δν; (bottom): Δf, ΔF were measured when the sample is at 0° orientation, (top): Δν was measured at 54.7° orientation.

The Δf as a function of water content is plotted in Figure 4.31a, the separation decreases from 6.7 kHz to 1.5 kHz as the water content increases from 6.0 wt% to 15.7 wt%. The linewidths Δν for central transition and the linewidths of two satellites ΔF are plotted in Figure 4.31b. The linewidth Δν decreases 4.1 kHz to 1.9 kHz, and the linewidth for the satellites ΔF decreases from 18.3 kHz to 3.9 kHz. All of these results provide evidence for rapid exchange and motional effects at higher water content.

Reproduced with permission of the copyright owner. Further reproduction prohibited without permission.

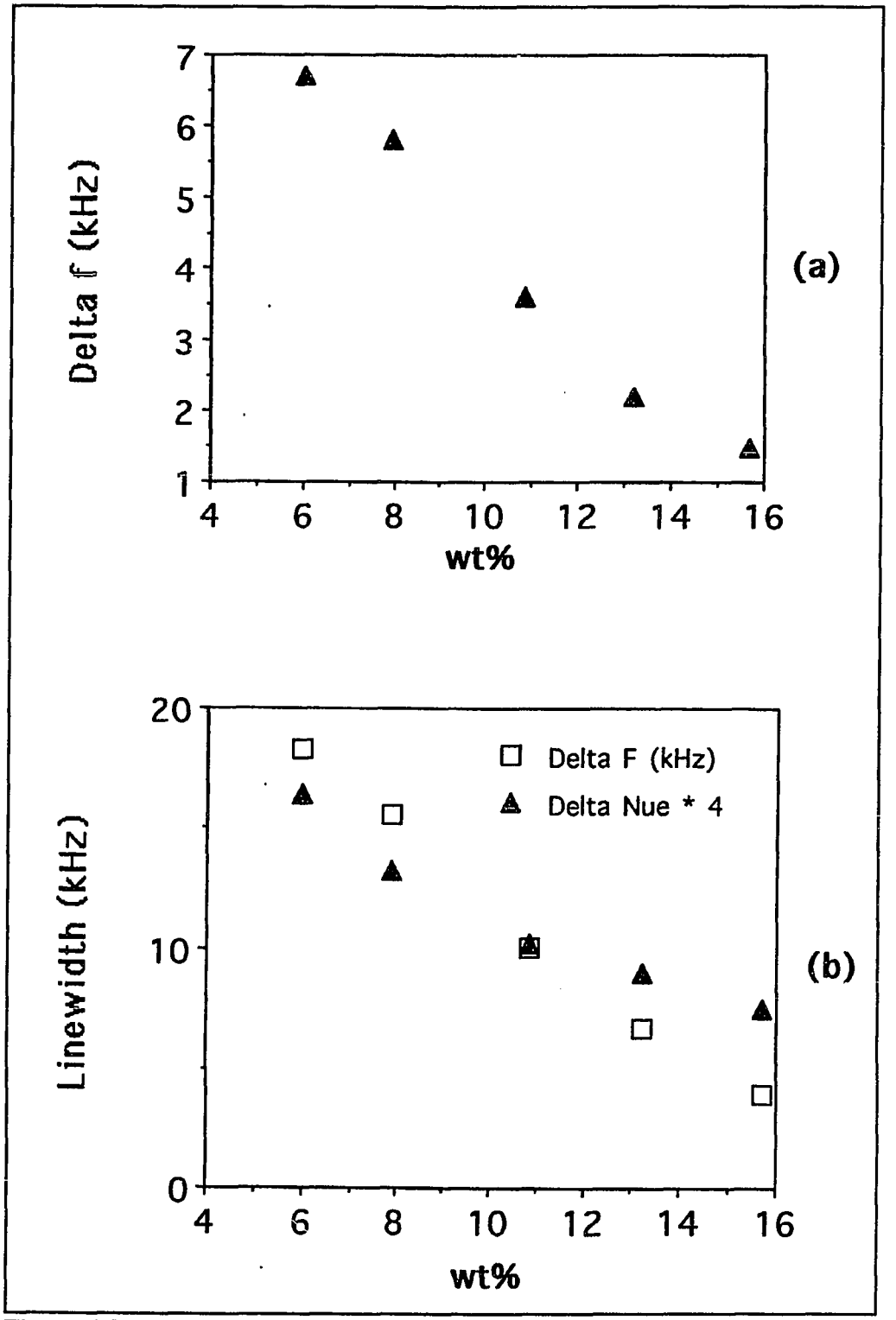

Figure 4.31: The linewidths and separations as a function of water content, (a) The separation of two satellites (Δf) at 0°, (b) The linewidths (Δν) at 54.7° and the linewidth of satellites (ΔF) at 0° orientation.

Reproduced with permission of the copyright owner. Further reproduction prohibited without permission.

4-3.2. Low Temperature Behavior

In order to obtain additional information regarding the dynamics of water in NAFION-117, variable temperature linewidth and T_1 measurements were performed. For linewidth measurements, samples orientated close to magic angle were utilized in order to suppress the anisotropies as described for the deuteron measurements. T_1 as a function of temperature for NAFION containing various $H_2{}^{17}O$ contents is plotted in Figure 4.32, The three different water contents (10.9 wt%, 13.2 wt%, and 15.7 wt%) apparently yield the same temperature dependence. At temperatures below ~ 225 K, the value of T_1 is very short (ca. 20 μs), and cannot be measured reliably because it becomes comparable to the width of the inverting pulse. The minimum T_1 occurs at about 201 K for 13.2% water content, which is close to the T_1 minimum for the deuterons. The Larmor frequency for oxygen-17 is 42 MHz, compared with for deuteron, the ^{17}O results thus yield estimated correlation time consistent with ^2H results. Arrhenius plots of ^{17}O T_1 in NAFION-117 containing various water contents are displayed in Figure 4.33. The thermal activation energies extracted from the data in Figure 4.33 are listed in Table 4.5. The trend of increasing activation energy as the larger water contents is the same as the deuteron results, but the E_A obtained from ^{17}O is somewhat larger than that from ^2H.

Table 4.5: Activation Energies From Figure 4.32.

Water content (wt%)	E_A (eV) $\pm$ 0.01eV
10.9	0.22
13.2	0.24
15.7	0.28

Reproduced with permission of the copyright owner. Further reproduction prohibited without permission.

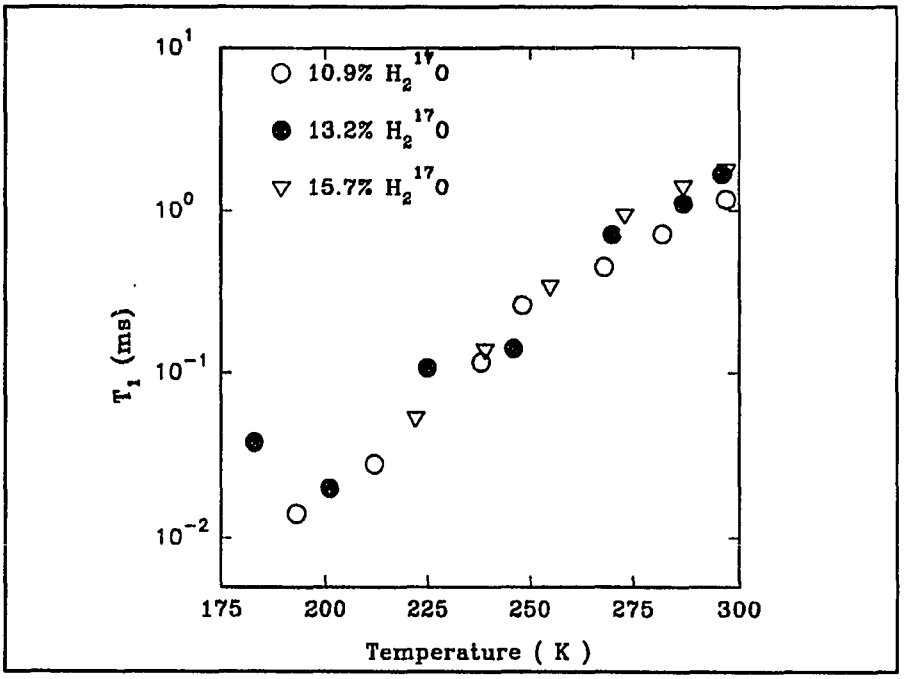

Figure 4.32: Oxygen-17 T_1 temperature dependence for NAFION-117 containing various water contents.

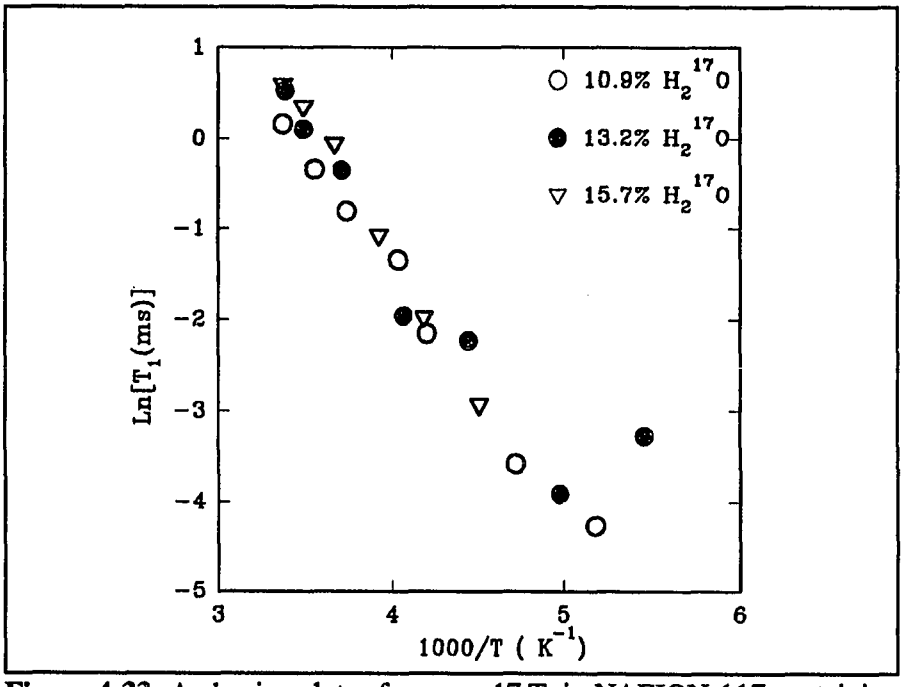

Figure 4.33: Arrhenius plots of oxygen-17 T_1 in NAFION-117 containing various water contents.

Reproduced with permission of the copyright owner. Further reproduction prohibited without permission.

The general shapes of the ^{17}O spectra for NAFION-117 containing 6.0 wt% and 15.7 wt% water are displayed in Figure 4.34 and 35, respectively. For 6.0 wt% sample, the spectra show a central transition peak as well as two satellites at 24 °C, the satellites disappear at -15°C, the line broadens as the temperature decreases until reaching 32 kHz, at -64°C, then the linewidth begins to decrease as the temperature decreases. Further decreasing of temperature will lead to line broadening again. The 15.7 wt% sample shows the same features as the 6.0 wt% sample. The linewidth starts from 3 kHz at room temperature and increases as the temperature decreases, reaching a value of 33.7 kHz, when T = -65°C. Upon further decrease in temperature, the linewidth then decreases to a minimum, 13.5 kHz, at T = -98°C, below this temperature the line then broadens again as the temperature keeps decreasing. The temperature dependences of the linewidth for NAFION-117 containing various water contents are plotted in Figure 4.36. Arrhenius plots of the data in Figure 4.36 are plotted in Figure 4.37. The curves in the Arrhenius plots follow the temperature dependence predicted for a second-order quadrupole broadened central transition, shown schematically in Figure 4.38[77]. The high-T region, equivalent to short motional correlation time τ, corresponds to the extreme narrowing limit $\omega_L\tau << 1$, where ω_L is the Larmor frequency. As T is lowered (or τ increased) the linewidth reaches a maximum associated with the T_1 minimum occurring at ca.$\omega_L\tau = 1$. Lowering T further reduces the linewidth until a minimum is reached, corresponding to a τ-value of the order of $1/\omega_Q$, where ω_Q is the strength of the quadrupole interaction (on the order of several MHz). Further reduction in T (increases in τ) broadens the line until the rigid limit of the second-order linewidth, ω_Q^2/ω_L is reached. Evaluation of the correlation times from the data in Figure 4.37 yields τ =

Reproduced with permission of the copyright owner. Further reproduction prohibited without permission.

3.8×10^{-9} s at ca. 205 K and $\tau \sim 1.6\times10^{-7}$ s at ca. 180 K, and approaching to 6.7×10^{-6} s for T lower than 150 K.

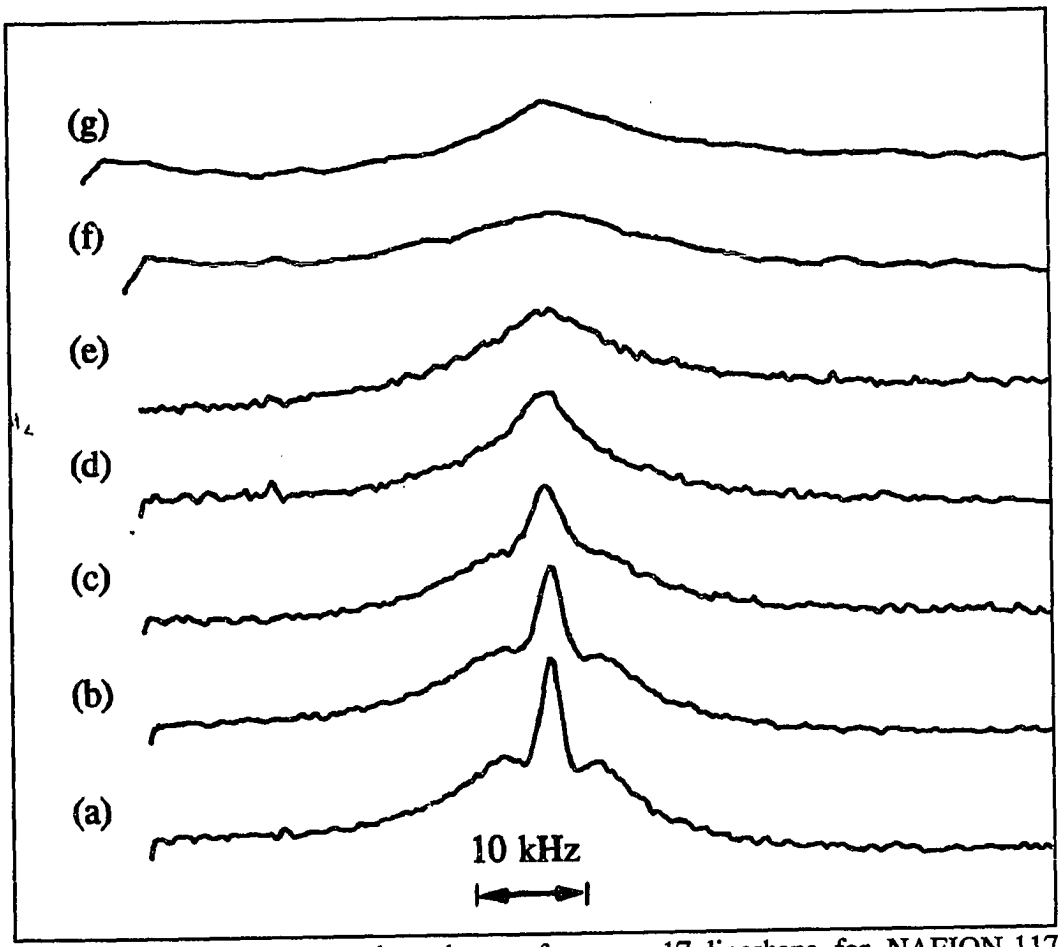

Figure 4.34: Temperature dependence of oxygen-17 lineshape for NAFION-117 containing 6.0% $H_2{}^{17}O$. (a) 24 °C, (b) 15 °C, (c) 0 °C, (d) -15 °C, (e) -32 °C, (f) -64 °C, (g) -80 °C.

Reproduced with permission of the copyright owner. Further reproduction prohibited without permission.

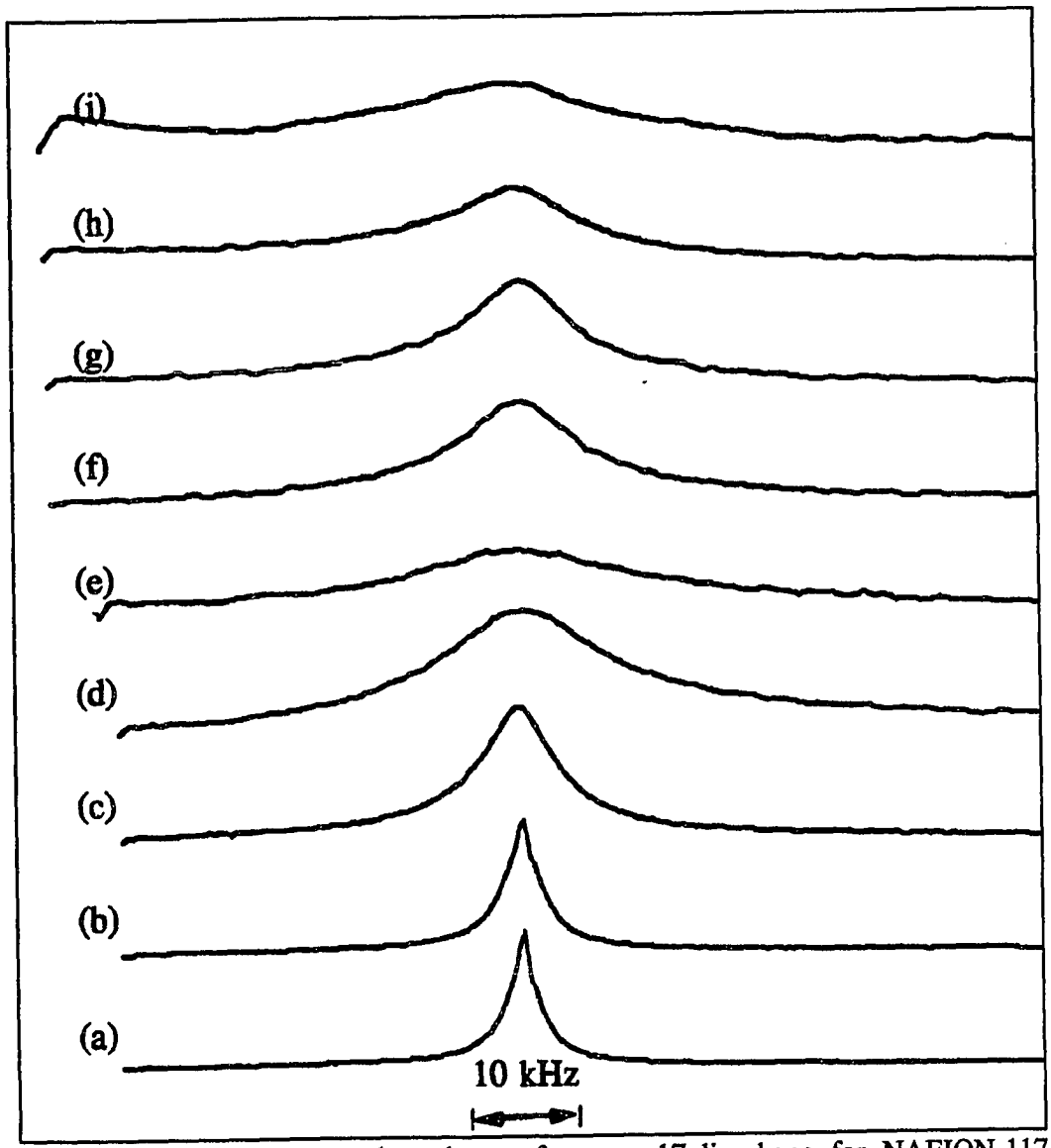

Figure 4.35: Temperature dependence of oxygen-17 lineshape for NAFION-117 containing 15.7% $H_2{}^{17}O$. (a)-(i) 24 °C, 0 °C, -34 °C, -53 °C, -65 °C, -90 °C, -98 °C, -104 °C, -110 °C.

Reproduced with permission of the copyright owner. Further reproduction prohibited without permission.

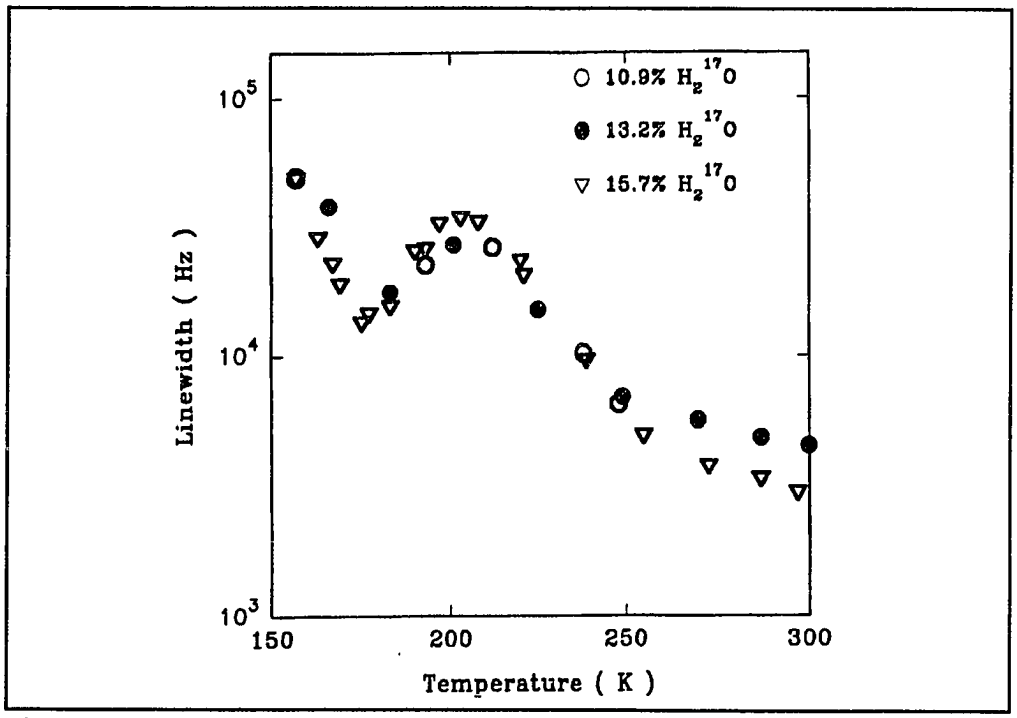

Figure 4.36: Oxygen-17 NMR linewidth temperature dependence for Nafion containing various water contents.

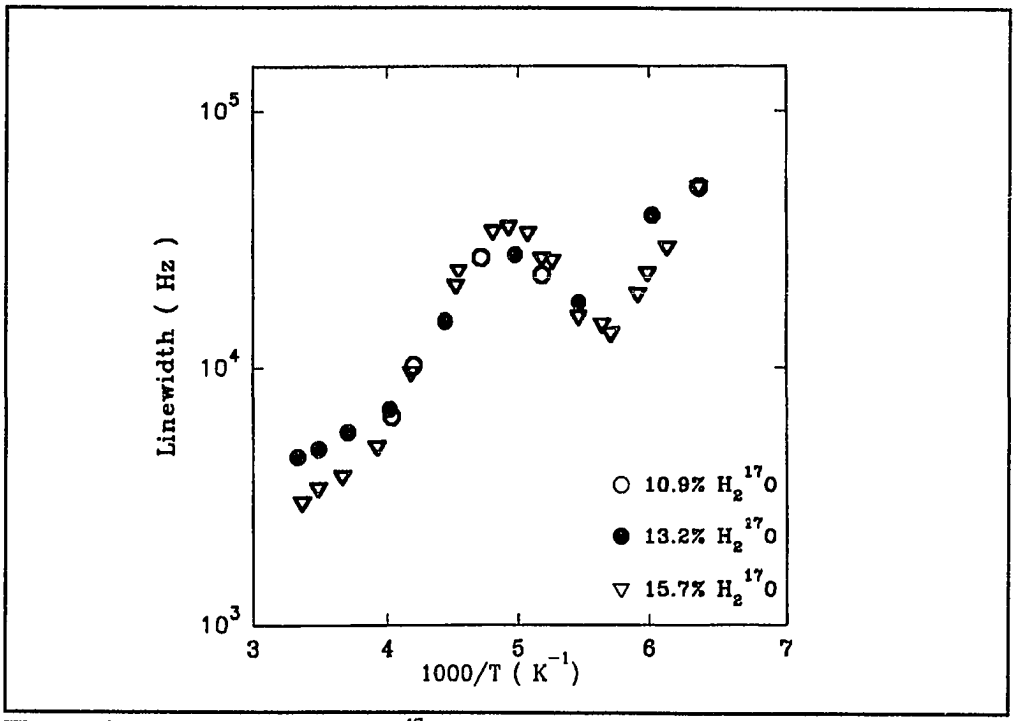

Figure 4.37: Arrhenius plots of ^{17}O linewidth in NAFION-117 containing various water contents.

Reproduced with permission of the copyright owner. Further reproduction prohibited without permission.

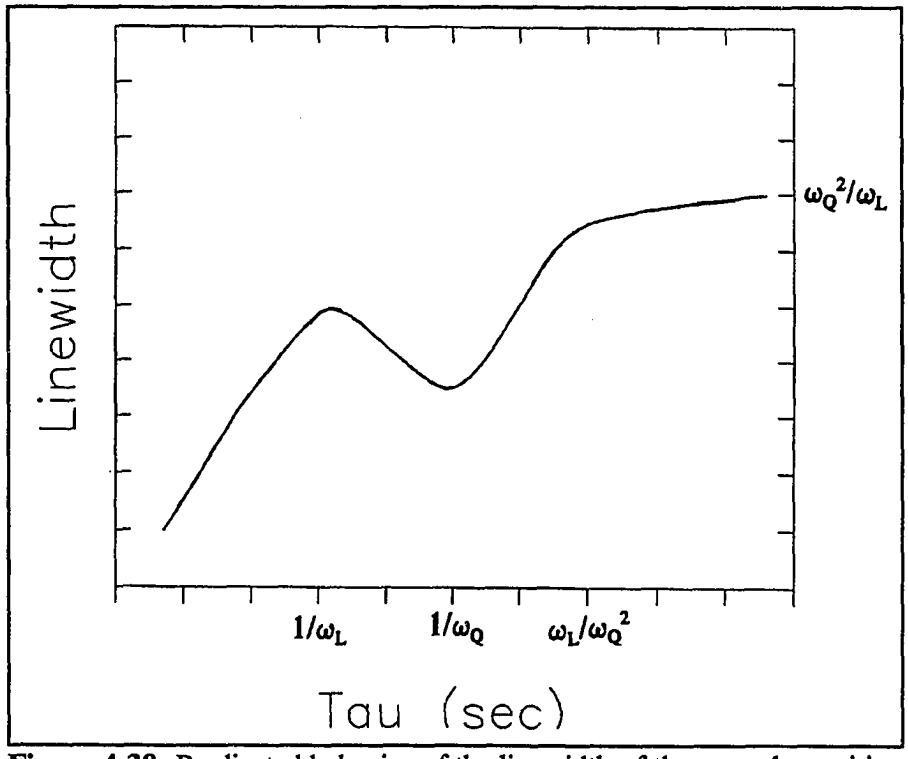

Figure 4.38: Predicated behavior of the linewidth of the central transition for a half-integer spin quadrupole nucleus, as a function of molecular correlation time. Adapted from [77].

Another observation at the temperature lower than ca. 185 K is that the 90° pulse width suddenly changes. The intensity of the FID increases as the pulse width decreases, providing evidence of the second order quadrupole interaction on the central transition. A typical example as shown in Figure 4.39 was taken at 183 K for NAFION-117 containing 13% $H_2{}^{17}O$. We observed that the largest intensity occurs at a pulse width of 3 μs, the smallest intensity occurs when the pulse width = 10 μs. This is because the $\pi/2$ pulse width for -1/2 to 1/2 transition for I = 5/2 is 1/3 the length of a $\pi/2$ pulse for an equivalent I = 1/2 nucleus with the same γ[78]. At this low temperature, the satellites have moved away from the central peak, the excited transition observed is only the central transition, and the line broadening is the second order perturbation of the central

Reproduced with permission of the copyright owner. Further reproduction prohibited without permission.

line. Fenzke[79] et al. calculated the intensities of central line with second order quadrupole interactions in the conditions of $\gamma H_1 = 41$ kHz, $\omega_Q = 300$ kHz and $\eta = 0$ with various pulse width, their results show the intensities of the spectra are 0.26; 0.46; 0.40 and 0.02 for the width equal to 1, 2, 4, and 6 μs, respectively. Our data follow the same trend.

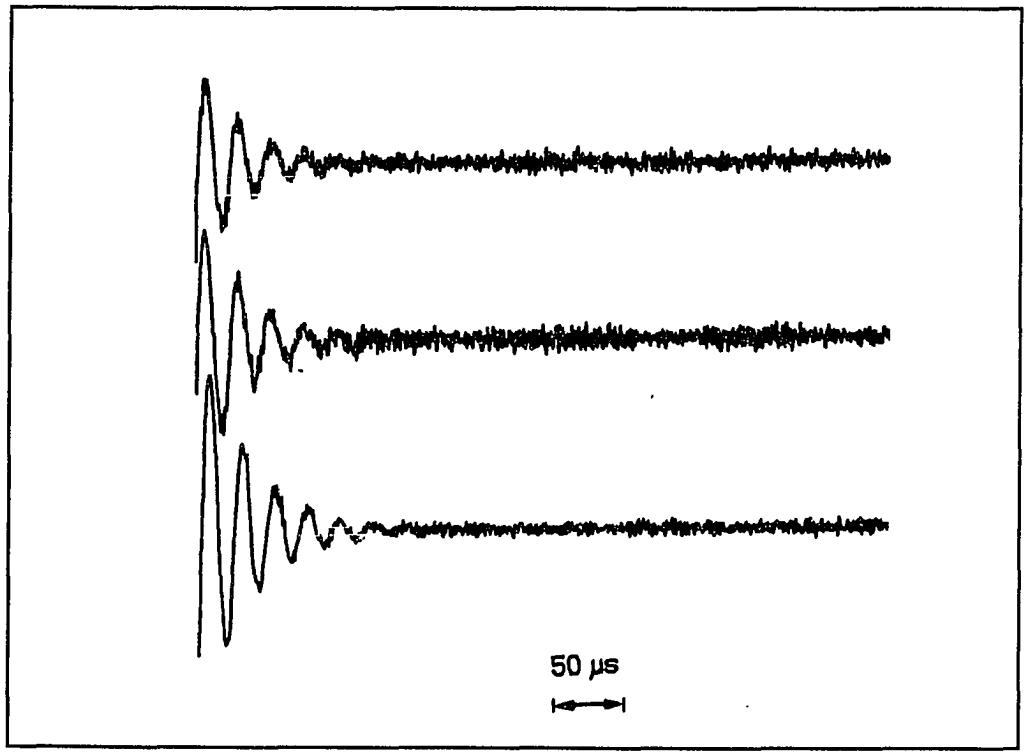

Figure 4.39: Evidence of the second order quadrupole interaction of central transition. top: the smallest intensity; middle: intermediate; bottom: largest intensity, corresponding the pulse width 10, 6, 3 μs, respectively.

4-3.3. Orientation Effect

^{17}O NMR spectra of NAFION-117 membrane stacks containing various water contents are shown in Figures 4.40-44. Because of the considerably larger quadrupole interaction of ^{17}O relative to ^{2}H (for the same molecule), the spectra are correspondingly broader than in Figures 4.12-17. The spectra exhibit unresolved satellite transitions with

Reproduced with permission of the copyright owner. Further reproduction prohibited without permission.

an angular dependence similar to that of Figures 4.12-17, demonstrating that the EFG principal axis (for the ^{17}O quadrupole interaction) is in the plane of the membrane. Thus both the ^{2}H and ^{17}O results indicate that residual molecular orientation for unstretched films resides in the plane of the film.

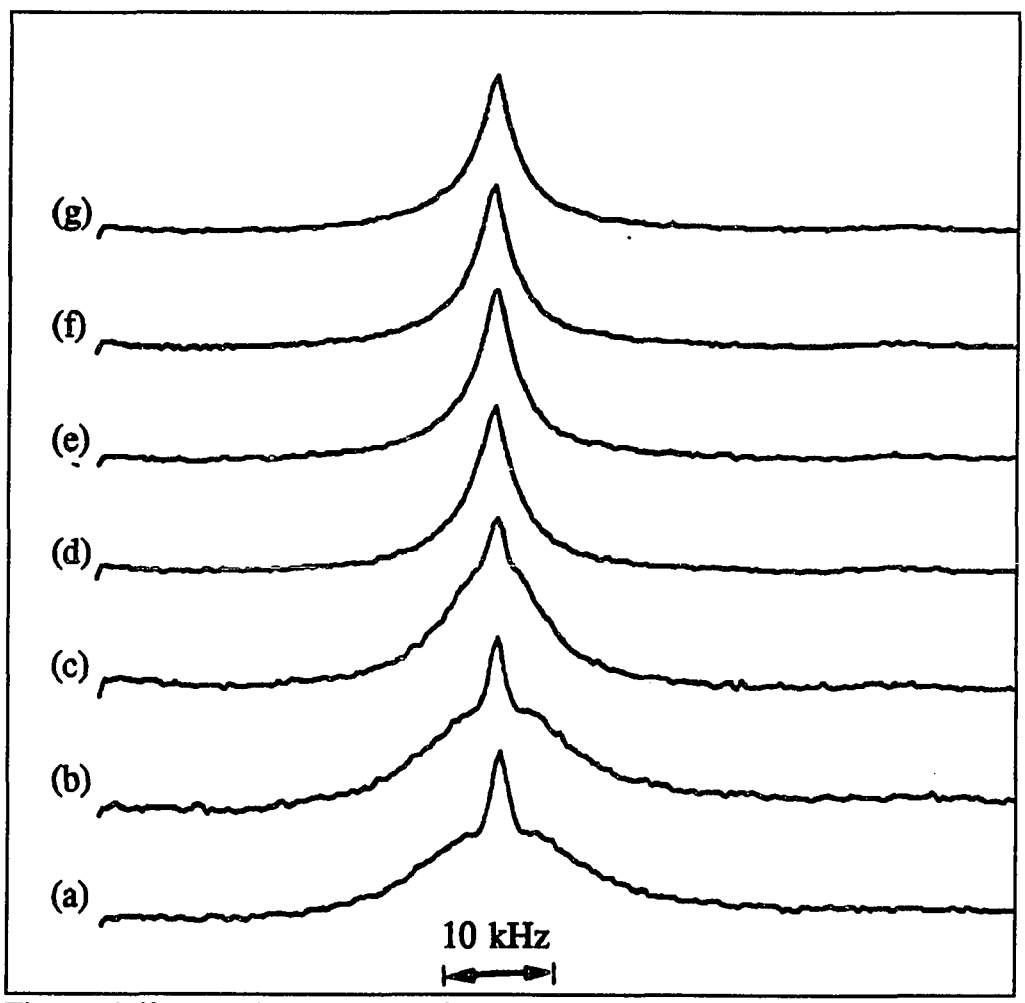

Figure 4.40: Angular variation of oxygen-17 NMR spectra for NAFION-117 containing 6.0 wt% $H_2{}^{17}O$. (a)-(g), θ = 0°, 15°, 30°, 45°, 60°, 75°, and 90°.

Reproduced with permission of the copyright owner. Further reproduction prohibited without permission.

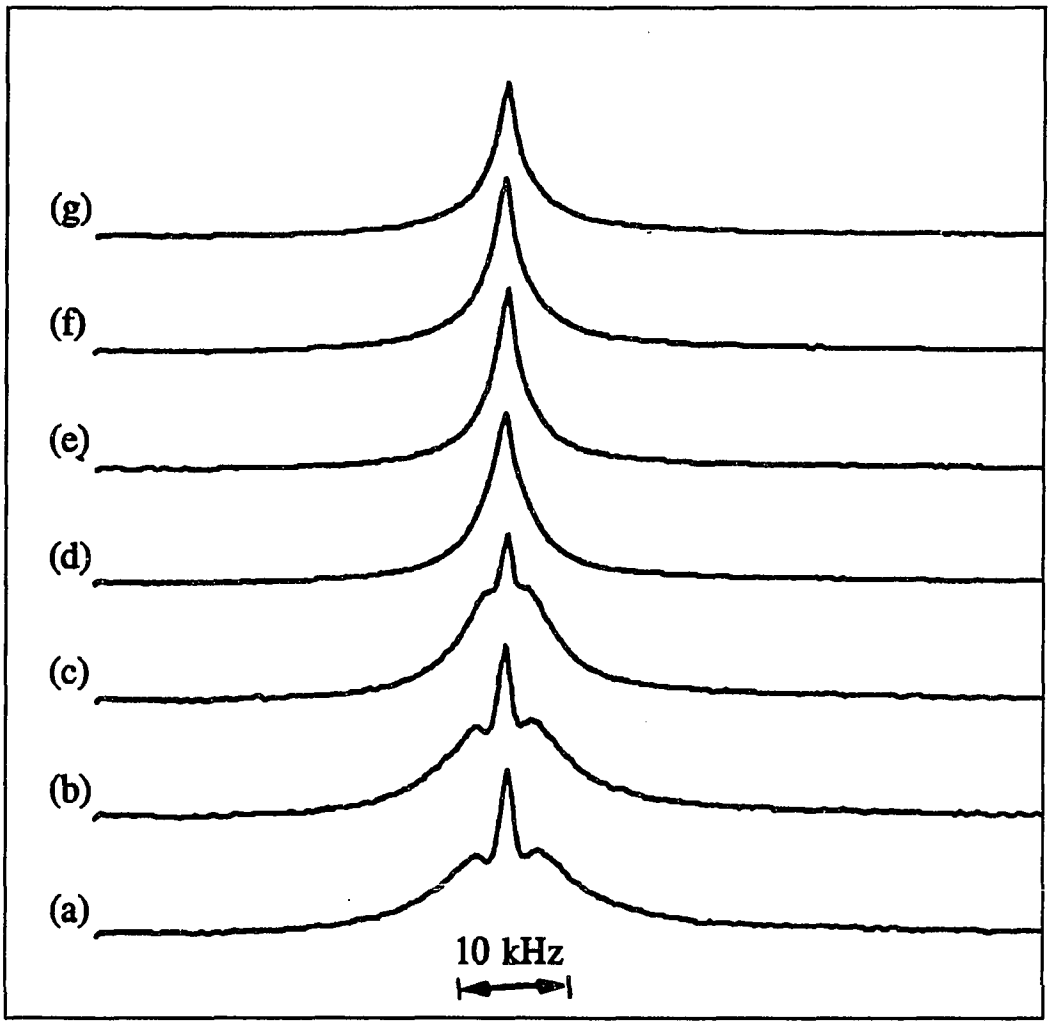

Figure 4.41: Angular variation of oxygen-17 NMR spectra for NAFION-117 containing 7.9 wt% $H_2{}^{17}O$. (a)-(g), θ = 0°, 15°, 30°, 45°, 60°, 75°, and 90°.

Reproduced with permission of the copyright owner. Further reproduction prohibited without permission.

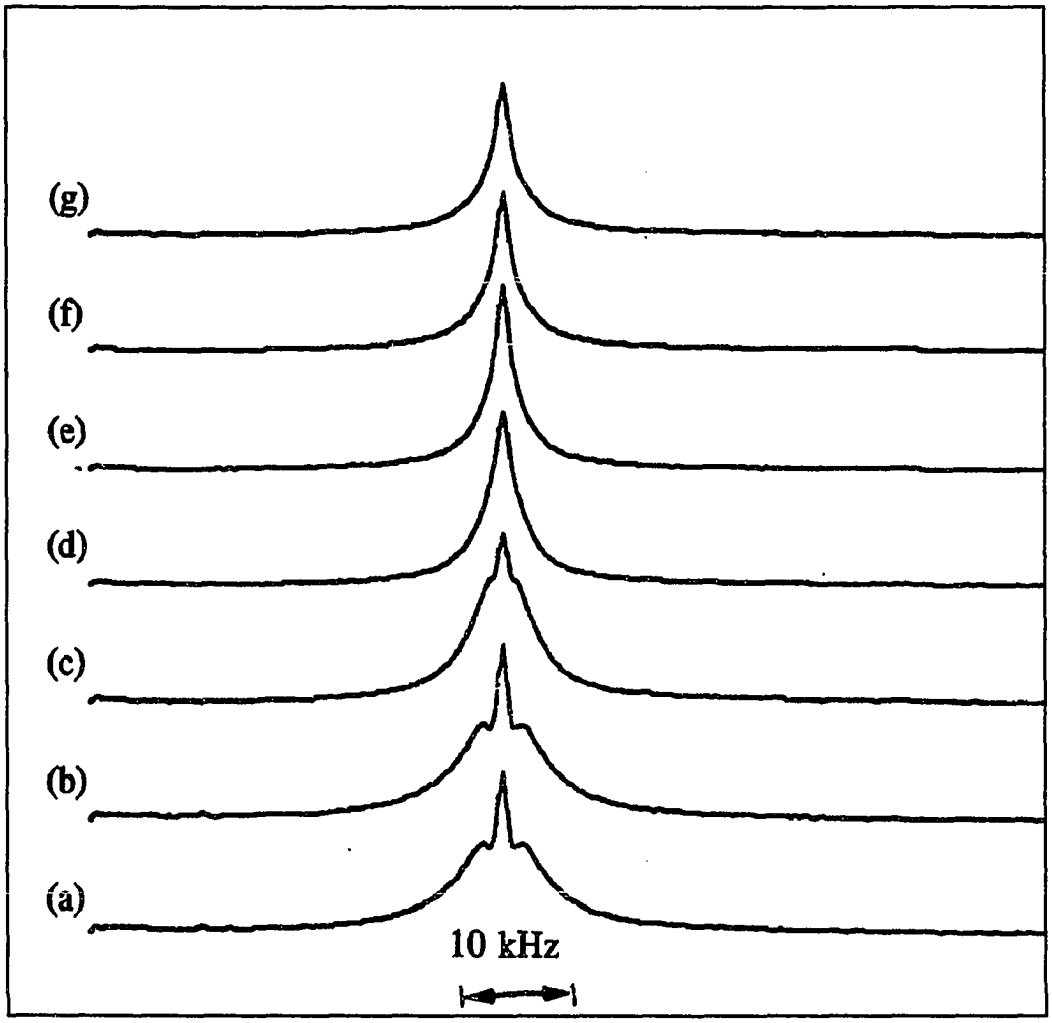

Figure 4.42: Angular variation of oxygen-17 NMR spectra for NAFION-117 containing 10.9 wt% $H_2{}^{17}O$. (a)-(g), θ = 0°, 15°, 30°, 45°, 60°, 75°, and 90°.

Reproduced with permission of the copyright owner. Further reproduction prohibited without permission.

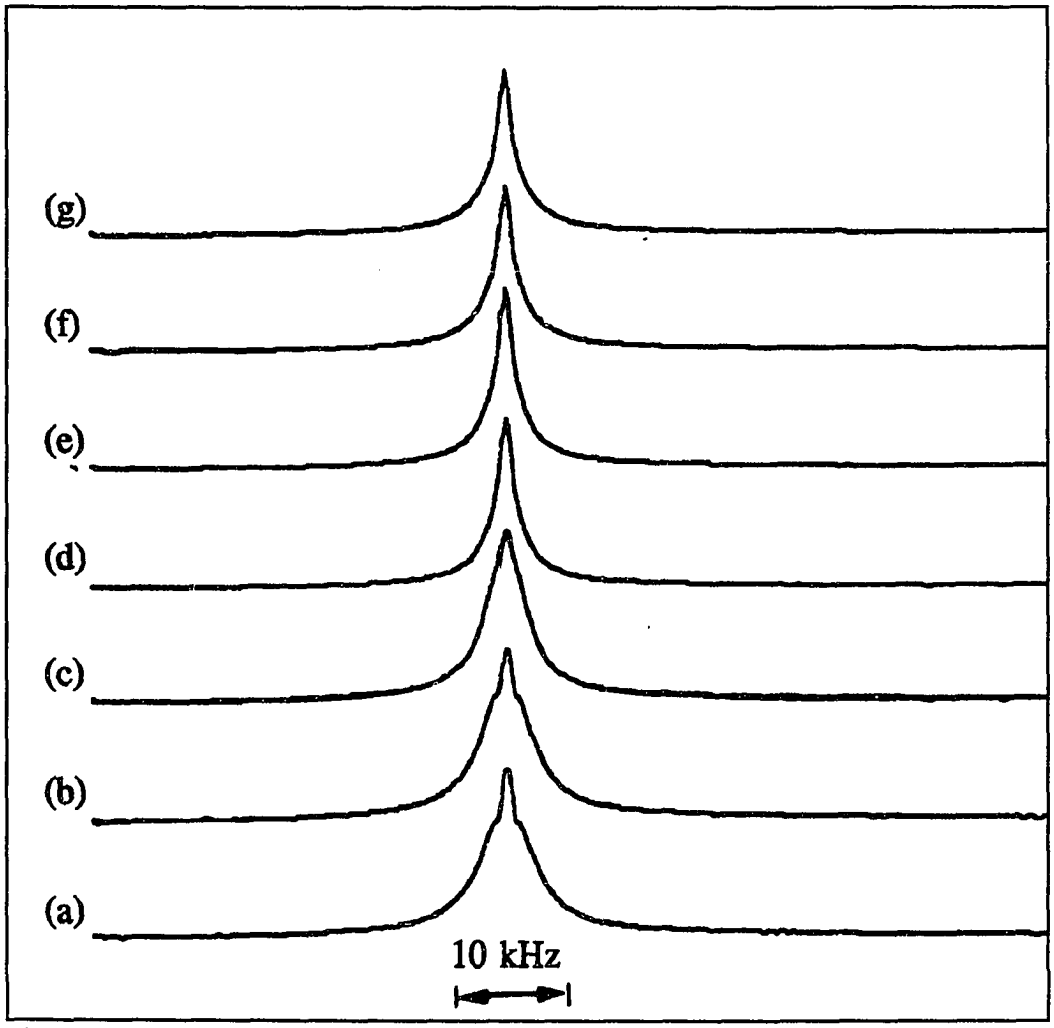

Figure 4.43: Angular variation of oxygen-17 NMR spectra for NAFION-117 containing 13.2 wt% $H_2{}^{17}O$. (a)-(g), θ = 0°, 15°, 30°, 45°, 60°, 75°, and 90°.

Reproduced with permission of the copyright owner. Further reproduction prohibited without permission.

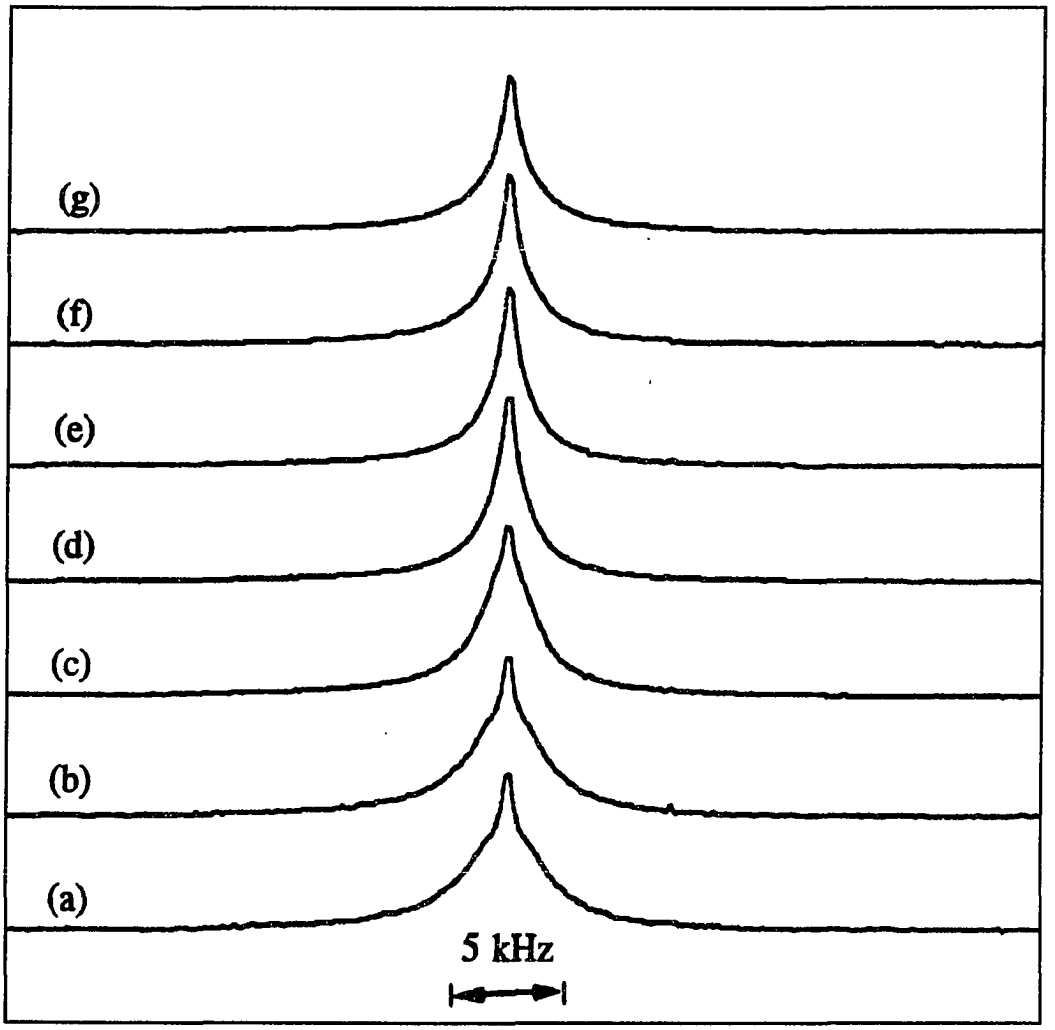

Figure 4.44: Angular variation of oxygen-17 NMR spectra for NAFION-117 containing 15.7 wt% $H_2{}^{17}O$. (a)-(g), θ = 0°, 15°, 30°, 45°, 60°, 75°, and 90°.

Reproduced with permission of the copyright owner. Further reproduction prohibited without permission.

4-3.4. Sample Stretching Effect

As we have seen in deuteron spectra, stretched samples show a doublet splitting as much as seven times larger than that of the unstretched sample. Oxygen-17 also shows dramatic increasing of the splitting in the spectra. Figure 4.45-46 display ^{17}O spectra of a 19%-stretched film containing 6.2 wt% and 13.3% ^{17}O-enriched H_2O, respectively. The unresolved satellites in the spectra of unstretched sample are resolved in the stretched sample. Comparison of the spectra for stretched and unstretched sample is replotted in Figure 4.47. The resolution of the satellite transitions in the 13.3% sample and their angular dependence for the relatively modest anisotropy imposed by the 19% elongation are striking.

Since the spectra show a large orientation effect in the stretched film, examination of the orientation effect on T_1 measurements was also undertaken on the stretched sample. The T_1 values as a function of orientation for 19% stretched NAFION-117 containing 13 wt% $H_2{}^{17}O$ content are listed in Table 4.6. The values in Table 4.6 show a small change when the orientation of the sample varies. The results most likely reflect differences in T_1 for the central and satellite transitions. These were not measured separately but the results in Table 4.6 represent weighted averages of the two contributions. T_1 results quated for all other samples were therefore taken on films oriented at ca. 55° to suppress the anisotropy.

Table 4.6: Angular variation of oxygen-17 T_1 for NAFION-117 containing 13 wt% $H_2{}^{17}O$.

Orientation	0°	15°	30°	45°	60°	75°	90°
T_1 (ms)	1.33	1.33	1.30	1.38	1.43	1.42	1.41

Reproduced with permission of the copyright owner. Further reproduction prohibited without permission.

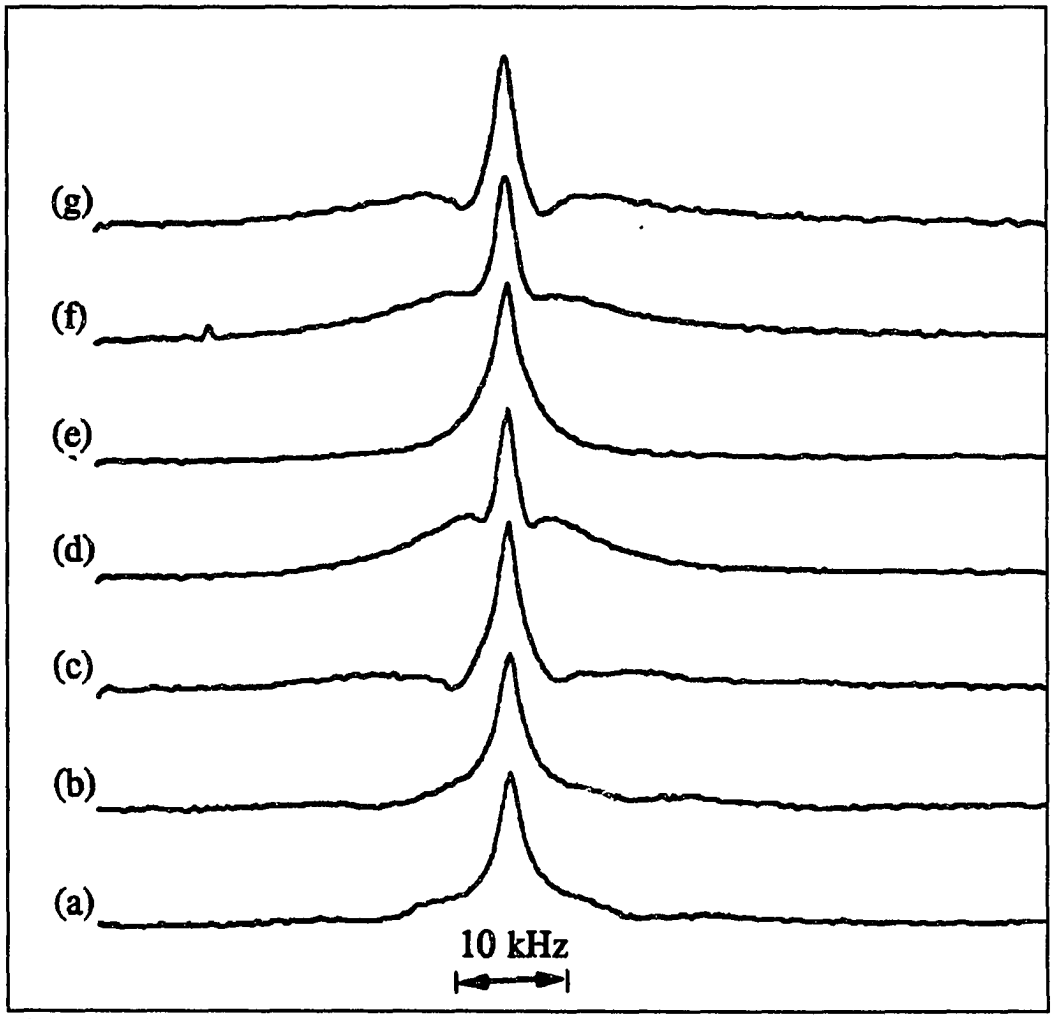

Figure 4.45: Angular variation of oxygen-17 NMR spectra for 19% stretched NAFION-117 containing 6.2 wt% $H_2{}^{17}O$. (a)-(g), θ = 0°, 15°, 45°, 60°, 75°, and 90°.

Reproduced with permission of the copyright owner. Further reproduction prohibited without permission.

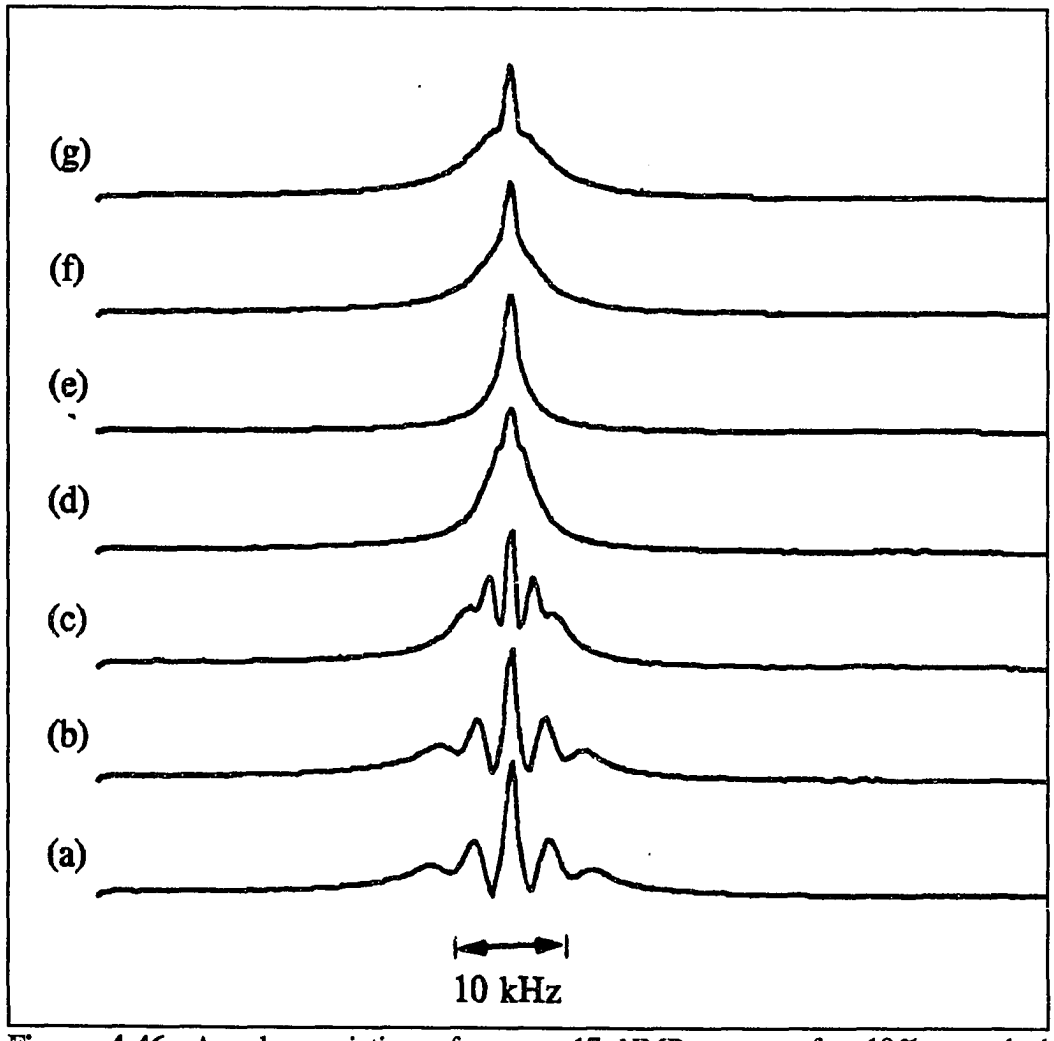

Figure 4.46: Angular variation of oxygen-17 NMR spectra for 19% stretched NAFION-117 containing 13.3 wt% $H_2{}^{17}O$. (a)-(g), θ = 0°, 15°, 45°, 60°, 75°, and 90°.

Reproduced with permission of the copyright owner. Further reproduction prohibited without permission.

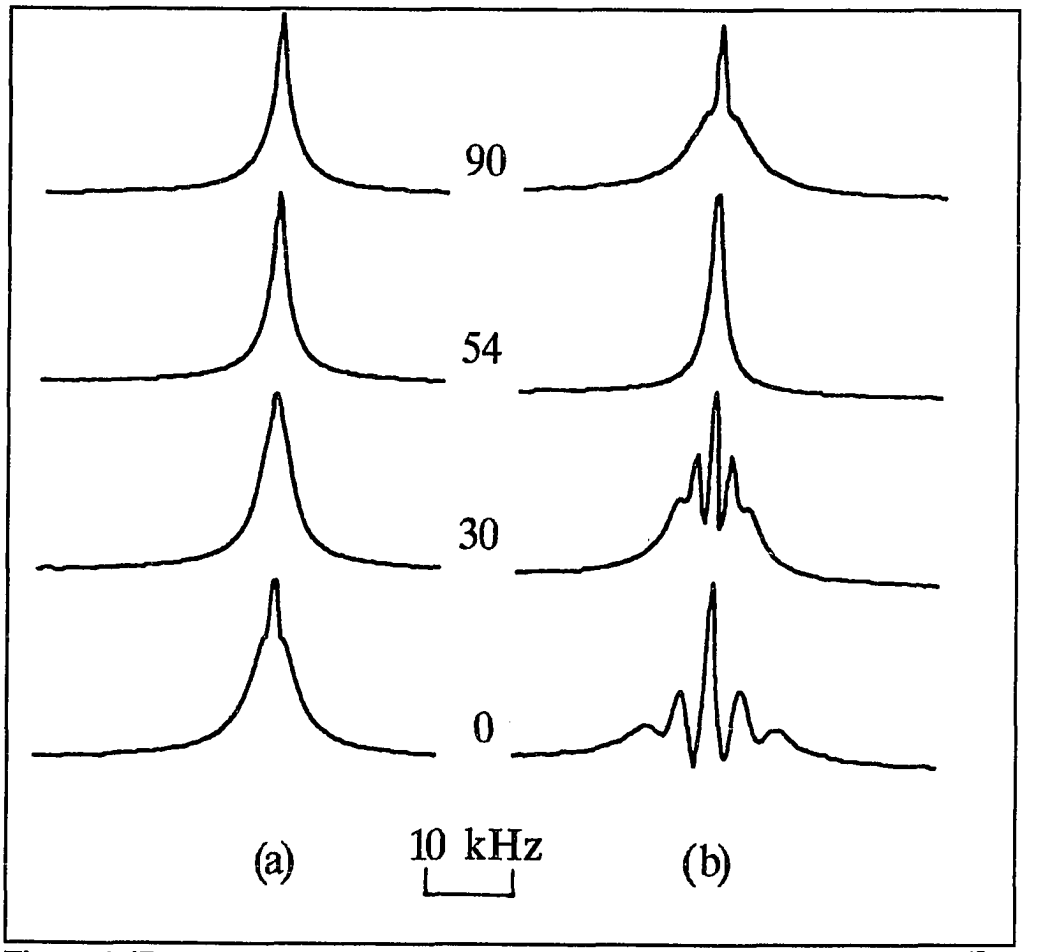

Figure 4.47: Oxygen-17 NMR spectra of NAFION-117 containing 13.3 wt% ^{17}O-enriched H_2O at θ=0°,30°,54°,90°. (a) unstretched, (b) stretched to 19% elongation.

Reproduced with permission of the copyright owner. Further reproduction prohibited without permission.

4-4. High Pressure NMR

Temperature and pressure are the thermodynamic variables which determine the state of a system. In some cases, they are complementary variables, while in others, pressure is the essential variable. Understanding of ion transport processes in polymers can be greatly assisted by employing pressure as the dynamic variable. Activation volumes associated with ionic and molecular motion can be derived directly from the pressure data. As discussed later, such motion includes both translation and rotation. In this section, proton, deuteron, and oxygen-17 spin-lattice relaxation times (T_1) as a function of pressure are presented, the activation volume evaluated from the T_1 pressure dependence are introduced. Analysis of activation energies from T_1 temperature dependence presented in previous sections compared with the activation volume obtained in this section suggests a water cluster model for water in NAFION membranes which will be discussed in detail in the next section.

All measurements were made at 24 °C. T_1 measurements were made using the inversion recovery pulse sequence describe previously. T_1 data were recorded as the pressure was first increased, then deceased, and increased again. Figures 4.48-50 display the proton, deuteron and oxygen-17 T_1 pressure dependence for all stages of the pressure cycle. Except for the ^{17}O results, only minor variations as a function of pressure history were noted.

Reproduced with permission of the copyright owner. Further reproduction prohibited without permission.

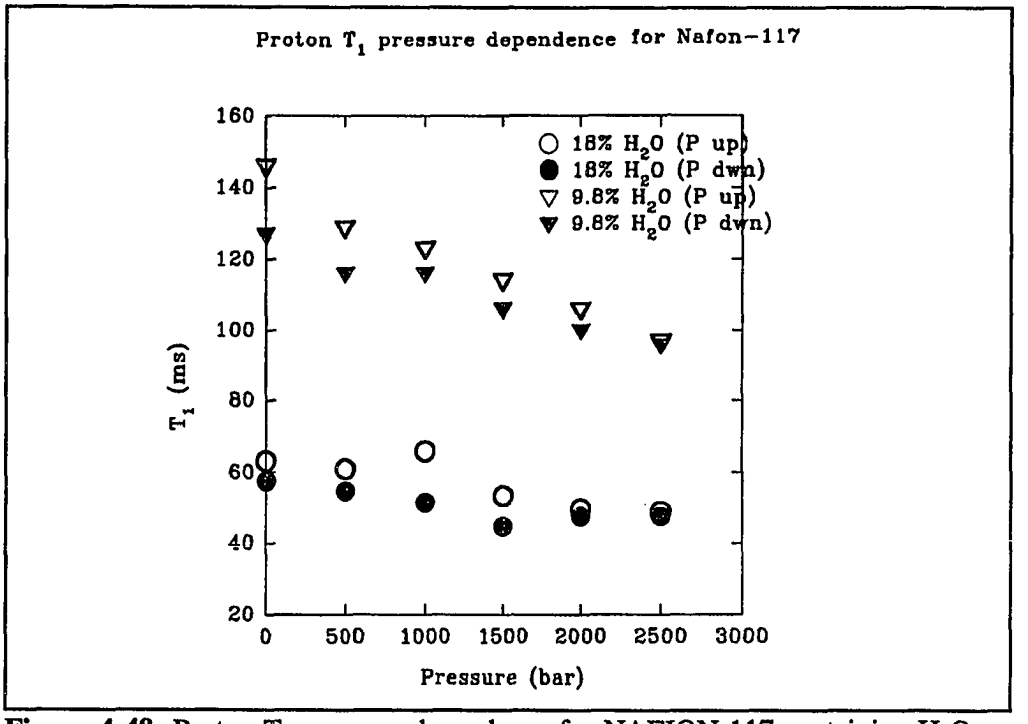

Figure 4.48: Proton T_1 pressure dependence for NAFION-117 containing H_2O.

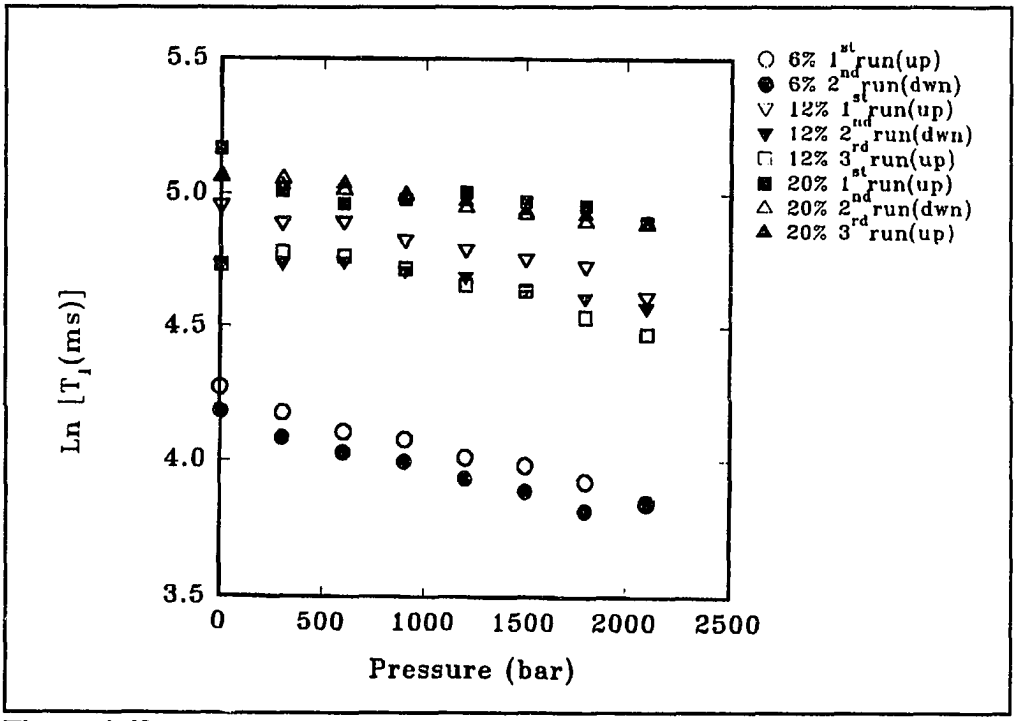

Figure 4.49: Deuteron T_1 pressure dependence for NAFION-117 containing D_2O.

Reproduced with permission of the copyright owner. Further reproduction prohibited without permission.

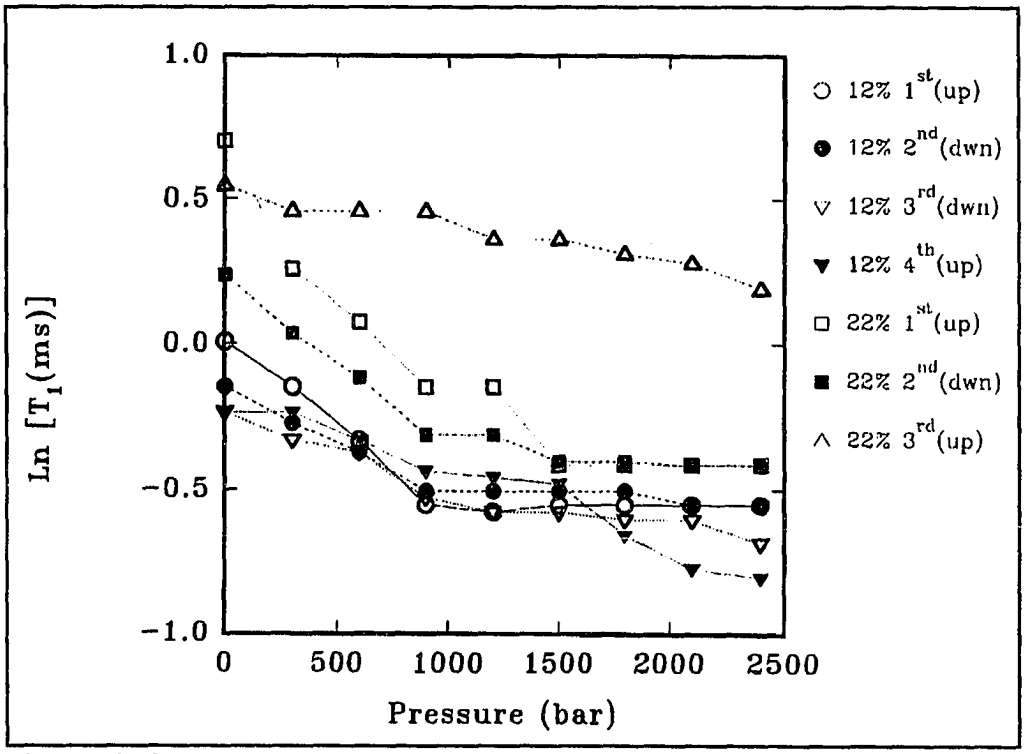

Figure 4.50: Oxygen-17 T_1 pressure dependence for NAFION-117 containing $H_2{}^{17}O$.

In order to analyze our data systematically, all results calculated for discussion are extracted from the data corresponding to the middle stage of the cycle, i.e. pressure decreasing from the maximum value of 0.25 GPa. Figure 4.51 displays the proton NMR results for two samples, containing 9.8 and 18 wt% H_2O (corresponding to roughly 5 and 10 water molecules, respectively, per sulfonate). Activation volumes can be extracted from the data by applying Equation 1.3, yielding $\Delta V = 2.7$ and 2.0 (both $\pm$ 0.2) cm^3/mole for the lower and higher water content samples, respectively.

Deuteron T_1 data for samples with water content 6, 12, and 22 wt% are plotted in Figure 4.52. The results are $\Delta V = 4.6 \pm 0.3$, 2.8 ± 0.7 and 2.6 ± 0.3 cm^3/mole, respectively. The calculated activation volumes for the proton and deuteron T_1's are in surprisingly good agreement with each other and with the conductivity results[80].

Reproduced with permission of the copyright owner. Further reproduction prohibited without permission.

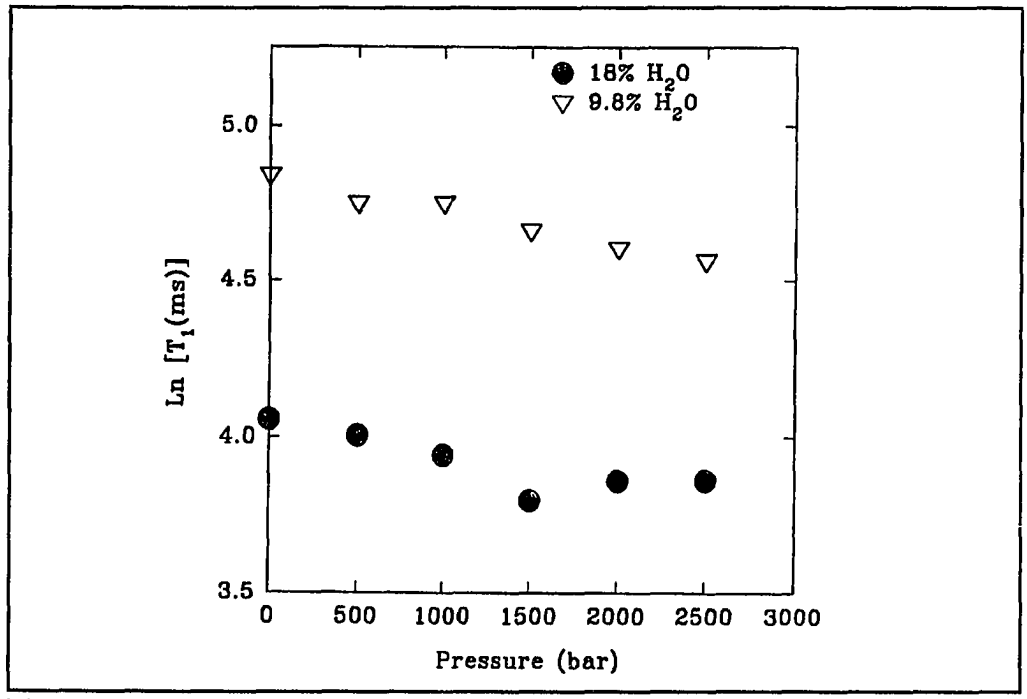

Figure 4.51: Pressure dependence of proton T_1 in NAFION-117 with two different water contents at 24 °C. (second stage of cycle).

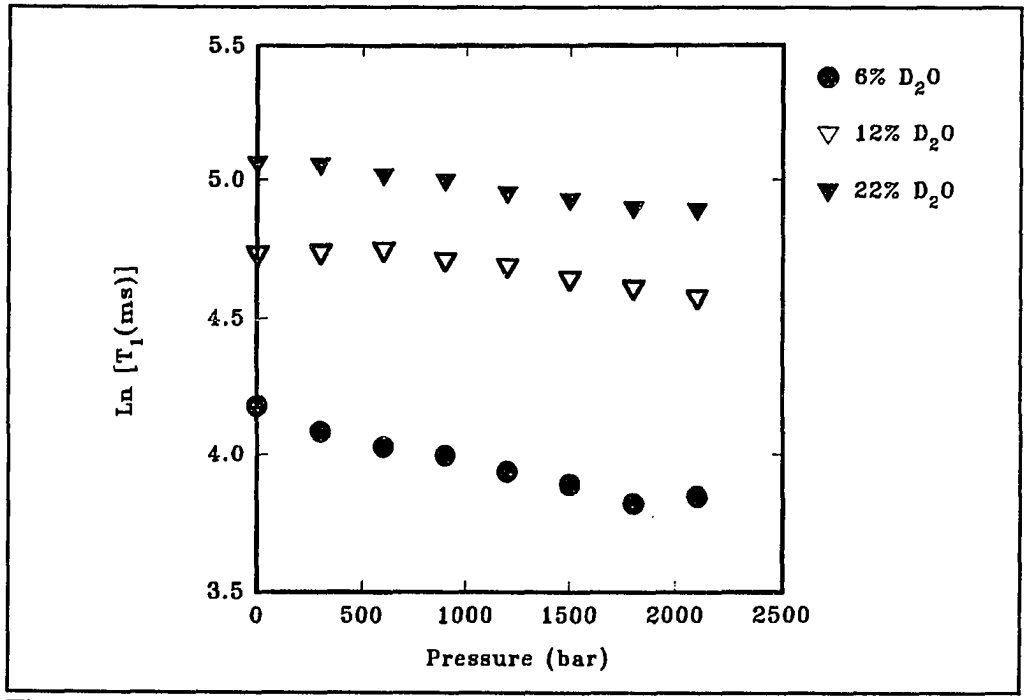

Figure 4.52: Pressure dependence of deuteron T_1 in NAFION-117 with three different water contents at 24 °C. (second stage of cycle).

Reproduced with permission of the copyright owner. Further reproduction prohibited without permission.

Moreover, the trend of increasing activation volume with decreasing water content is maintained in all of the measurements. However, the ^{17}O T_1 pressure dependence is considerably different from the proton and deuteron results. In particular, following a fairly steep drop in T_1 for both the 12 and 22 wt% samples as the pressure is increased to about 0.1 GPa, T_1 remains relatively constant. The situation just described and observed corresponds to the initial application of pressure, increasing from ambient (shown in Figure 4.50). The data in Figure 4.53, however, were recorded during the decreasing portion of the pressure cycle, for consistency with the proton and deuteron measurement conditions. Furthermore, the slopes of the pressure dependencies up to 0.1 GPa reflect a higher activation volume for the sample with higher water content, which is opposite to the trends observed in the proton and deuteron NMR and conductivity measurements[80].

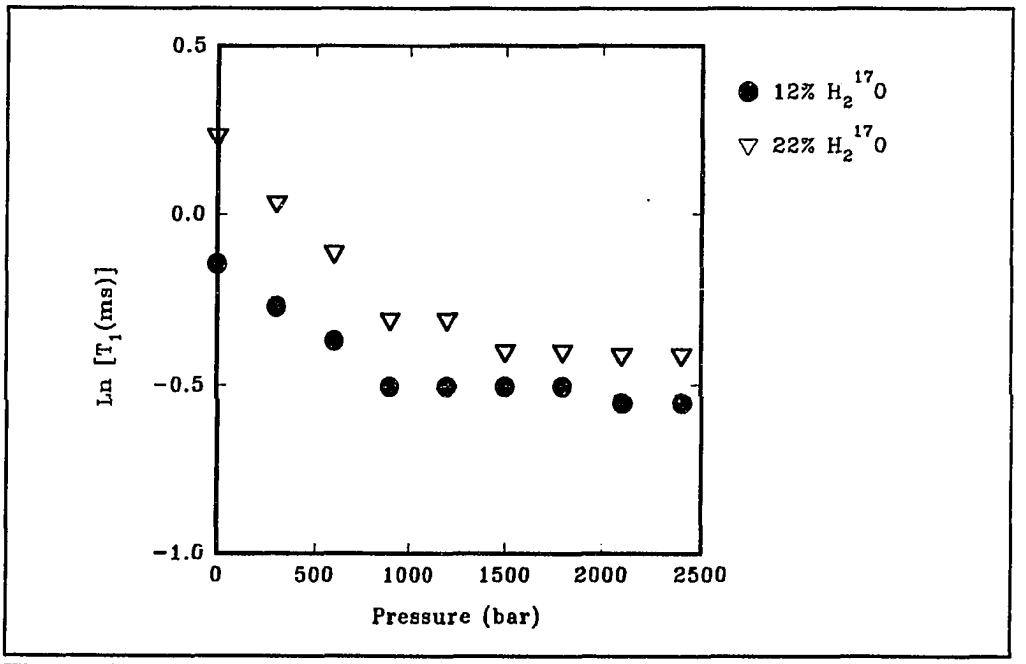

Figure 4.53: Pressure dependence of oxygen-17 T_1 in NAFION-117 with two different water contents at 24 °C. (second stage of cycle).

Reproduced with permission of the copyright owner. Further reproduction prohibited without permission.

That the proton and deuteron results should yield similar activation volumes is not obvious because their relaxation mechanisms are significantly different. In liquid water, protons relax by magnetic dipole-dipole interactions, which are primarily *inter*molecular in nature, while deuterons (and for that matter ^{17}O, discussion of which is momentarily deferred) relax through the electric quadrupole interaction which is primarily *intra*molecular in nature[59]. Thus relaxation measurements of protons are sensitive to translation while deuteron and ^{17}O relaxation is sensitive to rotation. However in liquids, there can be significant coupling between rotational and translational motion[81]. In acidic solutions, proton transport and molecular rotation are also correlated [82]. The reasonably close agreement between the proton and deuteron NMR and conductivity results implies that the electrical transport process in NAFION is correlated with water molecular rotation. The trend of increasing activation volume with decreasing water content is consistent with a rotational proton transfer mechanism between adjacent water molecules, and with the well-known result that the electrical conductivity increases with increasing water content. Proton, deuteron, and ^{17}O T_1's in pure water have a very weak pressure dependence over the range studied in this work, i.e. the activation volume associated with relaxation is very small[73]. Of course comparison with results for acidic solutions, if they were available, would be more appropriate. Nevertheless, because pressure effects on NAFION containing water are so much larger than on bulk water, these results could shed light on the nature of the interaction between water molecules and the host polymer matrix.

Interpretation of the ^{17}O NMR results remains problematic at this time. The two essential differences between ^{2}H and ^{17}O NMR are the much stronger quadrupole

Reproduced with permission of the copyright owner. Further reproduction prohibited without permission.

coupling in the latter (by about a factor of 30) and, in the context of this investigation, the fact that deuteron NMR samples both water molecules and the mobile charge while ^{17}O NMR samples only the water molecules. Given these differences, the behavior shown in Figure 4.53 is still, however, not presently understood.

4-5. The Cluster Model

As we reported in the previous sections, the activation energies, extracted from both deuteron and oxygen-17 T_1 temperature dependence, increase as the water contents increase. On the other hand, the activation volumes, obtained from proton, deuteron as well as conductivity pressure dependence, show a trend of decreasing with water contents increasing. It seems that these two results are conflict since the activation volume must related to the energy needed for diffusing species. However, if we notice that the activation energies were obtained in low temperature measurements while the activation volumes were taken at room temperature, therefore, activation energy represents the low temperature behavior and activation volume reflects water behavior at room temperature, it is not surprising that they have different dependences on water content. If we attribute these observations to a water cluster model, this paradox can be easily explained. Water clusters in NAFION, proposed originally by Gierke and Falk, as reviewed in Section 1-4, are formed by ionizable sulfonate groups when water is incorporated in the polymer[25,29], The diameter of the clusters in NAFION-H increases from 19 Å for the dry polymer up to 41 Å for one containing 20% water. Recently, Verbrugge[83] estimated the pore breadths. Using the Kozeny-Carmen relationship for the electrokinetic permeability through the porosity and the surface exposed to fluid per unit volume of

Reproduced with permission of the copyright owner. Further reproduction prohibited without permission.

solid, he obtained that the size of the pore depends on the thickness of the membranes, thick membranes have larger pore size. Typical pore breadth is about 50 Å in NAFION-117. We believe that these pores are aqueous clusters containing sulfonate sites, protons and water molecules. The larger the water content in NAFION membrane, the larger the size of the cluster. We may estimate how many water molecules there are in such a cluster, the average volume of one water molecule is about 30 $Å^3$, the volume of a spherical cluster with 50 Å diameter is about 6.5×10^4 $Å^3$, therefore more than 2000 water molecules are in the cluster. A large number of hydrogen bonds could be created between these water molecules. The behavior of the water cluster differs from the bulk water because it depends on its environment, i.e. polymer host. At room temperature, the hydrogen bonds between the water molecules can be easily broken in the larger cluster because of the higher mobility of water molecules, and the life of hydrogen bonds is short, thus the activation volumes are decreasing with increasing of water content, approaching to the bulk water behavior. At low temperature, those hydrogen bonds attached between water molecules are more rigid because the molecules have less thermal energies and are not so mobile, the larger the size of the cluster, the larger numbers of hydrogen bonds in the cluster, therefore motion associated with molecular reorientation is more cooperative when the water content is larger. This leads a larger activation energy when the water content is larger. It is expected that activation volumes at lower temperature would be higher than at room temperature. Upon further lowering the temperature, the clusters in the membranes form a glassy domain, this can explain why the temperature where glassy domain occurs shifts to lower T when the water contents are higher. The extremely small value of activation volumes (at room T) may also be

Reproduced with permission of the copyright owner. Further reproduction prohibited without permission.

consistent with the cluster model, in that molecular rotation and ion transport are independent of the polymer segmental motions but rather occur within the cluster. Of cause, if we could do low temperature high pressure measurements, we might observe that the activation volume would increase at lower temperature.

4-6. Methanol in NAFION-117

The prospect of employing methanol directly as a fuel in low temperature fuel cells has obvious appeal, but there are formidable problems that must be addressed. Principal among these are the choice of a suitable catalyst to facilitate oxidation at the anode, and finding a membrane in which the methanol itself is inhibited from diffusing. In the latter case, methanol transporting across the membrane would be spontaneously oxidized at the cathode, leading to a chemical "short-circuit" in the fuel cell[19]. In this section, we employ NMR to investigate issues related to methanol molecular mobility in NAFION-117 containing CH_3OD and $CH_3{}^{17}OH$ (15% ^{17}O-enrichment)[84].

4-6.1. Room Temperature Behavior

Room temperature deuteron NMR spectra of NAFION-117 films containing 24 wt% CH_3OD are shown in Figure 4.54, for both unstretched (a) and 11% stretched (b) samples. The angles listed between the spectra correspond to the relative orientation between the stretch direction and the static magnetic field, as described previously. Comparison of the spectra in (a) and (b) clearly demonstrates that some molecular anisotropy is generated by stretching. The splitting in (b) appears to follow the $3\cos^2\theta$ - 1 dependence of the quadrupole interaction. Close examination of the spectra in

Reproduced with permission of the copyright owner. Further reproduction prohibited without permission.

unstretched films (a) also shows some anisotropy though much smaller than (b). It is necessary to point out that stretched films containing a comparable molecular concentration of D_2O (about 14.5% D_2O by weight) exhibited splittings about a factor of 4 larger than shown in (b), (see Figure. 4.21).

Room temperature oxygen-17 NMR spectra of unstretched (a) and stretched (b) NAFION-117 films containing 22 wt% $CH_3{}^{17}OH$ are displayed in Figure 4.55. No angular dependence is apparent, even in the stretched samples. This is in stark contrast to the situation observed in stretched samples containing 13.3 wt% $H_2{}^{17}O$ (Figure 4.47). Although some of the anisotropy could be masked by lifetime broadening of the rapidly relaxing ^{17}O nuclei, it is clear that methanol molecular motion retains almost none of the anisotropy generated in the stretched perfluoropolymer host, again in contrast to the situation concerning water molecular motion. The results are consistent with rapid molecular motion of methanol in NAFION, for which further evidence from low temperature measurements is described next.

Reproduced with permission of the copyright owner. Further reproduction prohibited without permission.

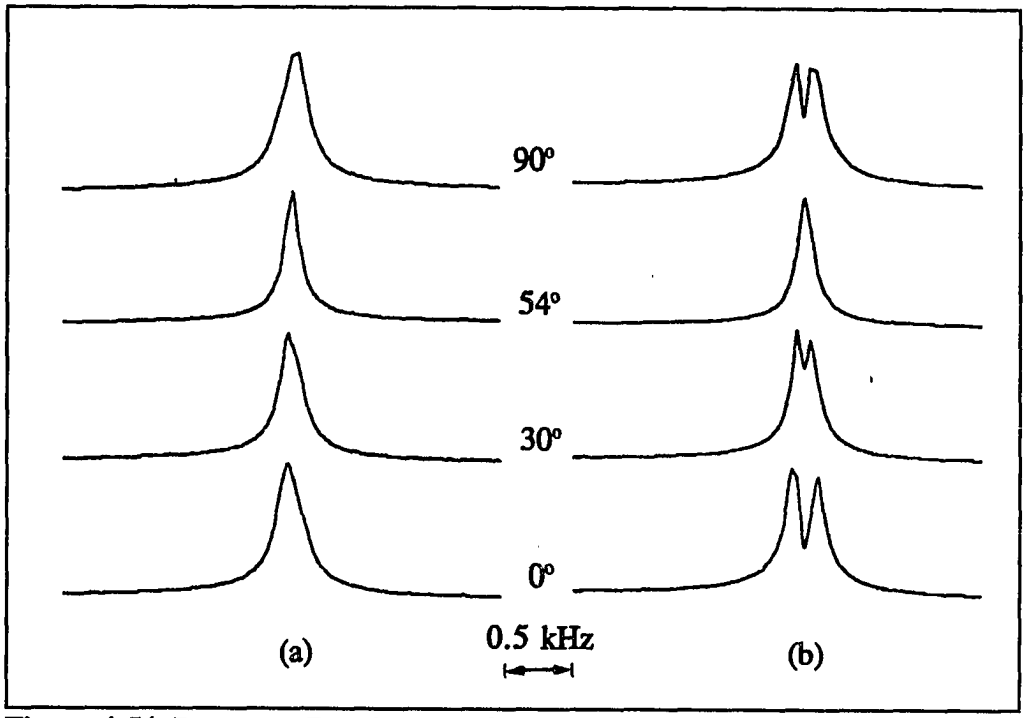

Figure 4.54: Deuteron NMR Spectra of unstreched (a) and stretched (b) NAFION-117 containing 24 wt% CH_3OD at various orientation.

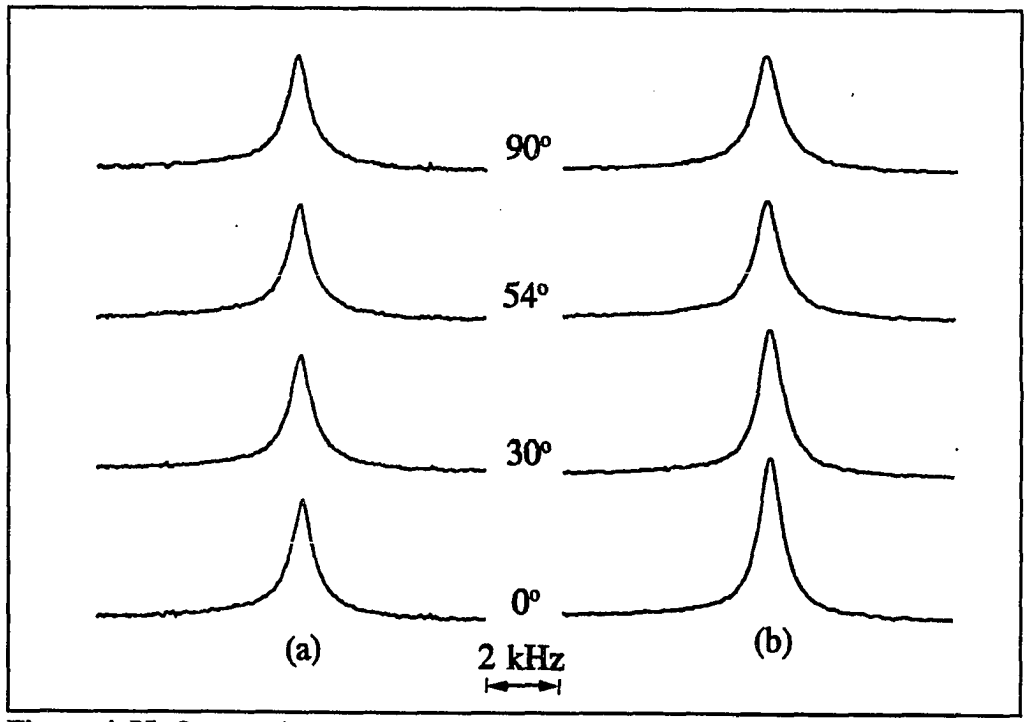

Figure 4.55: Oxygen-17 NMR spectra of unstreched (a) and stretched (b) NAFION-117 containing 22 wt% of 15% enriched $CH_3{}^{17}OH$ at various orientation.

Reproduced with permission of the copyright owner. Further reproduction prohibited without permission.

4-6.2. Low Temperature Behavior

In order to obtain additional information regarding the dynamics of methanol in NAFION, variable temperature linewidth and T_1 measurements were performed. For linewidth measurements, unstretched samples oriented close to 54° were used for suppressing the small anisotropies. Arrhenius plots of deuteron linewidth of two samples, one saturated with CH_3OD (24 wt%) and the other containing 17 wt%, are displayed in Figure 4.56. The linewidth of the 17 wt% sample is characterized by a low activation energy (~0.05 eV) region above 240 K, steepening to ~ 0.20 eV between 180 and 240 K. The sample exhibits a highly unusual line-narrowing phenomenon as T is decreased below 170 K. The origin of this line-narrowing is presently unknown, but could possibly be attributed to a subtle phase transition. The 24 wt% sample follows the same kind of behavior as the unsaturated one. It is interesting that at the lowest temperature at which measurements were made (140 K), the linewidth (~ 12 kHz) was still observed to be an order of magnitude smaller than that corresponding to a rigid quadrupole interaction for an O-D bond. In NAFION containing D_2O, the deuteron linewidth was observed 80 kHz at around 170 K. Thus molecular motion is frozen out at much higher T in the NAFION-water system than in NAFION-methanol. Arrhenius plots of T_1 of these samples are shown in Figure 4.57. Again, the two curves exhibit similar behavior with the features, most notably the T_1 minimum, of the 24 wt% sample shifted to lower T (by 5 - 10 K) relative to the 17 wt% sample. This means the larger methanol content is characterized by more motion than that of lower content at a given temperature.

Reproduced with permission of the copyright owner. Further reproduction prohibited without permission.

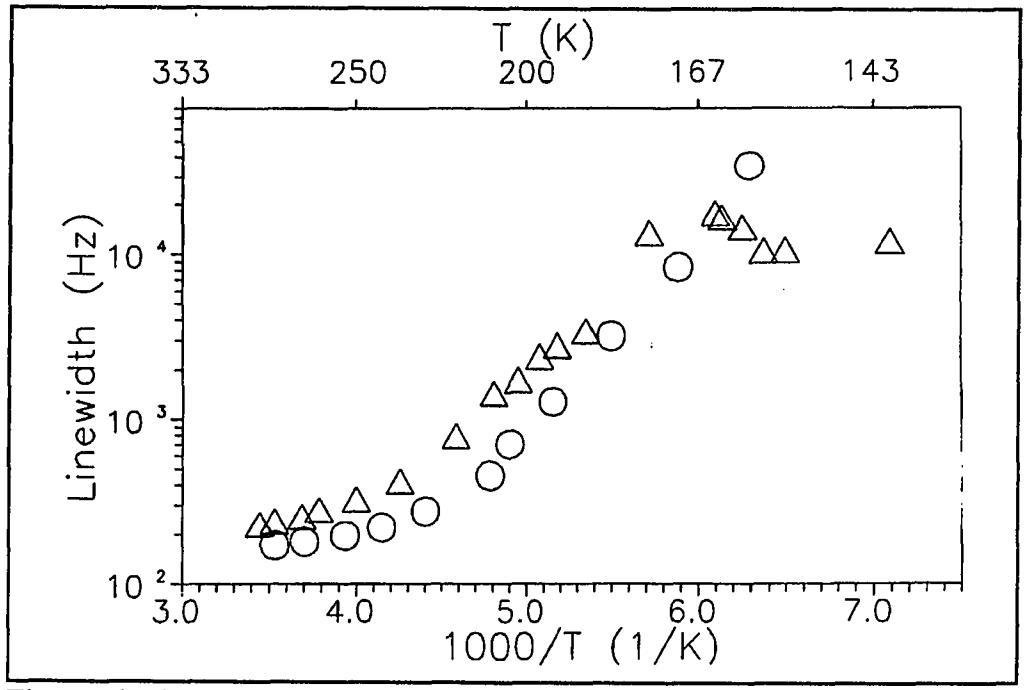

Figure 4.56: Arrhenius plots of deuteron NMR linewidth in NAFION-117 containing 17 wt% (triangles) and 24 wt% (circles) CH_3OD.

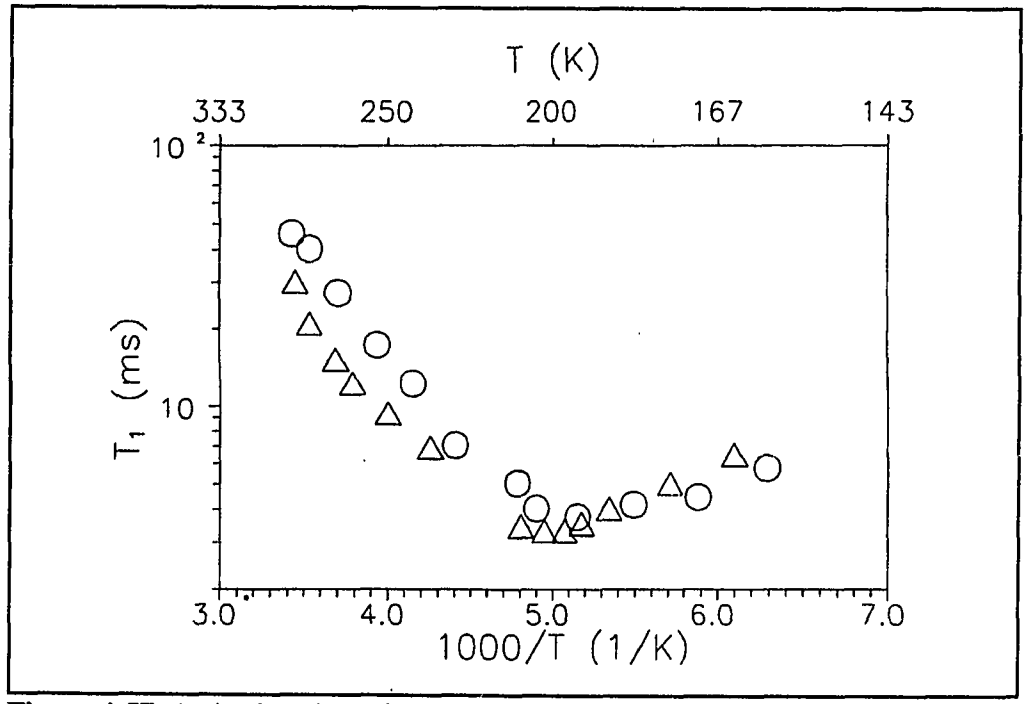

Figure 4.57: Arrhenius plots of deuteron spin-lattice relaxation time T_1 in NAFION-117 containing 17 wt% (triangles) and 24% (circles) CH_3OD.

Reproduced with permission of the copyright owner. Further reproduction prohibited without permission.

Although the molecular motion time-scale probed by linewidth and T_1 are considerably different (10^{2-5} Hz in the former and 10^{7-8} Hz in the latter), the dominant motional process responsible for both linewidth and T_1 behavior is assumed to be molecular rotation, as in the case of liquid CH_3OD[72]. Molecular rotation provides an even more efficient relaxation pathway for $CH_3{}^{17}OH$ because of the considerably larger (than deuterons in the same molecule) quadrupole interaction experienced by the ^{17}O nucleus. Figure 4.58 displays Arrhenius plots of ^{17}O T_1 in NAFION-117 samples containing 22 wt% and 18 wt% CH_3OH enriched 15% in ^{17}O. At temperatures below ~220 K, T_1 is too short to be measured reliably as discussed in the case of $H_2{}^{17}O$ before. Oxygen-17 linewidths of the same samples are plotted in Figure 4.59. It is interesting to note that the ^{17}O linewidths are determined, in large part, by lifetime (i.e. T_1) effects. For example, the T_1 contribution to the linewidth, which can be estimated as $(\pi T_1)^{-1}$, is approximately half of the total linewidth at 295 K. This is at least partly responsible for the absence of ^{17}O spectral anisotropies in Figure 4.55. Not surprisingly, the activation energies which characterize the T_1 and linewidth temperature dependencies are quite similar (~0.20 ev). The general shapes of the linewidth curves in Figure 4.60 follow the temperature dependence predicted for a second-order quadrupole broadened central transition (lifetime effects are included) similar to the case of $H_2{}^{17}O$ (see Figures 4.37-38). As in the case of the deuteron NMR results, the oxygen-17 linewidths of the two samples follow similar trends, with the main features of the higher methanol-content sample shifted to lower T. Thus the molecular dynamics at a given temperature are somewhat faster in the saturated sample.

Reproduced with permission of the copyright owner. Further reproduction prohibited without permission.

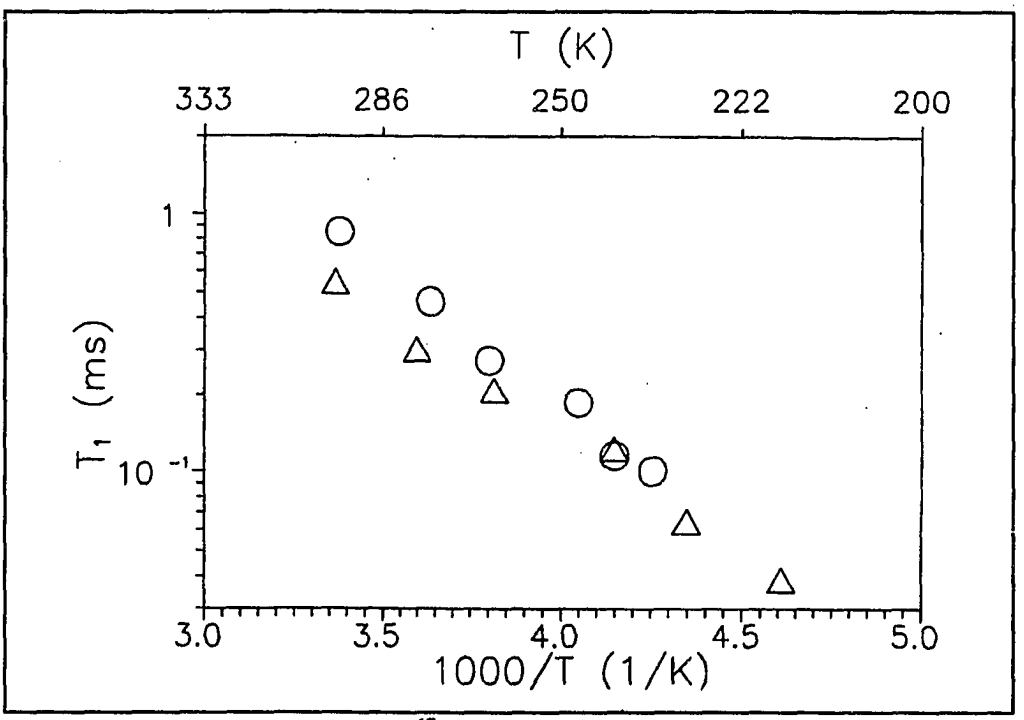

Figure 4.58: Arrhenius plots of ^{17}O spin-lattice relaxation time in NAFION-117 containing 18 wt% (triangles) and 22 wt% (circles) of 15% ^{17}O-enriched CH_3OH.

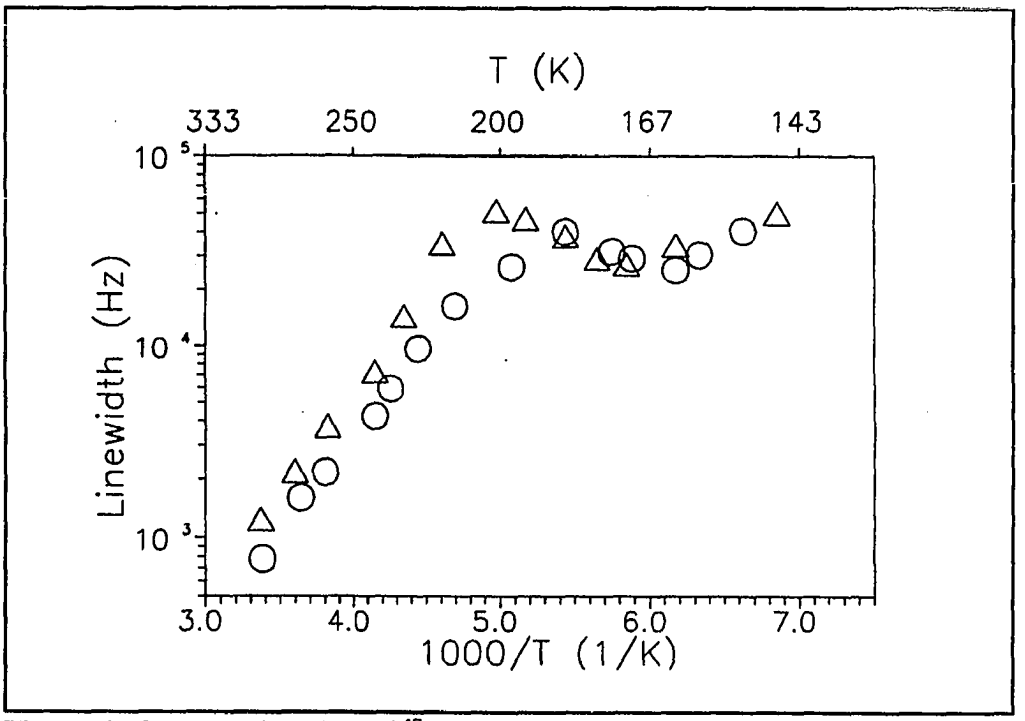

Figure 4.59: Arrhenius plots of ^{17}O linewidth in NAFION-117 containing 18 wt% (triangles) and 22 wt% (circles) of 15% ^{17}O-enriched CH_3OH.

Reproduced with permission of the copyright owner. Further reproduction prohibited without permission.

Although there is no simple and direct relationship between relaxation processes dominated by molecular rotation and methanol diffusion across the membrane as there may be for water molecular rotation and proton transport, as described in Section 4-4, the results reported here clearly suggest that methanol is highly mobile in NAFION-117, considerably more so than water. A brief summary of the experimental evidence supporting this conclusion is given: (i) near absence of anisotropic molecular motion in stretched films; (ii) deuteron linewidth at 140 K is still an order of magnitude smaller than that corresponding to a rigid O-D bond; (iii) molecular dynamics are somewhat faster at higher methanol content. Previous considerations of NAFION-117 as membrane separator in a methanol fuel cell led to diffusion measurements and mathematical modelling. The main conclusion of this study was that methanol transport across the membrane is probably too high, thus other membrane separators were deemed more promising[19]. The results reported in the present investigation are not inconsistent with this assessment.

4-7. Water in NAFION-127

The preceding sections discussed water and methanol behaviors in NAFION-117. This section consists of deuteron and oxygen-17 NMR studies of water in NAFION-127 membranes, comparisons of T_1 data for NAFION-117 and 127 are presented. NAFION-127, a member of NAFION family, has equivalent weight (EW) 1200, the repeat number of the tetrafluoroethylene unit is about 7.5, one more than that of NAFION-117. Its thickness is about 0.25 mm, 0.06 mm thicker than NAFION-117. All the measurements were performed in a 4.5 tesla magnetic field with Larmor frequency 29 MHz for

Reproduced with permission of the copyright owner. Further reproduction prohibited without permission.

deuteron and 26 MHz for oxygen-17. T_1 measurements have been checked for no significant difference in high field (7.2 T) and in lower field (4.5 T) as shown in Figure 4.60. From which we can see that the T_1 values for NAFION containing a comparable water content under different field are in good agreement. A shortcoming of lower field is that the T_1 data for ^{17}O at low temperatures are not available because of spectrometer ring-down which masks most of the NMR signal. In comparing NAFION-117 results (taken in high field) with NAFION-127 results (taken in low field), we make use of the field-independence of T_1, shown in Figure 4.60.

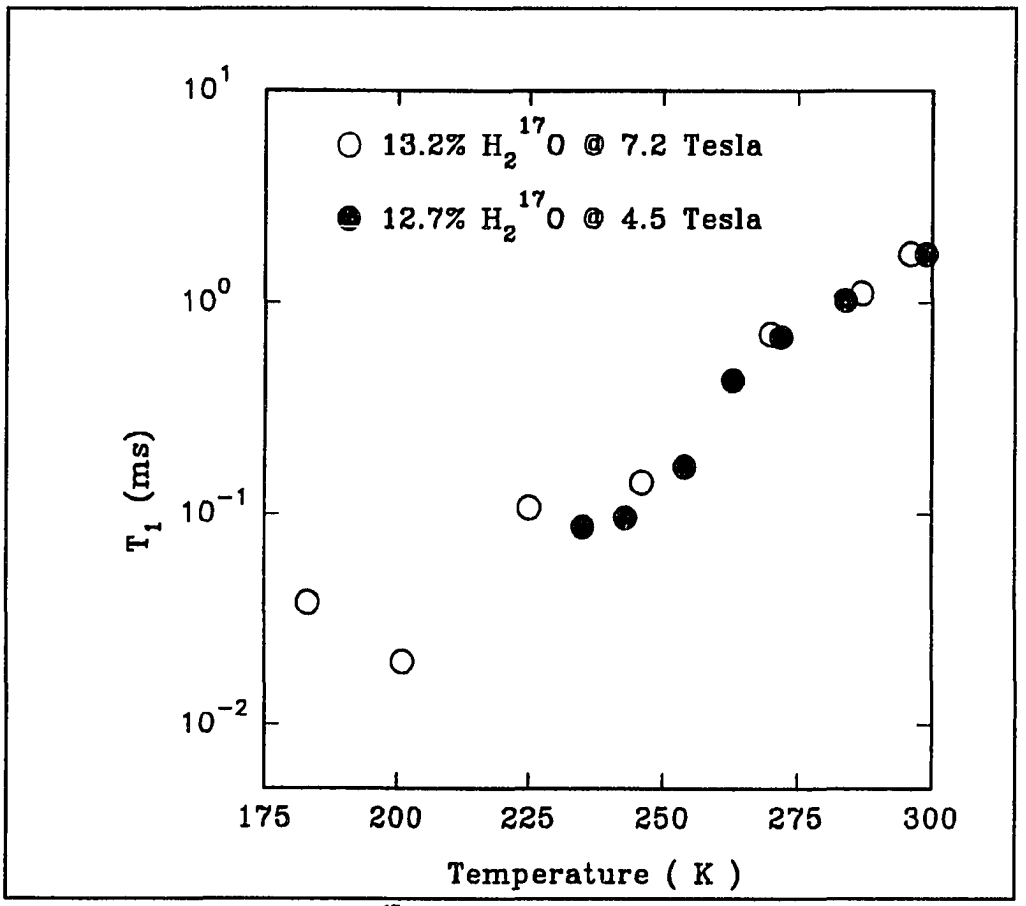

Figure 4.60: A comparison of ^{17}O T_1 deference taken under high and low magnetic field in NAFION-117 containing comparable water contents.

Reproduced with permission of the copyright owner. Further reproduction prohibited without permission.

Deuteron T_1s for NAFION-127 containing two different water contents are plotted in Figure 4.61. The T_1 inversion recovery profile is a single exponential over the entire temperature range that we measured. The same trend of T_1 vs. water content observed in NAFION-117 was observed in NAFION-127. At room temperature, T_1 is 180 ms for larger water content and 110 ms for lower water content. As the temperature decreases, the two water contents show a same trend of decreasing T_1, the T_1 minima reach about 1.7 ms at ca. 203 K. Figure 4.62 displays the Arrhenius plot of the data in Figure 4.61. The activation energies extracted from the Arrhenius plots are 0.25 eV for 9.4 wt% and 0.26 eV for 14.7 wt%, suggesting an increase of activation energy at higher water content, as in the case of NAFION-117. However it is also possible that the activation energy difference is within the experimental uncertainty.

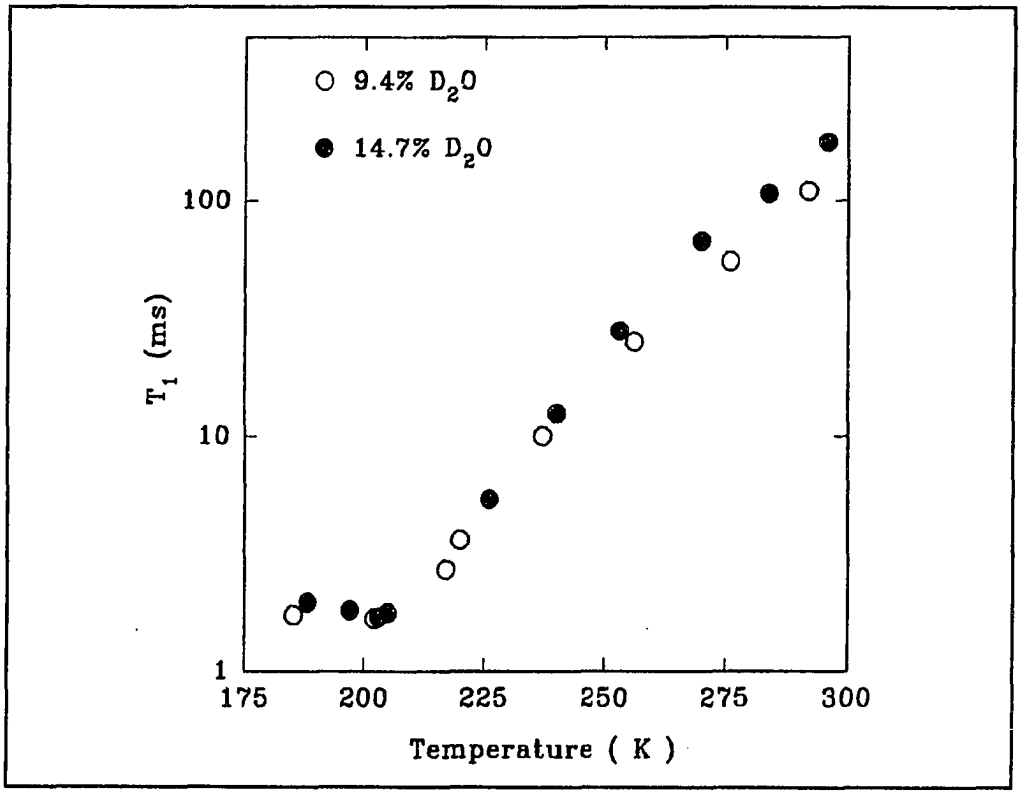

Figure 4.61:Temperature dependence of deuteron T_1 for NAFION-127 containing two D_2O contents.

Reproduced with permission of the copyright owner. Further reproduction prohibited without permission.

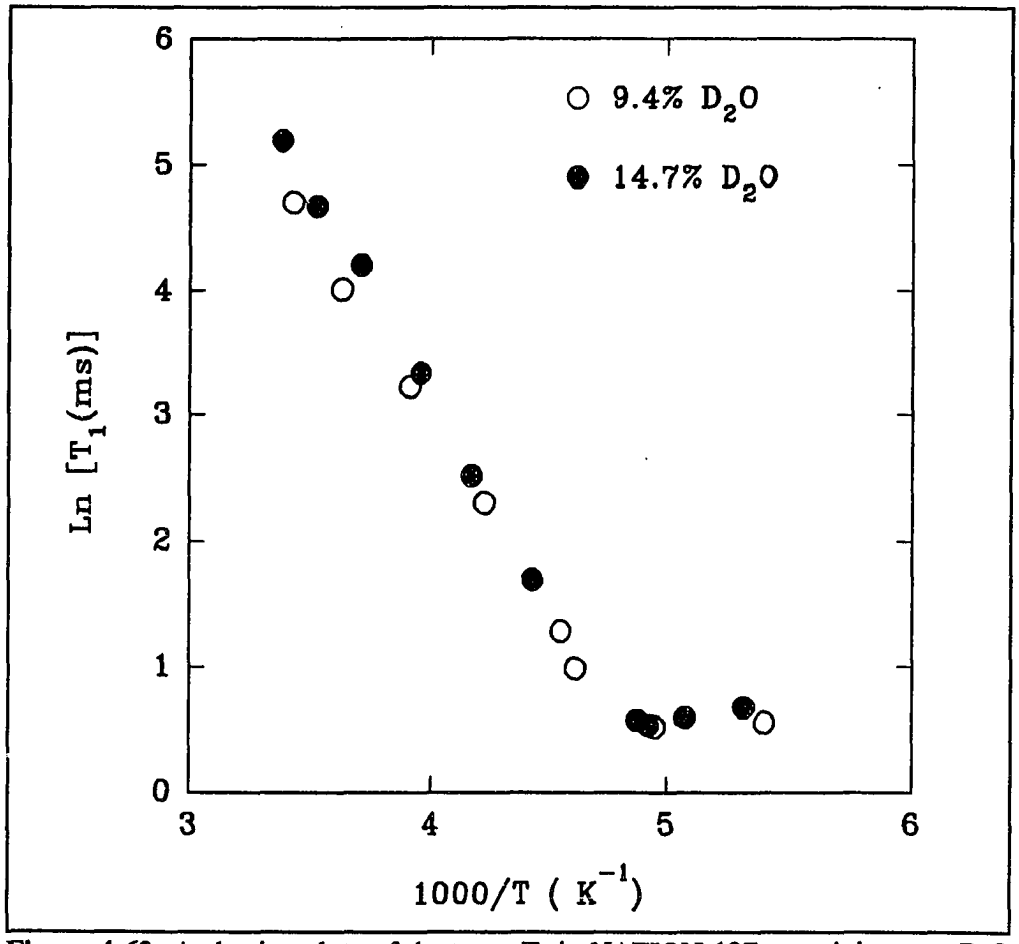

Figure 4.62: Arrhenius plots of deuteron T_1 in NAFION-127 containing two D_2O contents.

Oxygen-17 T_1s for NAFION-127 containing 7 wt% and 15.8 wt% $H_2{}^{17}O$ are plotted in Figure 4.63. The T_1 is from 0.93 ms for 7 wt% and 2.02 ms for 15.8 wt% at room temperature and decreases to about 0.05 ms at ca. 223 K for both samples. As the shortcoming in low field measurements mentioned previously, T_1 minima are not available. However, we still can obtain the activation energies in the range from room temperature to 223 K. The Arrhenius plots of oxygen-17 T_1 in NAFION-127 containing these two $H_2{}^{17}O$ contents are displayed in Figure 4.64. The activation energies extracted from Figure 4.64 are 0.28 eV for 7 wt% and 0.32 eV for 15.8 wt%. The values are slight larger than those of deuterons.

Reproduced with permission of the copyright owner. Further reproduction prohibited without permission.

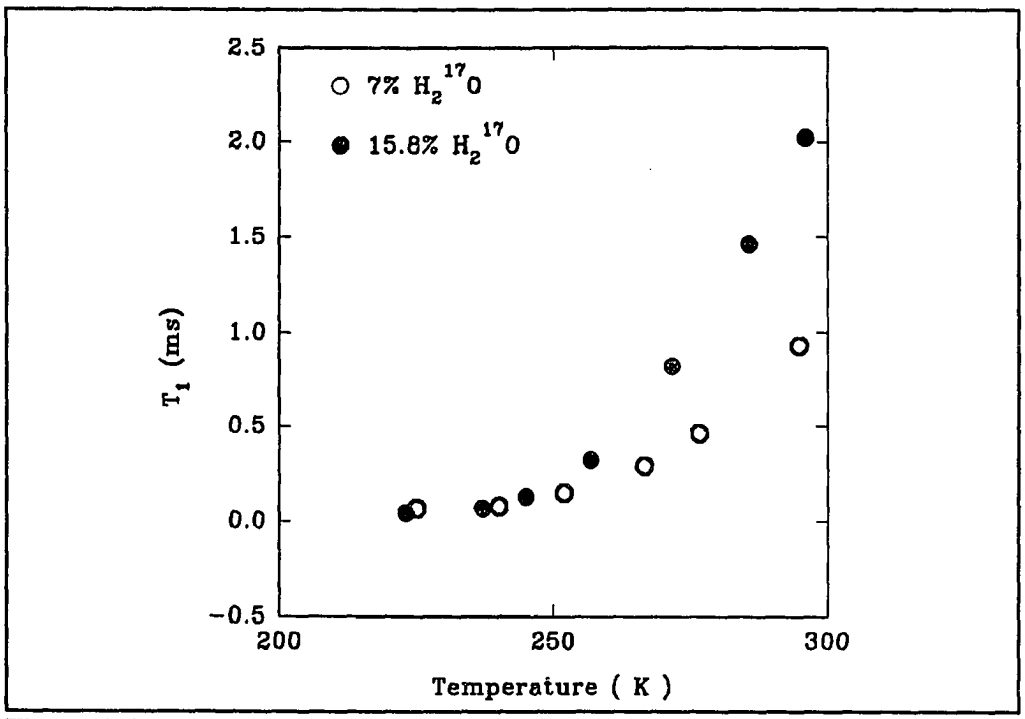

Figure 4.63: Temperature dependence of oxygen-17 T_1 for NAFION-127 containing two $H_2{}^{17}O$ contents.

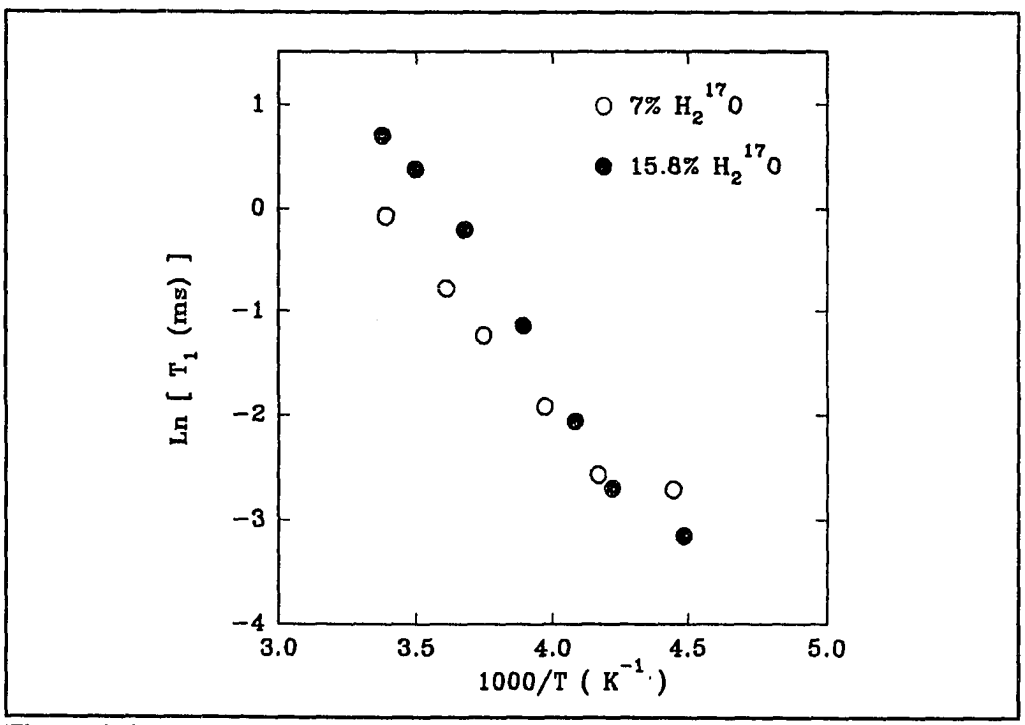

Figure 4.64: Arrhenius plots of oxygen-17 T_1 in NAFION-127 containing two $H_2{}^{17}O$ contents.

Reproduced with permission of the copyright owner. Further reproduction prohibited without permission.

Comparison of NMR behaviors of NAFION-117 and NAFION-127 can shed light on which one shows more promise for utility in fuel cell operations. Figure 4.65 displays the temperature dependence of deuteron T_1 for NAFION-117 and NAFION-127 containing comparable percentage D_2O by weight. We can see that the T_1 value for NAFION-127 is larger than that of NAFION-117 at room temperature, but it becomes smaller than that of NAFION-117 at lower temperature. This yields a larger activation energy (0.26 eV) for NAFION-127 than for NAFION-117 (0.25 eV). Considering that this comparison is based on the weight percent, but the number of the water molecules per sulfonate is different, another set of T_1 plots for both NAFION-117 and 127 containing the same number of water molecules per sulfonate is displayed in Figure 4.66. Both NAFION membranes contain 5.6 D_2O molecules per sulfonate. Examination of the difference between two samples also shows the same trend described in the case of NAFION containing same weight percent shown in Figure 4.65. The activation energy is 0.25 eV for NAFION-127 and 0.22 eV for NAFION-117. Again, these observations can be explained by our cluster model. Since the pore size is larger in the thicker membranes than in the thinner membranes[83], the size of the water cluster is somewhat larger in the NAFION-127. The T_1 is larger for NAFION-127 than that of NAFION-117 at room temperature because the T_1 behavior of larger cluster is closer to that of bulk water. At low T, the activation energies are higher for NAFION-127, this is the expectation that the larger cluster gives higher activation energy as discussed in the previous section.

The NMR results described above may be of use in explaining the different performance characteristics of NAFION membranes employed in fuel cells. As

Reproduced with permission of the copyright owner. Further reproduction prohibited without permission.

Verbrugge pointed out, more facile proton transport and reduction of water flow rates are desirable qualities for fuel cell membranes, the small pore size yields more facile proton transport[83]. Our results may support the conclusion that NAFION-117 is more promising for fuel cell membranes than NAFION-127 because of the smaller pore size.

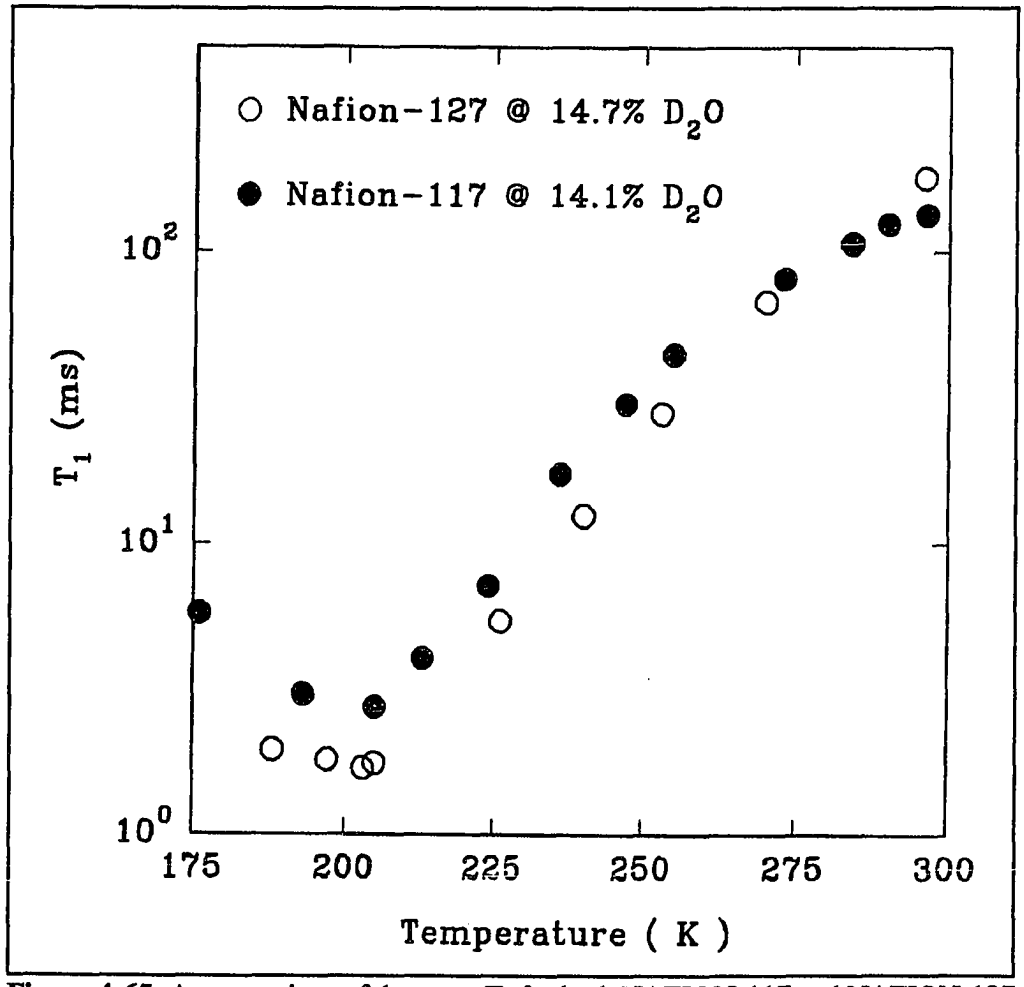

Figure 4.65: A comparison of deuteron T_1 for both NAFION-117 and NAFION-127 containing near same water percentage by weight.

Reproduced with permission of the copyright owner. Further reproduction prohibited without permission.

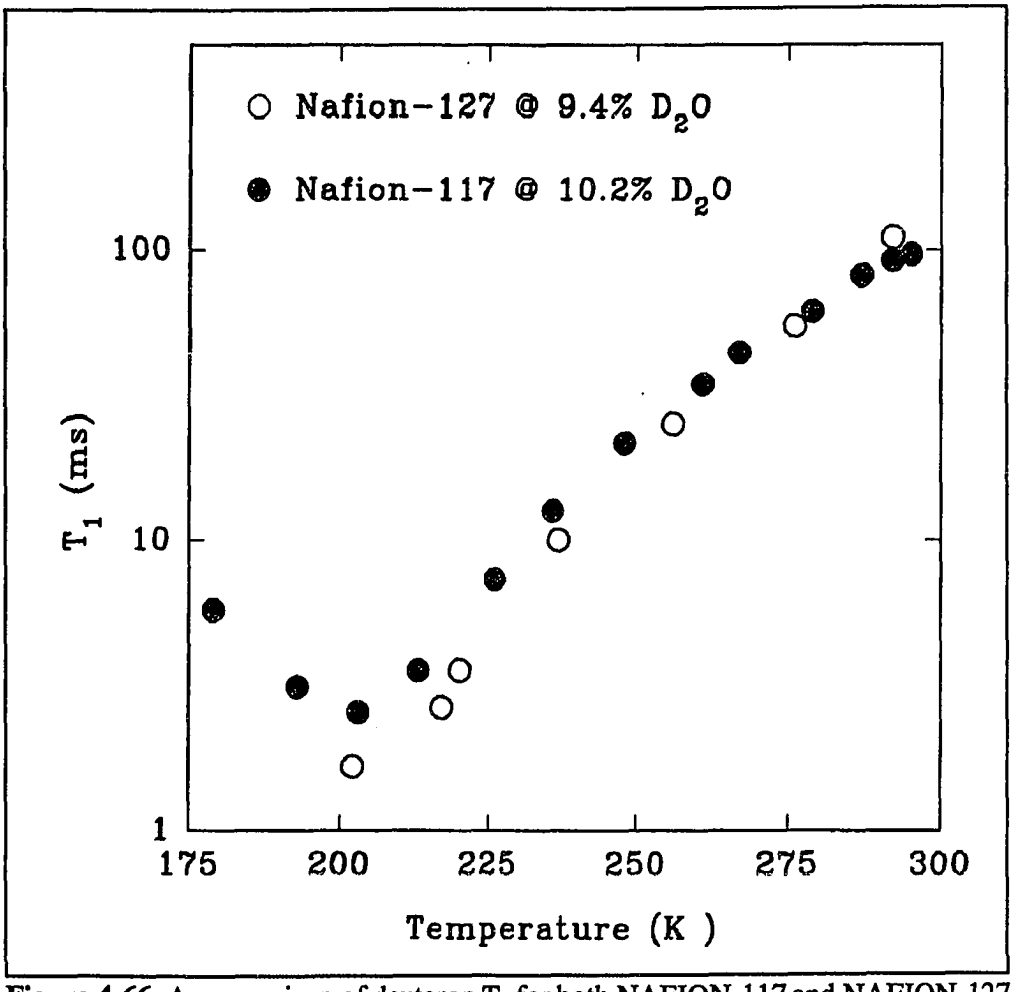

Figure 4.66: A comparison of deuteron T_1 for both NAFION-117 and NAFION-127 containing same numbers of water molecules per sulfonate.

Reproduced with permission of the copyright owner. Further reproduction prohibited without permission.

4-8. Conclusions

Based on all the results of NMR studies of water and methanol in NAFION-117 and NAFION-127 membranes presented and discussed in the previous sections, clearly the water behavior in the NAFION membranes demonstrates significant departures from that of bulk water because of its environment, i.e. NAFION polymer host. In particular there are several conclusions.

(1) Room temperature deuteron and oxygen-17 NMR spectroscopies reflect the underlying anisotropy of the host polymer. The water molecular motion in NAFION membranes is anisotropic in the membrane plane. The splitting of both deuteron and oxygen-17 spectra follow the quadrupole interaction orientation $3\cos^2\theta - 1$ relation, which implies that the averaged residual EFG axis is along the film plane. The splitting can be reduced with increasing of water content because of the more isotropic molecular motion at higher water contents. The splitting can also be enhanced dramatically by modest stretching (less than 20%) of the film, which indicates that the residual EFG tensor axis is along the stretching direction. The deuteron order parameter which is used for describing the anisotropy of D_2O motion in the NAFION varies from 3.6×10^{-3} to 6.2×10^{-4} depending on the water contents. The larger the water content, the smaller the order parameter. Stretching the sample to 13% elongation increases the order parameter by about one order of magnitude.

(2) The low temperature deuteron lineshape suggests that the water molecules reside in glassy domains below about 110 K. The temperature where the glassy domains occur shifts to lower temperature with increasing water content. The activation energy, extracted from both deuteron and oxygen temperature dependence of spin lattice

Reproduced with permission of the copyright owner. Further reproduction prohibited without permission.

relaxation time (T_1) on the high temperature side of the T_1 minimum, increase from 0.20 to 0.28 eV as the water content increases from 4.7 wt% to 18 wt%. This indicates that the motion associated with molecular reorientation in the temperature range ~ 210 to 295 K is more cooperative when the water content is larger. Fits to the data between 273-295 K indicate somewhat lower values of E_A, but these are still greater than the bulk water value. The correlation time, a measure of the time needed for a water molecule reorientation, evaluated from the NMR data of both deuteron and oxygen-17 T_1 minima and oxygen-17 linewidth temperature dependence, is approximately 1.4×10^{-11} s at room temperature, 3.6×10^{-9} s at ca. 205 K, 1.6×10^{-7} s at ca. 180 K, and approaching to 6.7×10^{-6} s for T lower than 150 K for NAFION containing water in the range of 10 to 15 wt%. Note that the correlation time for bulk water at room temperature is about 2.0×10^{-12} s. The second order quadrupole broadening of the central transition was observed in the ^{17}O temperature dependence of linewidth for NAFION containing either 20% ^{17}O enriched H_2O or 15% ^{17}O enriched CH_3OH at temperature lower than ca. 180 K for $H_2{}^{17}O$ and ca. 170 K for $CH_3{}^{17}OH$, respectively. The temperature-shift also depends on methanol or water content.

(3) The activation volumes, calculated from proton and deuteron pressure T_1 dependences measured at room temperature (24 °C), are between 2.0 to 4.6 cm^3/mole and exhibit a trend of increasing with decreasing water content. The values of the activation volumes from the data of proton and deuteron are in surprisingly good agreement with each other and with the conductivity results[80]. Because the mechanisms of the relaxation for proton (primarily *inter*molecular in nature) and deuteron (primarily *intra*molecular in nature) are significantly different, this good agreement implies that the

Reproduced with permission of the copyright owner. Further reproduction prohibited without permission.

electrical transport process in NAFION is correlated with water molecular rotation.

(4) The observations listed above suggest that the water organization in NAFION membranes can be described by a water cluster model. The cluster contains sulfonate sites, protons and water molecules. The larger the water content the larger the cluster size. A large number of hydrogen bonds could be created between these water molecules in the cluster. At room temperature the larger size clusters with the higher water content exhibit behavior closer to bulk water, that is the NMR parameters (T_1 and linewidth) exhibit a trend approaching that of bulk water. For instance, the larger of the water content, the larger of the T_1, the narrower the linewidth, and the smaller the activation volume. At low temperature, the hydrogen bonds become rigid because the molecules have less thermal energies and are not so mobile; the larger of the cluster size has a correspondingly larger number of hydrogen bonds. This leads to a larger activation energy when the water content is larger because the molecular motion is more cooperative when the number of hydrogen bonds is larger. Voids to be exposed to the fluorocarbon containing free water proposed by previous investigators[27,29] can be ruled out based on the following observations: first, the activation energies for water in NAFION are larger than that of the free water and increase with increasing water content; secondly the lineshape and T_1 results do not show any two components for even fully saturated samples (although rapid exchange of water molecules may be responsible for this). This conclusion is consistent with the PFG result that no large "pockets" of bulk water exist in NAFION-117 reported by Zawodzinski[40].

(4) Deuteron and oxygen-17 NMR studies of NAFION-117 containing either deuterated methanol (CH_3OD) or oxygen-17 enriched methanol ($CH_3{}^{17}OH$) show that the

Reproduced with permission of the copyright owner. Further reproduction prohibited without permission.

methanol molecular motion in NAFION-117 is considerably faster than for water in NAFION. This can be supported by the near absence of anisotropic molecular motion in stretched samples and the narrower linewidth at low T compared with NAFION-water cases. Also shown is that the molecular dynamics are somewhat faster at higher methanol content. This conclusion is consistent with other studies which conclude that methanol transport across the membrane is probably too high for it to be used as the separator in a methanol fuel cell[19].

(5) By comparing the water behavior in NAFION-127 with that of NAFION-117 containing same percentage water by weight and same numbers of water molecules per sulfonate, the activation energy extracted from the T_1 temperature dependence is somewhat higher for NAFION-127 than for NAFION-117. This may be of use in explaining the different performance characteristics of NAFION membranes employed in fuel cells. Our results may support the conclusion that NAFION-117 is more promising for fuel cell membranes than NAFION-127 because its smaller cluster size may yield more facile proton transport which is desirable quality for fuel cell membranes[83].

Reproduced with permission of the copyright owner. Further reproduction prohibited without permission.

References

1. Matthew L. Wald, *New York Times*, A1, April 14, (1993).
2. R.A. Lemons, *J. Power Sources*, **29**, 251 (1990).
3. S. Srinivasan, D.J. Manko, H. Koch, M.A. Enayetullah, and J.A. Appleby, *ibid*, **29**, 367 (1990).
4. S.J. Sondheimer, N.J. Bunce, and C.A. Fyfe, *J. Macromol. Sci.-Rev. in Macromol. Chem. and Phys.*, **C26**, 353 (1986).
5. A. Eisenberg and H.L. Yeager (eds.), Perfluorinated Ionomer Membranes, ACS Symposium Series 180, American Chemical Society, Washington, D.C., (1982).
6. A. Eisenberg (ed.), Ions in Polymers, Advances in Chemistry Series 187, American Chemical Society, Washington, D.C., (1980).
7. S.P. Rowland (ed.), Water in Polymers, ACS Symposium Series 127, American Chemical Society, Washington, D.C., (1982).
8. A. Eisenberg and H.L. Yeager, Chap. 1 in Ref. 5.
9. U. Frese and U. Stimming, *J. Electroanal. Chem. Interfacial Electrochem.*, **198**, 409 (1986).
10. T.H. Huang, E. Davis, U Frese, and U. Stimming, *J. Phys. Chem.*, **92**, 6874 (1988).
11. T.D. Gierke, 152nd Meeting of the Electrochemical Society, Atlanta, Ga., Oct. 1977, Abstract No. 438J. *Electrochem. Soc.*, **124**, 319C (1977).
12. H.W. Starkweather, Jr., *Macromolecules*, **15**, 320 (1982).

Reproduced with permission of the copyright owner. Further reproduction prohibited without permission.

13. T.A. Zawodzinski, Jr., C. Derouin, S. Radzinski, R.J. Sherman, V.T. Smith, T.E. Spinger, and S. Gottesfeld, *J. Electrochem. Soc.*, **140**, 1041 (1993).

14. R.S. Yeo and H.L. Yeager, *Modern Aspects of Electrochemistry*, **16**, 437 (1985).

15. T. Kyu, Materials Science of Synthetic Membranes, D.R. Lloyd (ed.), ACS Symposium Series 269, 365 (1985).

16. K.K. Pushpa, D. Nandan, and R.M. Iyer, *J. Chem. Soc. Faraday Trans. 1*, **84**, 2047 (1988).

17. S.C. Yeo and A. Eisenberg, *J. Appl. Poly. Sci.*, **21**, 875 (1977).

18. M.W. Verbrugge and R.F. Hill, *J. Phys. Chem.*, **92**, 6778 (1988).

19. M.W. Verbrugge *J. Electrochem. Soc.*,**136**, 417 (1989).

20. R.F. Hill, and M.W. Verbrugge, *ibid.*, **137**, 886,893 (1990).

21. E.R. Bauminger, I. Nowik and S. Ofer, and C. Heitner-Wirguin, *Ploymer*, **26**, 1829 (1985).

22. Noel. G. Boyle, Vincent J. McBriety, and Dean C. Douglass, *Macromolecules*, **16**, 75 (1983).

23. N.G. Boyle, J.M.D. Coey, and V.J. McBriety, *Chem. Phys. Lett.*, **86**, 16 (1982).

24. H.L.Yeager and A. Einsenberg, Chap.1, Chap.3, in Ref.5.

25. T.D. Gierke, G.E. Munn, and F.C. Wilson, *J. Polym. Sci., Polym. Phys. Ed.*, **19**, 1687 (1981).

26. B. Rodmacq, J.M. Coey, M. Escoubes, E. Roche, R. Duplessix, A.

Reproduced with permission of the copyright owner. Further reproduction prohibited without permission.

Eisenberg, and M. Pineri, Chap. 29 in Ref.7.

27. H.L.Yeager, Chap.4 in Ref.5.

28. J. Ceynowa, *Polymer,* **19**, 73 (1978).

29. M. Falk, *Can J. Chem.*, **58**, 1495 (1980).

30. M. Pineri, R. Duplessix, and F. Volino, Chap. 12 in Ref.5.

31. F. Volino, M. Pineri, A.J. Dianoux, and A. DeGeyer, *J. Polym. Sci., Polym. Phys. Ed.*, **20**, 481 (1982).

32. R. Duplessix, M. Escoubes, B. Rodmacq, F. Volino, E. Roche, A. Eisenberg, and M. Pineri, Chap.28 in Ref.7.

33. N. Bloembergen, E.M. Purcell and R.V. Pound, *Phys. Rev.*, **73**, 679 (1948).

34. Howard W. Starkweather, Jr., and James J. Chang, *Macromolecules*, **15**, 752 (1982).

35. N. Sivashinsky and G.B. Tanny, *J. Appl. Poly. Sci.*, **26**, 2625 (1981).

36. M. Pineri, F. Volino, and M. Escoubes, *J. Polym. Sci., Polym. Phys. Ed.*, **23**, 2009 (1985).

37. R.C.T. Slade, J. Barker, and J.H. Strange, *Solid State Ionics*, **35**, 11 (1989).

38. T.F. Fuller, and J. Newman, *J. Electrochem. Soc.*, **139**, 1332 (1992).

39. T.A. Zawodzinski, Jr., T.E. Spinger, J. Davey, R. Jestel, C. Lopez, J. Valerio, and S. Gottesfeld, *J. Electrochem. Soc.*, **140**, 1981 (1993).

40. T.A. Zawodzinski, Jr., M. Neeman, L.O. Sillerud, and S. Gottesfeld, *J. Electrochem. Soc.*, **95**, 6040 (1991).

Reproduced with permission of the copyright owner. Further reproduction prohibited without permission.

41. T.E. Spinger, T.A. Zawodzinski, and S. Gottesfeld, *J. Electrochem. Soc.*, **138**, 2334 (1991).

42. Noel. G. Boyle, Vincent J. McBriety, and A. Eisenberg, *ibid*, **16**, 80 (1983).

43. S. Schlick, G. Gebel, M. Pineri, and F. Volino, *Macromolecules*, **24**, 3517 (1991).

44. Lynn W. Jelinski, High-Resolution NMR Spectroscopy of Synthetic Polymers in Bulk, Ch.10, Komoroski (ed.), VCH Publisher, New York (1986),

45. Ian C.P. Smith, NMR of Newly Accessible Nuclei, Vol. 2, Ch.1, P. Laszlo (ed.), Academic Press, New York (1983).

46. H.W. Spiess, Advances in Polymer Science, Vol **66**, 24, Springer-Verlag, Berlin Heidelberg, (1985).

47. R.S. Chen, J.R.P. Jayakody, S.G. Greenbaum, Y.S. Pak, G. Xu, M.G. McLin and J.J. Fontanella, *J. Electrochem. Soc.*, **140**, 889 (1993).

48. S.Z. Li, Y.S. Pak, K. Adamic, S.G. Greenbaum, B.S. Lim, G. Xu, and A.S. Nowick, *J. Electrochem. Soc.*, **139**, 662 (1992).

49. R.E. Dehl, *J. Chem. Phys.* **48**, 831 (1968).

50. K. Matsumura, K. Hayamizu, T. Nakane, H. Yanagishita, and O. Yamamoto, *J. Polym. Sci.: Polym. Phys.* **25**, 2149 (1987).

51. K. Matsumura, K. Hayamizu, T. Nakane, H. Yanagishita, and O. Yamamoto, *J. Polym. Sci.: Polym. Phys.* **26**, 2215 (1988).

52. K. Matsumura, K. Hayamizu, and O. Yamamoto, *J. Polym. Phys.: Polym. Phys.* **27**, 2407 (1989).

Reproduced with permission of the copyright owner. Further reproduction prohibited without permission.

53. J.C. Hindman, A.J. Zielen, A. Svirmickas, and M. Wood, *J. Phys. Chem.* **76**, 1266 (1970).

54. J.C. Hindman, A.J. Zielen, A. Svirmickas, and M. Wood, *J. Phys. Chem.* **72**, 4188 (1968).

55. D. Brinkmann, High Pressure NMR, Chap. 1, J. Jonas, P. Diehl, E. Fluck, H. Gunther, R. Kosfeld, J. Seelig (eds.), Springer-Verlag, Berlin, Heidelberg (1991).

56. M.G. Mclin, M.C. Wintersgill, J.J. Fontanella, R.S. Chen, J.P. Jayakody, and S.G. Greenbaum, *Solid State Ionics*, **60**, 137 (1993).

57. C.P. Flynn, Point defects and diffusion, 319-325, 415-418, Clarendon Press, Oxford (1972).

58. J.H. Walton, M.J. Lizak, M.S. Conradi, T. Gullion, and J. Schaefer, *Macromolecules*, **23**, 416 (1990).

59. A. Abragam, The Principles of Nuclear Magnetism, Chap.7&8, Clarendon Press, Oxford (1961).

60. J. Jonas, P. Diehl, E. Fluck, H. Gunther, R. Kosfeld, and J. Seelig (eds.) High Pressure NMR, Springer-Verlag, Berlin, Heidelberg (1991).

61. Nan-I Liu and J. Jonas, *J. Magn. Reson.* **18**, 444 (1975).

62. S.G. Greenbaum, Y.S. Pak, K.J. Adamic, M.C. Wintersgill, J.J. Fontanella, D.A. Beam, H.L. Mei, and Y. Okamoto, *Mol. Cryst. Liq. Cryst.*, **160**, 347 (1988).

63. S.M. Klainer, T.B. Hirschfeld, and R.A. Marino, Fourier Transform Nuclear Quadrupole Resonance Spectroscopy, 166-178, A.G. Marshall

Reproduced with permission of the copyright owner. Further reproduction prohibited without permission.

(ed.), Plenum Press, New York, (1982).

64. C. P. Slichter, Principles of Magnetic Resonance, III Edition, Springer-Verlag (New York, 1990), Chapter 1-3, 5-6, 10.

65. E. Fukushima and S.B.W. Roeder, Experimental Pulse NMR, A Nuts and Bolts Approach, Chap. 3, 156, Addison-Wesly Publishing Company, Inc. (1981).

66. I.D. Weisman and L. H. Bennett, *Phys. Rev.* **181**, 1341 (1969).

67. I. Solomon, *Phys. Rev.* **110**, 61 (1958).

68. A.R. Edmonds, Angular Momentum in Quantum Mechanics, Chap.4, Princeton University Press, (1974).

69. N.J. Bunce, S.J. Sondheimer, and C.A. Fyfe, *Macromolecules*, **19**, 333 (1986).

70. J.C. Hindman, A. Svirmickas, M. Wood, *J. Phys. Chem.* **59**, 1517 (1973).

71. J.C. Hindman, A.J. Zielen, A. Svirmickas, M. Wood, *J. Phys. Chem.*, **54**, 621 (1971).

72. D.E. O'Reilly and E.M. Peterson, *J. Phys. Chem.* **55**, 2155 (1971).

73. E.W. Lang, H.-D Ludemann, Chap. 4, 129 in Ref. 60.

74. B. Halle and H. Wennerstrom, *J. Chem. Phys.* **75(4)**, 1928 (1981).

75. J.C. Gore, M.S. Brown, J. Zhong, and I.M. Armitage, *J. Magn. Reson.* **83**, 246 (1989).

76. K. Uosaki, K. Okazaki, and H. Kita, *J. Electroanal. Chem.*, **287** 163 (1990).

Reproduced with permission of the copyright owner. Further reproduction prohibited without permission.

77. (a) A. Baram, Z. Luz, and S. Alexander, *J. Chem. Phys.* **58**, 4558 (1973); (b) A. Vega, presented at the Bat-Sheva Workshop on New Developments and Applications in ESR and NMR Spectroscopy, Israel, (1990) (unpublished).

78. E. Fukushima and S.B.W. Roeder, p.108 in Ref.65.

79. Fenzke, D. Freude, T. Frohlich, and J. Haase, *Chem. Phys. Lett.*, **111**, 171 (1984).

80. R.S. Chen, P.E. Stallworth, S.G. Greenbaum, J.J. Fontanella, and M.C. Wintersgill, *Electrochemical Acta*, submitted.

81. D. Chandler, J. Chem. Phys. **60**, 3500 (1975).

82. B.E. Conway, J.O. Bockris and H. Linton, *ibid*, **24**, 834 (1956).

83. M.W. Verbrugge and R. Hill, *J. Electrochem. Soc.*, **137**, 3770 (1990).

84. R.S. Chen, J.R.P. Jayakody and S.G. Greenbaum, *Mat. Res. Symp. Proc. Solid State Ionics*, **293**, 99 (1993).

Reproduced with permission of the copyright owner. Further reproduction prohibited without permission.